MATHEMATICAL MODELING OF A THREE-DIMENSIONAL PERMEABILITY TENSOR FOR RESERVOIR SIMULATION

by

© Felix John Rogers

A Thesis submitted to the

School of Graduate Studies

in partial fulfillment of the requirements for the degree of

Masters of Engineering

Oil and Gas Engineering

Memorial University of Newfoundland

May 2015

St. John's, Newfoundland and Labrador

ABSTRACT

Anisotropy is generally formed as a result of systematic orientation and shape of asymmetric grains making up the solid matrix of porous media. It is well known that porous media are often anisotropic. To calculate flow in such three dimensional media a permeability tensor must be used in Darcy's law.

These anisotropic reservoirs cannot be properly studied with conventional simulators, which assume that the coordinate system used to describe the fluid flow aligns with the principal permeability axes. Thus, the coordinate axes are oriented in the same direction as these principal axes. Permeability actually varies in all directions and with increased use of directional wells, the ability to use correct permeability in the direction of fluid flow is important in predicting reservoir production characteristics. This will also help explain why and where oil accumulations occur.

Many investigators have attempted to either develop a mathematical model to calculate anisotropic permeability of a system or to experimentally develop a procedure to measure directional permeabilities.

This research involves creating this three-dimensional permeability tensor mathematically. Then, using the commercial reservoir simulator, the three-dimensional permeability tensor is

included in the reservoir model. The tensor is rotated within each grid block to align the principal coordinate axes with the actual well path. The model with the three-dimensional permeability tensor is used to predict the oil production rate. The oil production rates are then compared to the conventional reservoir simulator results.

Results from the reservoir simulations found that as the size reservoir grid refinement increased, so did the deviation in the oil production rates predicted comparing the conventional reservoir simulator wellpath and the simulation with the tensor aligned with the wellpath.

Also, from the simulations it was found that there is a difference in oil production rates when comparing the simulations with the tensor aligned with the wellpath to the conventional reservoir simulation approach. Further research using the tensor aligned with the wellpath in full field reservoir simulation and comparing the results to real field data will confirm which approach is more accurate.

ACKNOWLEDGEMENTS

I would like to express my gratitude to my academic advisors, Dr. Lesley James and Dr. Thormod Johansen, for allowing me to peruse my masters degree and their guidance and support throughout the process. They contributed to a rewarding graduate school experience by giving me intellectual freedom in my work, supporting my attendance at various conferences, engaging me in new ideas, and demanding a high quality of work in all my endeavours.

I would like to thank the Hibernia Management and Development Company Ltd. (HMDC) for providing the funding which allowed me to undertake this research.

This thesis would not have been possible without guidance from family members to initially pursue my masters degree. I would like to thank my mom and dad for their support and patience throughout this process. Finally, I want to express my gratitude to Matt, Melissa and Lisa for the help they provided me at various times over the last two years.

Table of Contents

List of Tables

List of Figures

List of Symbols, Nomenclature or Abbreviations

Darcy's Law

D	Space Differential Operator
$\vec{F}$	Mass Flux Vector
g	Gravitational constant [9.81 m/s^2]
K	Permeability [m^2 or mD]
$\underline{K}$	Permeability tensor
P	Absolute Pressure [Pa]
q	Fluid flow rate [m^3/s]
r	Radius [m]
u	Volumetric Flux [$m^3 \cdot s^{-1} \cdot m^{-2}$]
μ	Fluid viscosity [Pa·s]

Coordinate Systems

x, y, z	Coordinates of the principal permeability directions and the reservoir grid coordinates
β, ξ, ζ	Coordinates of the mathematically rotated permeability directions

List of Appendices

Chapter 1 Introduction

Reservoir simulation is used to help make large capital decisions, to estimate reserves, predict future oil production rates, and to diagnose, and improve the performance of producing reservoirs. The reservoir models have a large number of properties associated with them. Therefore, a better understanding of the variability of reservoir properties is needed. One of the most important properties governing fluid flow is permeability, which is a directionally, spatially and scale dependent variable describing the connectivity or transmissibility of the reservoir rock. This research focuses on the directional variability, or anisotropy, of permeability and its effect on predicting oil production rates.

Permeability anisotropy is formed by compaction due to gravity, depositional processes, the presence of fractures, diagenesis, biologic activity, etc. Permeability anisotropy results in a directionally variable permeability that can be modeled in three dimensions using a full tensor, represented by a 3x3 permeability matrix.

In reservoir simulation, the permeability tensor is used in Darcy's Law to model fluid flow in three dimensions. Typically, reservoir simulators ignore the full tensorial nature of the absolute permeability and assume the permeability can be represented by a diagonal tensor whose principal permeability axes coincide with the local coordinate system. Figure 1-1 depicts the

local grid coordinate system (x, y, z) and the principal permeability (K_x, K_y, K_z) having the same directions, resulting in a diagonal permeability tensor. The fluid flow does not align with the coordinate systems. The figure represents an offshore production platform producing hydrocarbons from a reservoir folded by tectonic forces. Also depicted is the location of a section of a reservoir simulation grid.

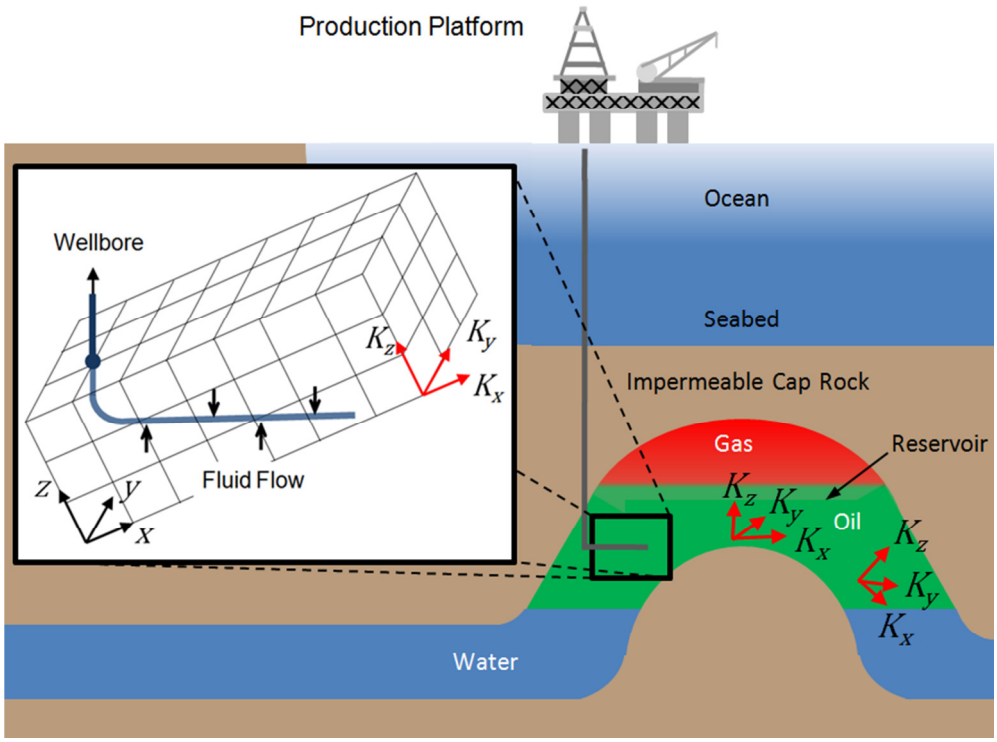

Figure 1-1: Representation of the Permeability Model Simulation Grid within the Oil Field Reservoir

Figure 1-1 depicts the local coordinate system as (x, y, z) therefore the principal permeability axes (K_x, K_y, K_z) are aligned with the depositional directions before folding occurred. The challenge with this approach arises when the flow path is not aligned with the local coordinate

system as seen in Figure 1-1. Also in Figure 1-1 the well cuts through the grid blocks rather than being aligned with them or the principal permeability directions.

Diagonal permeability tensors are used in each simulation grid block. This is obtained by having the well path aligned with either the x, y or z direction within each block. Commercial simulators also depict the well path as passing through the center of each block in either of the directions. This limits the ability of commercial simulators to accurately model well paths. The following Figure 1-2 is an example of how current reservoir simulators would depict the wellbore path in Figure 1-1. The lighter sections of the wellbore demonstrate that it is inside the reservoir and the dot followed by the darker section of the wellbore is where the well is exiting the simulation grid.

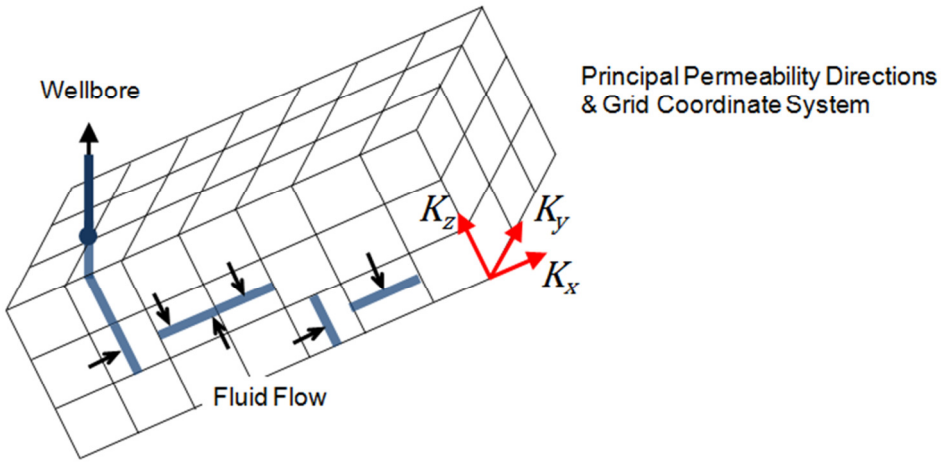

Figure 1-2: Reservoir Grid with Commercial Simulator Wellpath

An alternate method to model the hydrocarbon flow into the well is to rotate the permeability axes to match the wellbore path. This would create new directional permeabilities (K_β, K_ξ, K_ζ) that will differ from the principal permeabilities (K_x, K_y, K_z) and will require a full tensorial description as explained below. The new rotated coordinate system is illustrated in Figure 1-3.

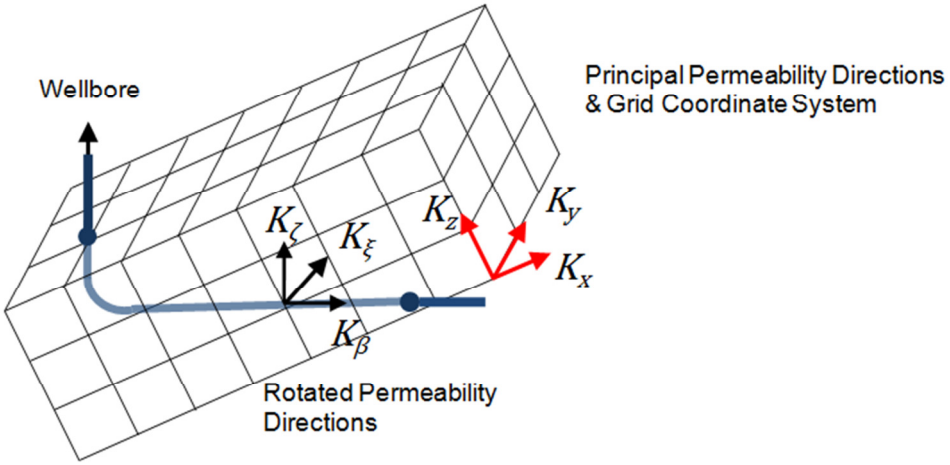

Figure 1-3: Reservoir with Rotated Permeability Tensor and Mathematical Representation of Wellpath

When the principal permeability tensor is rotated, cross permeability terms arise in the permeability matrix. These cross permeability terms have been investigated analytically and with numerical simulations, and the importance of including these terms has been established (Leung, 1986). However, through extensive literature review, the effect that cross permeability terms have on production and forecasting is not fully understood.

In order to orient the permeability tensor parallel to the wellbore, a matrix rotation is required. Rotation methods include the directional cosines method, and using an angle rotation about a secondary axis. By using these methods a new permeability tensor that contains cross terms in the permeability matrix can be generated. This new tensor is then used to calculate flow rate using Darcy's Law for fluid flow in a porous media.

In this thesis, reservoir simulations using the full permeability tensor, obtained from the mathematical rotation, are compared to the cases where the reservoir simulator uses a diagonal tensor. Oil production rates for the full permeability tensor and the diagonal tensor are examined to find any discrepancies between the two. Results show a difference in production rates depending on the method used.

Chapter 2 Literature Review

Through literature review it has been found that little work has been completed on the three dimensional permeability tensors for use in anisotropic and heterogeneous reservoir simulation. For this thesis, a good deal of work has been completed on understanding anisotropic reservoirs, fluid flow in porous media, reservoir modeling and other background information required.

In this chapter, absolute permeability is described, with information on isotropic, anisotropic and directional permeability. This is followed by sections outlining reservoir simulators, studies on modeling of three-dimensional anisotropic permeability and a section on permeability tensor.

2.1. Absolute Permeability

The absolute permeability of a rock is a measure of the ease with which a rock will permit the flow of fluids. A high permeability will allow a fluid to move rapidly through rocks. The permeability of a single phase fluid is different than the permeability where multiple fluid phases are flowing.

In 1856, Henry Darcy carried out simple experiments on packs of sand, and hence developed an empirical formula that remains the main permeability formula in use in the oil industry today. It has since been validated for most porous rock types and certain common fluids. Darcy's Law can be expressed as,

$$Q = \frac{KA(P_i - P_o)}{\mu L}. \tag{2.1}$$

Where*:*

Q = *flow rate (m^3/s)*
P_o = *outlet fluid pressure (Pa)*
P_i = *inlet fluid pressure (Pa)*
μ = *dynamic viscosity of the fluid (Pa·s)*
L = *length between inlet and outlet (m)*
K = *permeability of the sample (m^2)*
A = *area of the sample (m^2)*

In petroleum engineering, the unit used for permeability is the Darcy (D). A material is said to have a permeability equal to 1 Darcy if a pressure difference of 1 atmosphere will produce a flow rate of 1 cm^3/s of a fluid with 1 centipoise (cP) viscosity through a cube having sides equal to 1 cm (Darcy 1856). Therefore,

$$1\ Darcy = \frac{1\left(\frac{cm^3}{s}\right)1(cP)}{1(cm^2)1(\frac{atm}{cm})} = 0.987\ (\mu m)^2. \tag{2.2}$$

Darcy's law can also be expressed in terms of volumetric flux, $u = Q/A$. The differential form of Darcy's law can be written as,

$$u = -\frac{K}{\mu}\left(\frac{\partial p}{\partial s} + \rho g \sin\theta\right), \tag{2.3}$$

where s is the positive flow direction and θ is the angle between the positive x-axis and the positive flow direction measured counter clockwise.

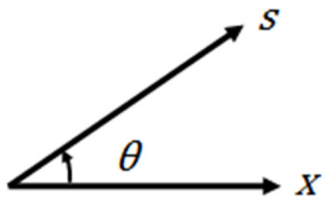

Figure 2-1: Arbitrary Flow Direction

Darcy's law applies for any direction and can therefore be formulated in three dimensions as a vector equation,

$$\vec{u} = -\frac{1}{\mu}\underline{K}(\nabla p - \rho\vec{g})\,. \tag{2.4}$$

In equation 2.3, $\underline{K}$ is a matrix of the following form,

$$\underline{K} = \begin{pmatrix} K_{xx} & K_{xy} & K_{xz} \\ K_{xy} & K_{yy} & K_{yz} \\ K_{xz} & K_{yz} & K_{zz} \end{pmatrix}. \tag{2.5}$$

A great deal of effort has been spent on proving that the permeability tensor $\underline{K}$ is symmetric and positive definite (Liakopoulos 1965). A symmetric matrix is a square matrix that is equal to its transpose, $A = A^T$. A *n* x *n* matrix, M, is positive definite when z^TMz is positive for every non-zero column vector z of *n* real numbers. Where z^T denotes the transpose of z. It is a mathematical fact that it is always possible to find three directions perpendicular to each other such that the permeability tensor becomes diagonal. These directions are called the principal directions for the permeability tensor. If *x, y, z* are the principal directions, $K_{xy} = K_{xz} = K_{yz} = 0$, and the permeability matrix becomes,

$$K = \begin{pmatrix} K_{xx} & 0 & 0 \\ 0 & K_{yy} & 0 \\ 0 & 0 & K_{zz} \end{pmatrix}. \tag{2.6}$$

When $K_{xx} = K_{yy} = K_{zz} = K$, the medium is called isotropic. In an anisotropic medium, the flow direction does not align with the pressure gradient (Liakopoulos 1965). The component volumetric flux (u) equation for *x, y,* and z becomes

$$u_x = -\frac{1}{\mu}\left[K_{xx}\frac{\partial p}{\partial x} + K_{xy}\frac{\partial p}{\partial y} + K_{xz}\frac{\partial p}{\partial z}\right], \tag{2.7}$$

$$u_y = -\frac{1}{\mu}\left[K_{xy}\frac{\partial p}{\partial x} + K_{yy}\frac{\partial p}{\partial y} + K_{yz}\frac{\partial p}{\partial z}\right], \tag{2.8}$$

$$u_z = -\frac{1}{\mu}\left[K_{xz}\frac{\partial p}{\partial x} + K_{yz}\frac{\partial p}{\partial y} + K_{zz}\frac{\partial p}{\partial z}\right]. \tag{2.9}$$

A property is said to be anisotropic when it is directionally dependent; otherwise, the property is said to be isotropic, which implies identical properties in all directions. Only flow or transport properties, which have a specific direction associated with their measurement, are anisotropic. This includes permeability, resistivity, thermal conductivity, and dispersivity. Properties such as density, porosity, and capillary pressure are considered intrinsically isotropic (Lake 1988). Nearly all reservoirs have some degree of anisotropy and heterogeneity (Fanchi 2006).

Permeability also varies spatially. A medium is homogeneous if the permeability is constant from point to point over the entire medium, while it is heterogeneous if permeability changes from point to point. An anisotropic medium has a different magnitude of permeability

depending on the direction (x, y or z) at each point, while the permeability of an isotropic medium is the same in each direction. Figure 2-2 illustrates four conditions of permeability. The arrows in each block indicate the magnitude of the permeability in each direction. It should be noted that these are scale dependent variables and what may be perceived as homogeneous or isotropic at one scale may be anisotropic or heterogeneous at another scale.

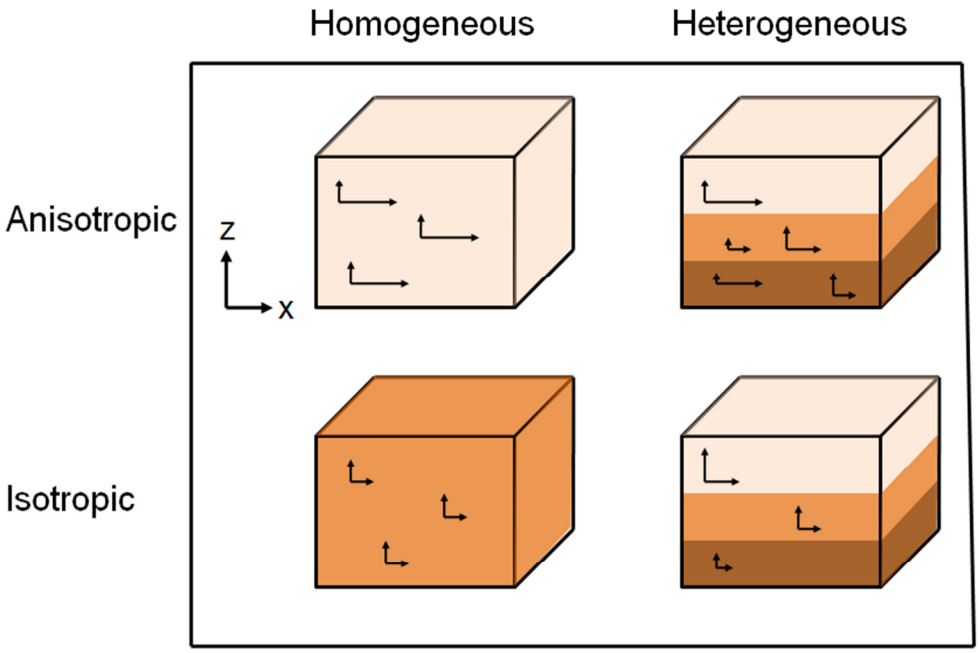

Figure 2-2: Four Possible Conditions for Isotropy / Anisotropy and Homogeneity / Heterogeneity

2.1.1. Isotropic Permeability

The permeability is considered to be isotopic if the elements of the diagonalized permeability tensor are equal, $K_{xx} = K_{yy} = K_{zz} = K$. Therefore, if the medium is isotopic, permeability does not depend on direction.

2.1.2. Anisotropic Permeability

In the anisotropic case the permeability tensor will have different values for K_{xx}, K_{yy} and K_{zz}. When the coordinate axes are not aligned with the principal permeability directions there will also be non-zero cross terms, which all have pairs; $K_{xy} = K_{yx}$, $K_{xz} = K_{zx}$ and $K_{yz} = K_{zy}$.

2.1.3. Directional Permeability Measurements

Measurement of isotropic permeability is usually performed on linear, mostly cylindrically shaped, 'core' samples. The core sample can be arrange to have either horizontal or vertical flow. Great care must be taken during fluid flow through the sample as to not allow fluids to bypass and cause a misreading.

Liquids and gases have been used to measure the permeability of the core using steady state and unsteady state methods. It has been found that liquids sometimes change the pore structure and therefore the permeability. This happens by rearrangement of some particles, swelling of material in pores, chemical reaction, etc (Rose 1982).

Directional permeabilities are measured for anisotropic materials. A couple of methods used to measure these permeabilities have been performed on anisotropic sandstone (Johnson and Hughes 1948; Johnson and Breston 1951). One method consists of cutting plug samples at various angles from the well core. The permeabilities of these plugs are then measured as mentioned previously. In the other method, a hole was drilled down the center of the cylindrical piece of a well core whose faces had been parallel. The equipment used allowed the hollow porous cylinder to be rotated to any position for flow measurement while the fluid was flowing from the center of the core to the outside of the cylinder. Darcy's Law is then used to calculate the directional permeabilities.

A more recent method to measure directional permeability is performed using three measurements on a laboratory sample to calculate the maximum and minimum permeabilities (Rose 1982). Rose used an angle which shows the direction of flow with respect to the direction of maximum permeability, an angle which shows the direction of flow with respect to the direction of the driving force gradient and an element, R_{ij}, of the resistivity tensor that appears when Darcy's law is given the special form, $R_{ij} \cdot \bar{q}\mu = -grad\ p$

2.2. Reservoir Simulators

Reservoir simulators progressed, between the early 1950s and 1970, from two dimensions and simple geometries to three dimensions, realistic geometry and a black oil fluid model. In the 1970s, researchers introduced compositional models and placed a heavy emphasis on enhanced oil recovery (Coats 1980).

Today, simulators are used to estimate production characteristics, calibrate reservoir parameters, visualise reservoir flow patterns, and much more. The main purpose is to provide an information database that can help the oil and gas companies to position and manage wells and well trajectories in order to maximize the oil and gas recovery and forecast production profiles for economic and life of field. Unfortunately, obtaining an accurate prediction of reservoir flow scenarios is a difficult task. One of the reasons is that it is not possible to obtain a complete and accurate characterization of the rock parameters that influence the flow pattern. Even if it was possible, reservoir simulators would not be able to exploit all available information, since this would require a tremendous amount of computer resources that exceed the capabilities of modern multi-processor computers.

Three categories of reservoir simulators exist; private, open source and commercial. The most well known open source software includes Black Oil Applied Simulation Tool (Boast), the MATLAB Reservoir Simulation Toolbox (MRST), and the Open Porous Media (OPM). Commercial

software includes Rock Flow Dynamics, CMG Suite (Three-Phase Black-Oil Reservoir Simulator, Compositional & Unconventional Reservoir Simulator and Advanced Processes & Thermal Reservoir Simulator), Schlumberger's Eclipse Suite (E100 and E300), and Halliburton's Landmark Nexus®.

For the purpose of this research the Schlumberger Eclipse E300 suite software was used, since Eclipse 300 allows a full tensor description of the absolute permeability and is licenced to Memorial University.

In order to confirm that the results from the Eclipse 300 reservoir simulator can be used, the diagonal tensor must have identical results as the case using the full tensor and having zero in the off diagonal components of the matrix. The only cases where the approaches should yield identical results are when the full tensor have zero in he off diagonal terms and have the same values in the diagonal terms as the diagonal tensor. If this occurs then it proves that the Eclipse 300 reservoir simulator have no error when comparing either approach.

2.2.1. Schlumberger ECLIPSE Suite

The Schlumberger ECLIPSE simulator is an industry standard for complete and robust set of numerical solutions and for fast and accurate prediction of dynamic behaviour for all types of reservoirs and development schemes. The ECLIPSE simulator has been a benchmark for

commercial reservoir simulators for more than 25 years thanks to its extensive capabilities, robustness, speed and parallel scalability (Schlumberger 2014).

Full tensor permeabilities are often required to describe complex reservoirs. Given a detailed heterogeneous reservoir description at the geological scale, upscaling is normally carried out to reduce the model size to one suitable for reservoir simulation. These upscaling procedures will generally create full tensor permeabilities, even if the permeabilities in the fine geological grid are not represented as tensors. Full tensor permeabilities also arise in complex crossbedded systems where the dip directions will not in general coincide with the local coordinate direction (Johansen 2008). A further case for full tensor permeabilities is in the modeling of fractured systems.

Conventionally, reservoir simulators ignore the full tensor nature of the absolute permeability and assume the permeability can be represented by a diagonal tensor whose principal axes coincide with the local coordinate system. This allows the construction of the usual five point discretization (the process of transferring continuous models and equations into discrete counterparts) in two dimensions or seven point in three dimensions which can be solved efficiently in the simulator. Ignoring the full tensor nature of the absolute permeability can lead to large reservoir simulation errors. Introduction of a full tensor permeability extends the arrangement of the discretization scheme to nine points in two dimensional cases and either 19

or 27 points in three dimensional cases. Figure 2-3 depicts the five (points P, N, S, E, W) and nine (points P, N, S, E, W, NW, NE, SW, SE) point discretization scheme's.

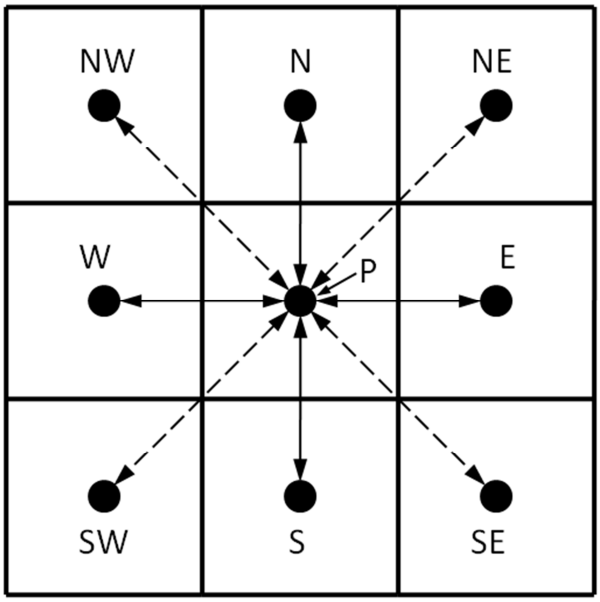

Figure 2-3: Five and Nine Point Discretization Scheme's

ECLIPSE 300 allows a full tensor description of the absolute permeability. The permeability tensor may either be supplied by a pre-processor by upscaling the properties on the geological model, or it may be entered by keywords PERMXX, PERMYY, PERMZZ (which describe the diagonal components for the tensor, *x*, *y* and *z*) and PERMXY, PERMYZ, PERMXZ to describe the off diagonal components (in the *xy*, *yz* and *xz* directions). Only positive definite symmetric tensors are allowed in the simulator. The principal directions of the tensor must also be supplied.

At present, the directions of the components of the tensor have three options, Figure 2-4. They can be aligned with the Cartesian axes (1), aligned with the axes joining the midpoints of each pair of opposite faces in the corner point cells (2), or aligned with the two axes formed by joining the midpoints of pairs of opposite faces in the "I" and "J" directions and with the third axis normal to the bedding plane (3).

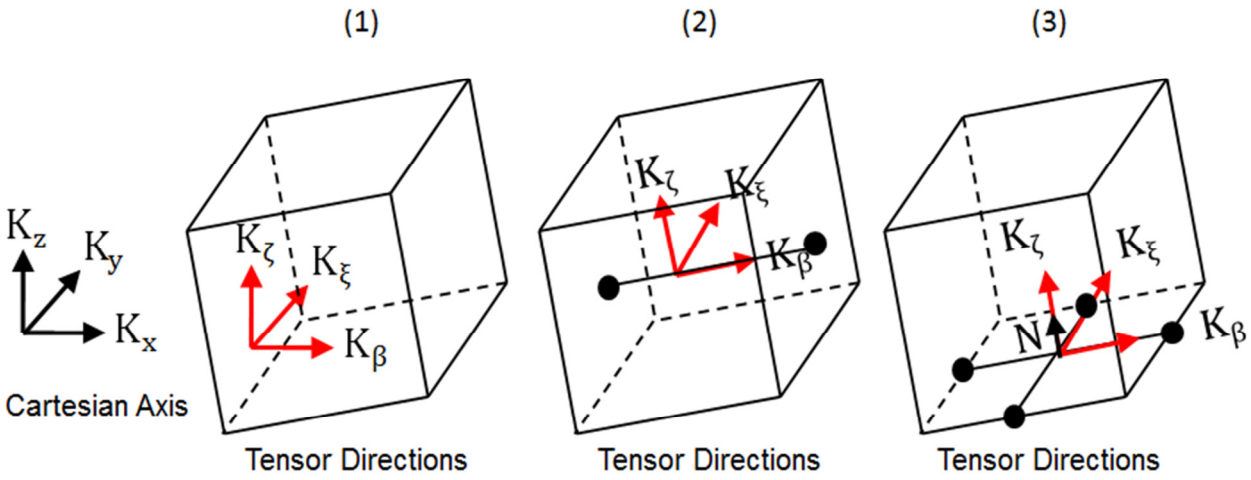

Figure 2-4: Three Options for Components of the Tensor

2.2.2. Traditional Reservoir Simulation Modeling

In reservoir simulation, the material balance equations must be discretized by choosing either an explicit or implicit method for pressure and saturation. For straight forward cases, the pressure is solved using an implicit equation, then the saturation using an explicit time stepping scheme. The algorithm is called the IMplicit Pressure Explicit Saturation (IMPES) (Sheldon et al. 1959).

The Eclipse E300 can use three calculation methods for the next time step; fully implicit (both saturation and pressure are implicit), adaptive implicit (tries to save computation time and memory by making cells implicit only when necessary) and IMPES. For the simulations related to this research the fully implicit method was used. This is the default case in Eclipse E300 and the most widely used in reservoir simulation.

Figure 2-4 illustrate the difference in implicit and explicit time discretization, where D is a space differential operator, $\vec{F}$ is mass flux vector and $\vec{X}(x,y,z)$ is known for every point in the reservoir.

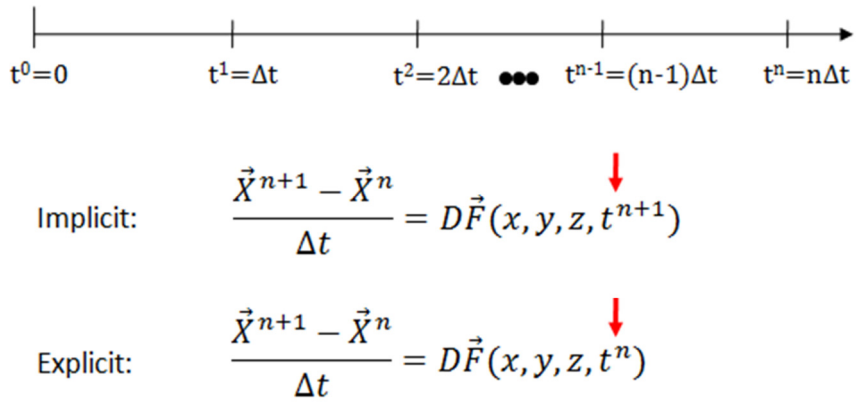

Figure 2-5: Time Discretization in Reservoir Simulation

When multiple blocks are added to the reservoir simulation, space discretization must be included. The simplest way to discretize space is to divide the whole simulation region into

many regions of the same size. Figure 2-5 demonstrates space discretization and the equation used in reservoir simulation.

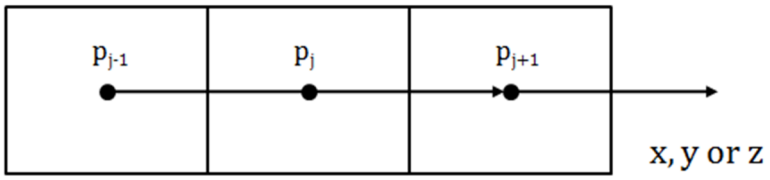

$$\frac{\partial}{\partial x}\left(\lambda\frac{\partial p}{\partial x}\right)=\frac{1}{\Delta\bar{x}_j}\left(\lambda_{j+1/2}\frac{p_{j+1}-p_j}{\lambda_{j+1/2}}-\lambda_{j-1/2}\frac{p_j-p_{j-1/2}}{\lambda_{j-1/2}}\right)$$

Figure 2-6: Space Discretization in Reservoir Simulation (Johansen 2008)

Near the wellbore, the linear Darcy's law may be inadequate to simulate the fluid flow. In the near wellbore region the flow rate from the reservoir is highly sensitive to the variation in permeabilities.

In the reservoir simulator, the wellbore is penetrates through the center of a box shaped reservoir grid, seen in Figure 1-2. These reservoir blocks are usually much larger than the wellbore and must be scaled accordingly. Equation 2.10 describes the steady state oil flow rate equation used to describe radial well models,

$$Q_o=\frac{2\pi Kh(p_e-p_w)}{\mu[\ln(r_e/r_w)+S]}, \tag{2.10}$$

where Q_o is the flow rate, K is the isotropic permeability, h is the height, p_e is the reservoir pressure at the drainage radius, p_w is the wellbore pressure, μ is fluid viscosity, r_e is the drainage radius and r_w is the wellbore radius. The variable S is called the skin. This represents an additional pressure drop (positive or negative) due to different irregularities in permeability in the near well region. A positive value would represent an impairment to flow, while a negative skin value would represent an enhancement to flow.

For the reservoir simulator the previous flow equation becomes,

$$Q_o = \frac{2\pi Kh(p_{block} - p_w)}{\mu[\ln(r_{block}/r_w) + S]}, \tag{2.11}$$

where p_{block} and r_{block} are the simulation grid block pressure and block radius, respectively. The problem arises in the so called block radius. It has been determined, through numerical simulations where analytical solutions exist, that the "correct" value to use for r_{block} in an anisotropic case with the well penetrating the center of the grid block and traveling in the y-direction is,

$$r_o = 0.28 \frac{\sqrt{\Delta x^2 \sqrt{\frac{K_z}{K_x}} + \Delta z^2 \sqrt{\frac{K_x}{K_z}}}}{\sqrt[4]{\frac{K_z}{K_x}} + \sqrt[4]{\frac{K_x}{K_z}}}. \tag{2.12}$$

This is called the Peaceman formula (Peaceman 1983). The following should be used for permeability in this anisotropic case in equation (2.12),

$$K = \sqrt{K_x K_z}\,. \tag{2.13}$$

In equation (2.12), Δx and Δz is the block size in the x- and z-directions, respectively. Similar formulas apply when the well path is aligned with other axis.

In reservoir simulation, it is standard to align the well in each grid block with the grid coordinate axis. Figure 2-6 depicts the well trajectory of simulator following the layers of the grid blocks as opposed to the actual well trajectory (Johansen 2008).

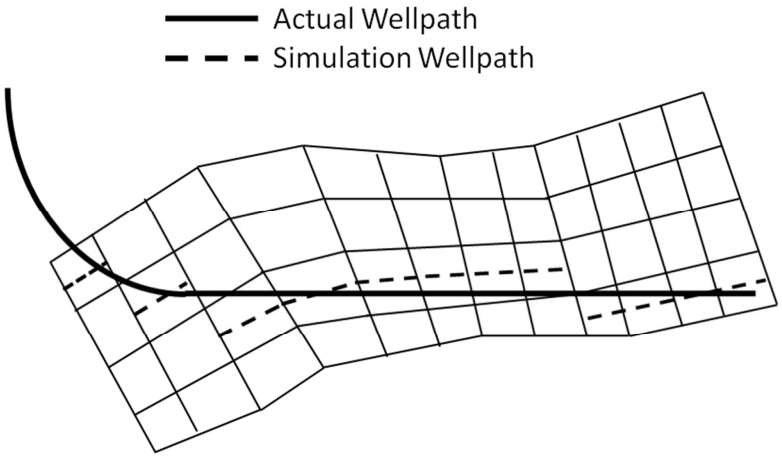

Figure 2-7: Actual and Simulated Wellpaths

2.3. Studies on Modeling of Three-Dimensional Anisotropic Permeability

Studies have been completed on understanding how anisotropic permeability is formed in reservoirs but little work has been done on the effects anisotropy has on predicting production profiles. However, the worth that has been done is described in this section.

2.3.1. Methods for Modeling Full Tensor Permeability in Reservoir Simulation

Bagheri and Settari's (2007) work examines methods for modeling reservoir flow using a permeability tensor. Instead of using the control volume multipoint discretizations, they used a simple extension of conventional finite difference method to handle both the permeability tensor and complex geometry. The work was initiated in order to find a more accurate way to model fluid flow in porous media. Dependency of simulation results of fluid flow in porous media to the type of grid mesh used is well-known and called the "grid orientation" effect. Many errors have been found depending on the gird method used. Figure 2-7 is an example used to demonstrate the effect the grid orientation has on production (Dalen et al. 1986). The reservoir simulation has two producing wells equidistant from an injection well and an orthogonal grid, Figure 2-7 (a). In order to investigate grid effects, the grid has been twisted so that the grid is no longer orthogonal, Figure 2-7 (b). Dalen's results showed the difference between the water cut values of the two wells increased dramatically when the angle between the grid lines is reduced to 45 degrees. The water reaches Well 2 before Well 1, in

correspondence with a faster flow parallel with the grid lines than the diagonal to the grid lines, using a skewed grid.

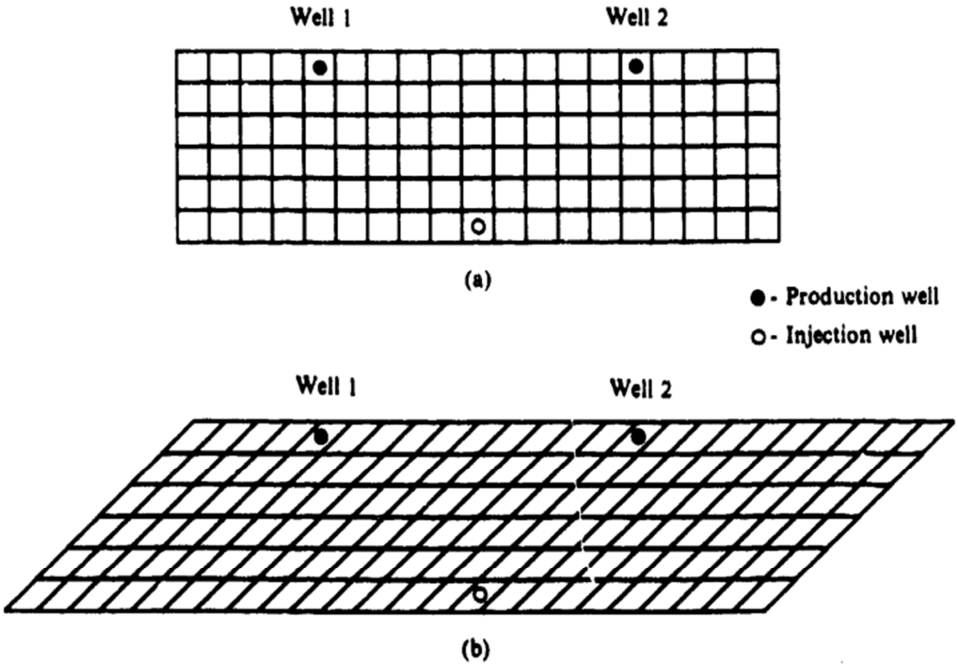

Figure 2-8: Grids for the Three-Well Problems: (a) Orthogonal grid and (b) Skew Grid with 45° Between Grid Lines (Dalen et al. 1986)

The nine point discretization method is the usual practice in reservoir simulation. Bagheri and Settari (2007) found that using a 9-point approximation with full tensor, in the presence of permeability anisotropy, could not accurately predict the behaviour of the reservoir, Figure 2-8. This was due to what they called a "tensor orientation" effect. This caused an error in the pressure and shape of the pressure field, which depends on the relative orientation of the grid in relation to the principal axes of the permeability tensor.

They showed that using a 13-point extension of the conventional 9-point finite difference method virtually eliminates the tensor orientation errors. The problem with the 13-point method is that it is impractical for conventional reservoir simulators because of the increased computer time required for simulation.

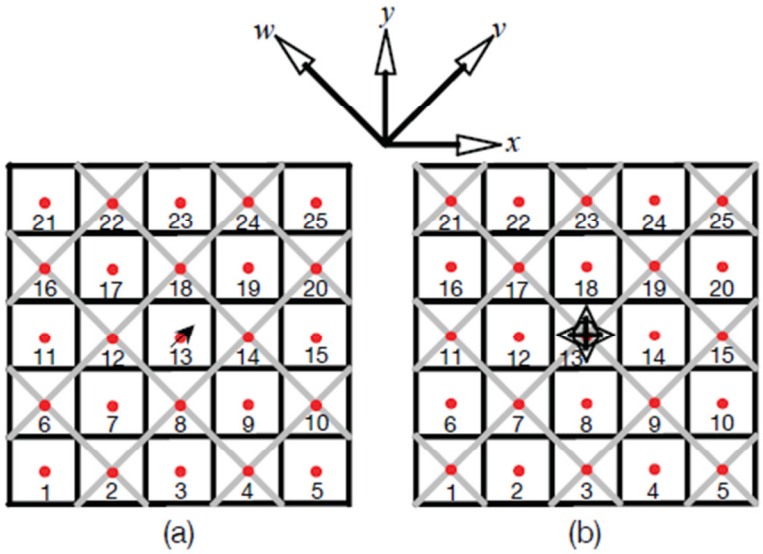

Figure 2-9: Overlapping Coordinate System used in 13-Point Method (Bagheri and Settari 2007)

Bagheri and Settari's research focused on x-y coordinate systems and not on a three-dimensional case. The base cases for each method (9-point and 13-point) used an isotropic model rather than a full tensor anisotropic model. Therefore, there is a lack of an analytical solution and full tensorial analysis to support their method.

In summary, their work describes the theory for modeling fluid flow in the presence of a permeability tensor. However, it does not look at rotation of the permeability tensor to align with the well trajectory.

2.3.2. A Tensor Model for Anisotropic and Heterogeneous Reservoirs with Variable Directional Permeabilities

Leung (1986) studied the permeability tensor to model fluid flow in complex reservoirs with multiple zones of directional permeability. He analyzed the cross permeability effects that arise when the coordinate axes are offset at an angle to the principal permeability axes. Nine and nineteen point finite difference methods have been derived for the tensor formation for two and three dimensional simulations, respectively.

His work explained the permeability tensor and its importance in Darcy's Law. He then provided mathematical and physical interpretation for the non-diagonal terms in the permeability tensor for a two-dimensional case. To show the cause and effect of the cross permeability terms of the tensor quantity, simple examples were used.

A finite difference formula was derived and implemented by Leung (1986), for use in a standard black oil simulator. Examples were performed in order to test the cross term permeability tensor derived from the formula. These examples focused solely on two dimensional cases with

the principal permeability axes rotated at an angle from the x-y axis. The examples demonstrated that neglecting the cross permeability terms in the tensor matrix may lead to serious errors in interpreting the well response. One example illustrated the importance of a permeability tensor used to study reservoirs with variable directional permeabilities in different zones. It showed that conventional simple anisotropy models are inadequate for studying this type of reservoir.

The work completed by Leung (1986) is helpful in understanding the use of a permeability tensor to model fluid flow in complex reservoirs with multiple zones of directional permeability. The research did not look at horizontal wells in anisotropic reservoirs and the problems that arise when simulating horizontal wells.

2.4. Permeability Tensor

Tensor calculus is a technique that can be regarded as a follow-up on linear algebra. It is a generalisation of classical linear algebra. In classical linear algebra one deals with vectors and matrices. Tensors are generalisations of vectors and matrices.

An example would be a tensor T at a point P is a property of the medium at P, such that T can be represented by a set of scalars depending on the coordinate system in which P is represented, Figure 2-9. Also, the components in another coordinate system depends uniquely on the linear transformation by which the two coordinate systems are related.

In Figure 2-9, X, Y and Z represent the principal permeability directions and x', y' and z' are the directions after the tensor (T') has been rotated.

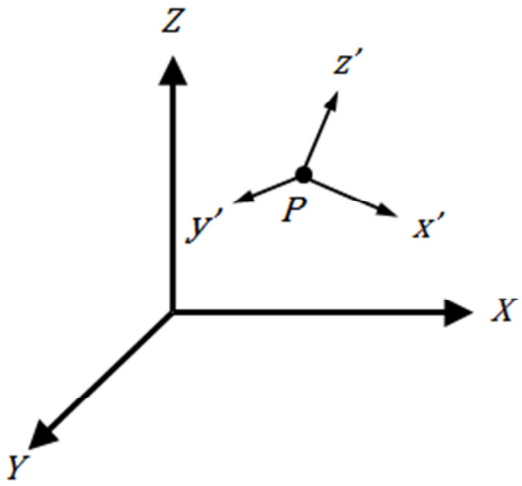

$$T'(@P) = \begin{bmatrix} T_{x'x'} & T_{x'y'} & T_{x'z'} \\ T_{y'x'} & T_{y'y'} & T_{y'z'} \\ T_{z'x'} & T_{z'y'} & T_{z'z'} \end{bmatrix}$$

Figure 2-10: Tensor T at Point P

Tensors often display a certain degree of symmetry, as is always the case in a diagonal matrix. Such symmetries have a strong effect on the properties of these tensors. Often, many of these properties or even tensor equations can be derived solely on the basis of these symmetries (Dellemond and Peeters 2010).

Darcy's law was originally derived for one dimensional single phase fluid flow. Permeability is a scalar quantity in the one dimensional flow case. The permeability tensor that can be

transformed by a rotation of the coordinate system has since been proven to be a symmetric property (Szabo 1968; Whitaker 1969; Case & Cochran 1972). Therefore, the eigenvalues of the tensor will be real. In 1988, Bear defined the tensor as positive definite, which guarantees that the energy is always dissipated during flow. If this were not true, then the flow would be against the pressure gradient (Durlofsky 1991).

Figure 2-10 depicts the direction of a flow field, $\vec{u}$ and the direction of a pressure gradient, ∇p. The definition of positive definite means that $x^T K x \geq 0$ for all vectors x. For this case take $x = \nabla p$ and $u = K \cdot \nabla p$. Therefore, $\nabla p \cdot (K \cdot \nabla p)$ equals components of $\vec{u}$ in the direction of ∇p. Components of $\vec{u}$ cannot be in the opposite direction of ∇p since the tensor is positive definite.

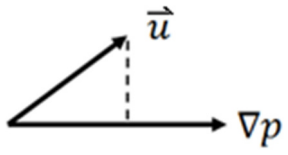

Figure 2-11: Directions of Tensor, $\vec{u}$, and Pressure Gradient, ∇p

Fluid flow in porous media is a transport phenomenon, fluid flow can be mathematically described by a linear law showing that the flow is directly proportional to the driving force (Scheidegger 1958). If the flow magnitude and direction are expressed in terms of a velocity vector and if the driving force is expressed by another vector given by the gradient in mechanical energy, such as pressure gradient, the constant of proportionality will be a simple

scalar quantity denoted by the absolute permeability divided by viscosity (K/μ), when the porous medium is an isotropic conductor. In an isotropic medium, K is a scalar quantity and has no directional sense. Mathematically, the direction of the flow and the driving force vectors are the same throughout the field of flow. This implies that in those domains, homogeneity of the system prevails. Sometimes, the constant of proportionality in Darcy's law between the flow and driving force vectors cannot be expressed in terms of a simple scalar number, but rather reference has to be made to a symmetric second rank tensor, which will have nine elements in a three dimensional case.

For an anisotropic porous media, Darcy's law can be described using a three dimensional matrix as shown (with gravity neglected),

$$\begin{bmatrix} u_x \\ u_y \\ u_z \end{bmatrix} = -\frac{1}{\mu} \begin{bmatrix} K_{xx} & K_{xy} & K_{xz} \\ K_{yx} & K_{yy} & K_{yz} \\ K_{zx} & K_{zy} & K_{zz} \end{bmatrix} \cdot \begin{bmatrix} \partial p/\partial x \\ \partial p/\partial y \\ \partial p/\partial z \end{bmatrix}. \quad (2.14)$$

The permeability tensor is used to model fluid flow in complex anisotropic and heterogeneous reservoirs. The orientation and magnitude of principal permeabilities may, in general, vary between different zones in the reservoir. This type of reservoir cannot be studied with conventional simulators, which assume that the orientation of the principal permeability axes are fixed in each grid block; thus, the coordinate axes can be oriented in the same direction as these principal axes.

Permeability actually varies in all directions and with the increased use of directional wells, the ability to simulate these wells using realistic permeability values is important in predicting reservoir production characteristics, as is the focus of this thesis.

2.4.1. Tensor Rotation

In cases where the coordinate system used to describe flow is not aligned with the principal permeability directions, the coordinates are obtained by a rotation of the principal coordinate system. According to the definition of a tensor, the tensor must be calculated from the same set of rotations. A case where this occurs would be when a wellbore path passes through a reservoir that is tilted as shown in the Figure 2-11. This two dimensional figure shows the principal permeability directions of the reservoir that are not in the same direction of the hydrocarbon flow.

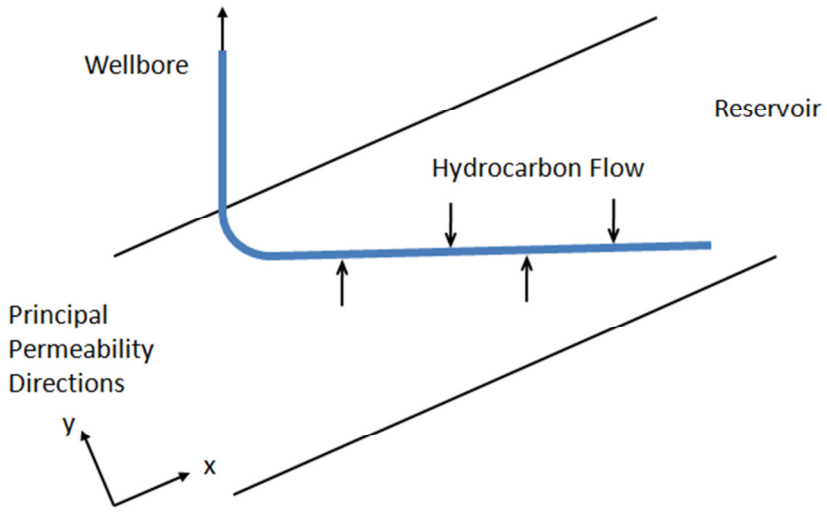

Figure 2-12: Wellpath in Reservoir Not Aligned with a Principal Permeability Direction

A simple test can be performed to determine if the matrix is symmetric, positive definite when the principal permeabilities K_1, K_2 and K_3 are known. After the tensor rotation calculation has been performed, a quick calculation using equations (2.21), (2.22) and (2.23) will determine if the calculation was performed correctly (Johansen 2013).

The theory for this simple test begins with symmetric matrices always having real eigenvalues and if the matrix is also positive definite then these eigenvalues are also positive. These facts are utilized in the search for a coordinate system that will simplify calculations using Darcy's law for a symmetric, positive definite permeability tensor $\underline{K}$. First, the following eigenvalue problem must be solved,

$$\underline{K} \cdot \vec{e} = \lambda \vec{e}\,, \tag{2.15}$$

where $\vec{e}$ is an eigenvector for the eigenvalue λ and the permeability tensor is symmetric, i.e.

$$\underline{K} = \begin{pmatrix} K_{xx} & K_{xy} & K_{xz} \\ K_{xy} & K_{yy} & K_{yz} \\ K_{xz} & K_{yz} & K_{zz} \end{pmatrix}. \tag{2.16}$$

Equation 2.15 determines the direction for which $\vec{e}$ and $\underline{K} \cdot \vec{e}$ are the same. These are the directions where the medium behaves isotropically. For (2.15) to have non-trivial solutions, the determinant of $\underline{K} - \lambda I$ must be zero, where I is the identity matrix. This leaves the cubic equation

$$\lambda^3 - I_1\lambda^2 + I_2\lambda - I_3 = 0 \tag{2.17}$$

in λ where the coefficients are given by

$$\begin{aligned} I_1 &= K_{xx} + K_{yy} + K_{zz}\ , \\ I_2 &= K_{xx}K_{yy} + K_{yy}K_{zz} + K_{zz}K_{xx} - K_{xy}^2 - K_{yz}^2 - K_{zx}^2\ , \text{and} \\ I_3 &= K_{xx}K_{yy}K_{zz} + 2K_{xy}K_{yz}K_{zx} + K_{xx}K_{yz}^2 - K_{yy}K_{zx}^2 - K_{zz}K_{xy}^2\ . \end{aligned} \tag{2.18}$$

It was assumed that (2.16) is a symmetric and positive definite permeability tensor, having real roots λ_1, λ_2, λ_3. The next step is to find the corresponding eigenvectors, once the eigenvalues are determined. The determinant, $Det\left(\underline{K} - \lambda_i I\right) = 0$ for each i, therefore one of the components of $\overrightarrow{e_i}$ can be chosen leaving a unique solution for the two remaining components. For a symmetric matrix, this will always result in three linearly independent orthogonal eigenvectors $\overrightarrow{e_1}$, $\overrightarrow{e_2}$, $\overrightarrow{e_3}$. Since one of the components in each eigenvector could be chosen, it is

also possible to choose these eigenvectors as unit vectors. Assuming an eigenvector as a unit vector, an orthonormal coordinate system corresponding to the eigenvalues of the given symmetric and positive definite matrix $\underline{K}$ is determined. These orthonormal eigenvectors can then be organized in a matrix as

$$R = [\overrightarrow{e_1}, \overrightarrow{e_2}, \overrightarrow{e_3}] , \tag{2.19}$$

where the i-th column of R is $\overrightarrow{e_i}$. Since the columns are linear independent, the inverse R^{-1} exists, $R^{-1} \cdot R = I$. Therefore,

$$R^{-1} \cdot \underline{K} \cdot R = R^{-1} \cdot \underline{K} \cdot [\overrightarrow{e_1}, \overrightarrow{e_2}, \overrightarrow{e_3}] = R^{-1} \cdot [\lambda_1 \overrightarrow{e_1}, \lambda_2 \overrightarrow{e_2}, \lambda_3 \overrightarrow{e_3}] = \begin{bmatrix} \lambda_1 & 0 & 0 \\ 0 & \lambda_2 & 0 \\ 0 & 0 & \lambda_3 \end{bmatrix}. \tag{2.20}$$

The transform $\underline{K} \rightarrow R^{-1} \cdot \underline{K} \cdot R$ gives a diagonal matrix with eigenvalues of $\underline{K}$ on the diagonal, and the corresponding coordinate system that gives this result is defined by three orthonormal eigenvectors.

For a symmetric positive definite matrix to be a permeability tensor, the diagonalization process applied to it must result in the same eigenvalues and eigenvectors, namely those given by the principal directions and principal permeabilities K_1, K_2, K_3. That is to say, all permeability tensors for a porous medium have the same eigenvalues and corresponding eigenvectors. Consequently, equation (2.17) always has K_1, K_2, K_3 as roots independent of the coordinate

system we started with. Therefore, the coefficients of (2.17) given by (2.18) are also independent of the coordinate system. As a result, I_1, I_2, I_3 in (2.18) are permeability invariants for the porous medium. These facts offer the simple test to determine if a given symmetric, positive definite matrix as (2.16) is a permeability tensor for the medium if the principal permeabilities (K_1, K_2, K_3) are known,

$$K_{xx} + K_{yy} + K_{zz} = K_1 + K_2 + K_2 \tag{2.21}$$

$$K_{xx}K_{yy} + K_{yy}K_{zz} + K_{zz}K_{xx} - K_{xy}^2 - K_{yz}^2 - K_{xz}^2 = K_1K_2 + K_2K_3 + K_1K_3 \tag{2.22}$$

$$K_{xx}K_{yy}K_{zz} + 2K_{xy}K_{yz}K_{xz} - K_{xx}K_{yz}^2 - K_{yy}K_{xz}^2 - K_{zz}K_{xy}^2 = K_1K_2K_3 \tag{2.23}$$

where, K_1, K_2, K_3 are the principal permeability values and $K_{xx}, K_{yy}, K_{zz}, K_{xy}, K_{yz}, K_{xz}$ are values from the full tensor created after rotation.

Orthogonal transformation of the permeability tensor can be done in many ways. This research will focus on three dimensional transformation using the directional cosine method and the angle rotation about a secondary axis. These are described next.

2.4.1.1. Directional Cosines

The directional cosines of a vector are the cosines of the angles between the vector and the three coordinate axes. They are useful in forming directional cosines matrices that express one set of orthonormal basis vectors in terms of another set. Sets of direction cosines can be used to construct a transformation matrix from the vectors (Tyldesley 1975).

The following figure illustrates an arbitrary direction $\vec{n}$ relative to the principal permeability directions,

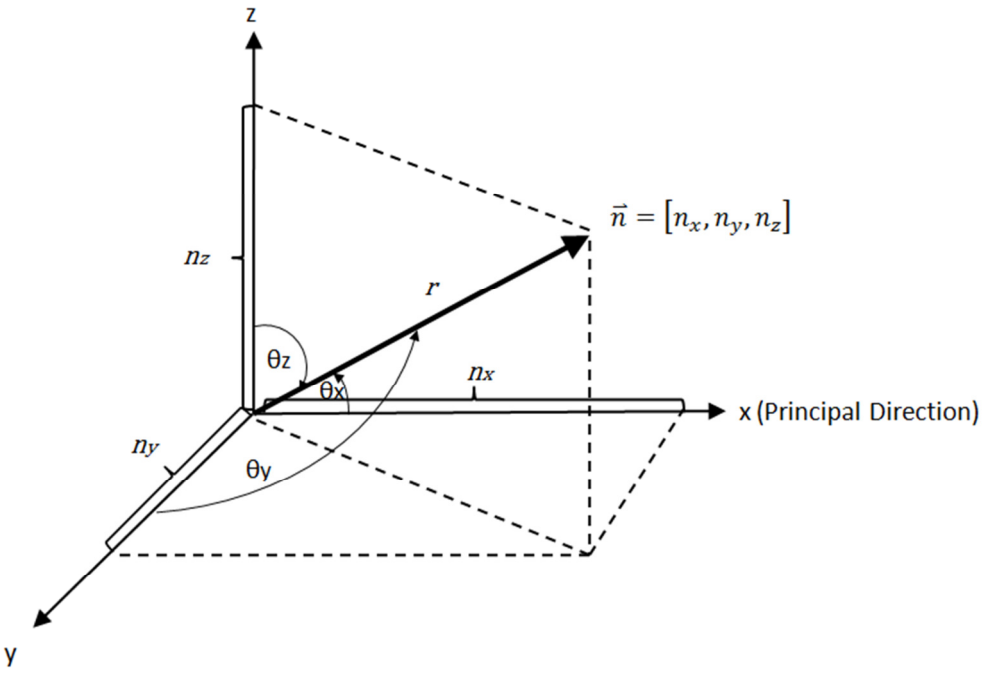

Figure 2-13: Principal Permeability Directions x, y, and z with Unit Vector $\vec{n}$

where the directional cosines for Figure 2-12 and 2-13 are,

$$\cos\theta_x = \frac{n_x}{r}, \tag{2.24}$$

$$\cos\theta_y = \frac{n_y}{r}, \tag{2.25}$$

$$\cos\theta_z = \frac{n_z}{r}. \tag{2.26}$$

We find that

$$\cos^2\theta_x + \cos^2\theta_y + \cos^2\theta_z = \frac{n_x^2}{r^2} + \frac{n_y^2}{r^2} + \frac{n_z^2}{r^2} = 1\,. \tag{2.27}$$

Therefore, $[\cos\theta_x\,, \cos\theta_y\,, \cos\theta_z]$ is a unit vector (length=1).

This method needs three angles, one from each of the principal permeability directions to the given direction. The given direction is the direction of the wellbore. The axis in Figure 2-13 below, represents the principal permeability directions and the arbitrary wellbore represented as β. Angles from the x, y and z-axis to the well path are required to describe the deviation of the arbitrary wellbore orientation from the principal permeability axes.

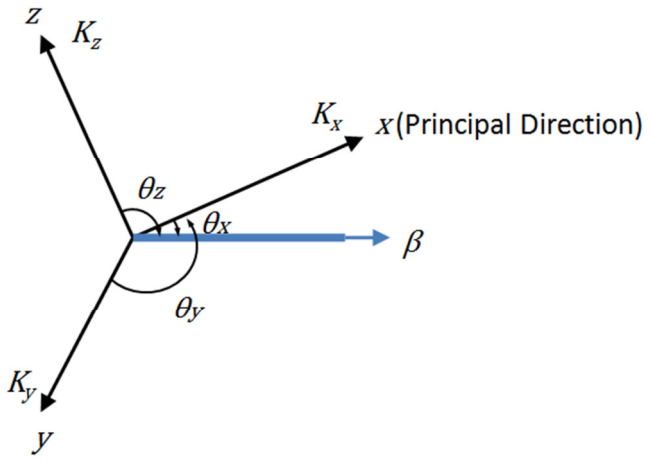

Figure 2-14: Coordinate System Rotation so the x-axis Aligns with the Wellbore (β) using Directional Cosines

A three dimensional rotated coordinate system is given by a matrix R. In this method R is given by,

$$R = R_x(\theta_x) \cdot R_y(\theta_y) \cdot R_z(\theta_z), \tag{2.28}$$

with coordinate system rotations of the x, y and z-axis in the counterclockwise direction when looking towards the origins give the matrices,

$$R_x(\theta_x) = \begin{bmatrix} 1 & 0 & 0 \\ 0 & \cos\theta_x & \sin\theta_x \\ 0 & -\sin\theta_x & \cos\theta_x \end{bmatrix}, \tag{2.29}$$

$$R_y(\theta_y) = \begin{bmatrix} \cos\theta_y & 0 & -\sin\theta_y \\ 0 & 1 & 0 \\ \sin\theta_y & 0 & \cos\theta_y \end{bmatrix}, \tag{2.30}$$

$$R_z(\theta_z) = \begin{bmatrix} \cos\theta_z & \sin\theta_z & 0 \\ -\sin\theta_z & \cos\theta_z & 0 \\ 0 & 0 & 1 \end{bmatrix}. \tag{2.31}$$

After matrix multiplication we find

$$R = \begin{bmatrix} \cos\theta_y \cos\theta_z & \cos\theta_y \sin\theta_z & -\sin\theta_y \\ \cos\theta_z \sin\theta_x \sin\theta_y - \cos\theta_x \sin\theta_z & \sin\theta_x \sin\theta_y \sin\theta_z + \cos\theta_x \cos\theta_z & \cos\theta_y \sin\theta_x \\ \cos\theta_x \cos\theta_z \sin\theta_y + \sin\theta_x \sin\theta_z & \cos\theta_x \sin\theta_y \sin\theta_z - \cos\theta_z \sin\theta_x & \cos\theta_x \cos\theta_y \end{bmatrix}. \tag{2.32}$$

This rotation method gives the permeability tensor with the following terms,

$$K_{\beta\beta} = K_x \cos^2\theta_y \cos^2\theta_z + K_y \cos^2\theta_y \sin^2\theta_z + K_z \sin^2\theta_y, \tag{2.33}$$

$$K_{\beta\xi} = K_x(\cos\theta_z \sin\theta_x \sin\theta_y - \cos\theta_x \sin\theta_z)\cos\theta_y \cos\theta_z + K_y(\cos\theta_x \cos\theta_z + \sin\theta_x \sin\theta_y \sin\theta_z)\cos\theta_y \sin\theta_z - K_z \cos\theta_y \sin\theta_x \sin\theta_y, \tag{2.34}$$

$$K_{\beta\zeta} = K_x(\sin\theta_x \sin\theta_z + \cos\theta_x \cos\theta_z \sin\theta_y)\cos\theta_y \cos\theta_z + K_y(\cos\theta_x \sin\theta_y \sin\theta_z - \cos\theta_z \sin\theta_x) * \cos\theta_y \sin\theta_z - K_z \cos\theta_x \cos\theta_y \sin\theta_y, \tag{2.35}$$

$$K_{\xi\beta} = K_x(\cos\theta_z \sin\theta_x \sin\theta_y - \cos\theta_x \sin\theta_z)\cos\theta_y \cos\theta_z + K_y(\cos\theta_x \cos\theta_z + \sin\theta_x \sin\theta_y \sin\theta_z) * \cos\theta_y \sin\theta_z - K_z \sin\theta_y \cos\theta_y \sin\theta_x, \tag{2.36}$$

$$K_{\xi\xi} = K_x(\cos\theta_x \sin\theta_x \sin\theta_z - \cos\theta_x \sin\theta_z)^2 + K_y(\cos\theta_x \cos\theta_z + \sin\theta_x \sin\theta_y \sin\theta_z)^2 + K_z \cos^2\theta_y \sin^2\theta_x, \tag{2.37}$$

$$K_{\xi\zeta} = K_x(\sin\theta_x \sin\theta_y + \cos\theta_x \cos\theta_z \sin\theta_y)(\cos\theta_z \sin\theta_x \sin\theta_y - \cos\theta_x \sin\theta_z)$$
$$+K_y(-\cos\theta_z \sin\theta_x + \cos\theta_x \sin\theta_y \sin\theta_z)(\cos\theta_x \cos\theta_z + \sin\theta_x \sin\theta_y \sin\theta_z)$$
$$+K_z \cos\theta_x \cos^2\theta_y \sin\theta_x \quad (2.38)$$

$$K_{\zeta\beta} = K_x(\sin\theta_x \sin\theta_z + \cos\theta_x \cos\theta_z \sin\theta_y)\cos\theta_y \cos\theta_z + K_y(\cos\theta_x \sin\theta_y \sin\theta_z$$
$$-\cos\theta_z \sin\theta_x) * \cos\theta_y \sin\theta_z - K_z \cos\theta_x \cos\theta_y \sin\theta_y, \quad (2.39)$$

$$K_{\zeta\xi} = K_x(\sin\theta_x \sin\theta_z + \cos\theta_x \cos\theta_z \sin\theta_y)(\cos\theta_z \sin\theta_x \sin\theta_y - \cos\theta_x \sin\theta_z)$$
$$+K_y(-\cos\theta_z \sin\theta_x + \cos\theta_x \sin\theta_y \sin\theta_z)(\cos\theta_x \cos\theta_z + \sin\theta_x \sin\theta_y \sin\theta_z)$$
$$+K_z \cos\theta_x \cos^2\theta_y \sin\theta_x, \quad (2.40)$$

$$K_{\zeta\zeta} = K_x(\sin\theta_x \sin\theta_z + \cos\theta_x \cos\theta_z \sin\theta_y)^2 + K_y(\cos\theta_x \sin\theta_y \sin\theta_z - \cos\theta_z \sin\theta_x)^2$$
$$+K_z \cos^2\theta_x \cos^2\theta_y. \quad (2.41)$$

For further derivation details, see Appendix A.

2.4.1.2. Angle Rotation About a Secondary Axis

The two rotation method uses a rotation about the y-axis followed by a rotation about the z-axis to align the x-axis of the principal permeability directions with the wellbore, β. This was performed using Euler's rotation theorem. See Appendix B for further details.

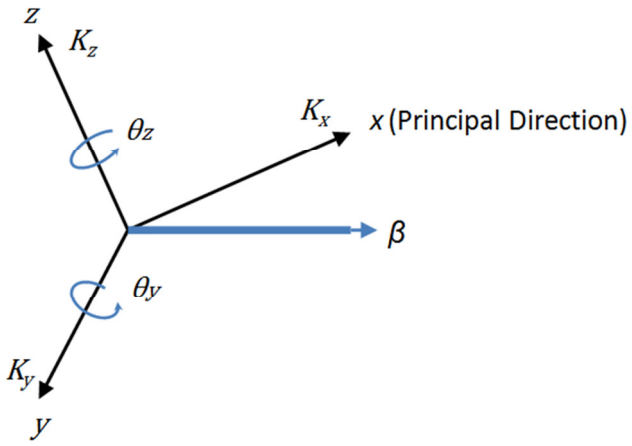

Figure 2-15: Coordinate System Rotation so the x-axis Aligns with the Wellbore (β) using two Axis Rotations

Figure 2-14 depicts the axis representing the principal permeability in the x, y and z direction. In order to align the x-axis with the wellbore, rotations about the y-axis and z-axis are performed. The mathematics for this method follows the same concept as the directional cosine method.

A three dimensional rotated coordinate system is given by a matrix R. In this two rotation method R equals,

$$R = R_y(\theta_y) \cdot R_z(\theta_z) \tag{2.42}$$

with coordinate system rotations of the y and z-axis in the counterclockwise direction when looking towards the origin, give the matrices

$$R_y(\theta_y) = \begin{bmatrix} \cos\theta_y & 0 & -\sin\theta_y \\ 0 & 1 & 0 \\ \sin\theta_y & 0 & \cos\theta_y \end{bmatrix}, \tag{2.43}$$

$$R_z(\theta_z) = \begin{bmatrix} \cos\theta_z & \sin\theta_z & 0 \\ -\sin\theta_z & \cos\theta_z & 0 \\ 0 & 0 & 1 \end{bmatrix}. \tag{2.44}$$

After matrix multiplication, R equals,

$$R = \begin{bmatrix} \cos\theta_y \cos\theta_z & \cos\theta_y \sin\theta_z & -\sin\theta_y \\ -\sin\theta_z & \cos\theta_z & 0 \\ \cos\theta_z \sin\theta_y & \sin\theta_z \sin\theta_y & \cos\theta_y \end{bmatrix}. \tag{2.45}$$

This rotation method give the permeability tensor with the following terms,

$$K_{\beta\beta} = K_x(\cos\theta_y \cos\theta_z)^2 + K_y(\cos\theta_y \sin\theta_z)^2 + K_z \sin\theta_y^2 , \tag{2.46}$$

$$K_{\beta\xi} = -K_x \cos\theta_y \cos\theta_z \sin\theta_z + K_y \cos\theta_y \cos\theta_z \sin\theta_z , \tag{2.47}$$

$$K_{\beta\zeta} = K_x \cos\theta_y \cos\theta_z^2 \sin\theta_y + K_y \cos\theta_y \sin\theta_y \sin\theta_z^2 - K_z \cos\theta_y \sin\theta_y , \tag{2.48}$$

$$K_{\xi\beta} = -K_x \cos\theta_y \cos\theta_z \sin\theta_z + K_y \cos\theta_y \cos\theta_z \sin\theta_z \,, \tag{2.49}$$

$$K_{\xi\xi} = K_x \sin\theta_z^2 + K_y \cos\theta_z^2 \,, \tag{2.50}$$

$$K_{\xi\zeta} = -K_x \cos\theta_z \sin\theta_y \sin\theta_z + K_y \cos\theta_z \sin\theta_y \sin\theta_z \,, \tag{2.51}$$

$$K_{\zeta\beta} = K_x \cos\theta_y \cos\theta_z^2 \sin\theta_y + K_y \cos\theta_y \sin\theta_y \sin\theta_z^2 - K_z \cos\theta_y \sin\theta_y \,, \tag{2.52}$$

$$K_{\zeta\xi} = -K_x \cos\theta_z \sin\theta_y \sin\theta_z + K_y \cos\theta_z \sin\theta_y \sin\theta_z \,, \tag{2.53}$$

$$K_{\zeta\zeta} = K_x(\cos\theta_z \sin\theta_y)^2 + K_y(\sin\theta_y \sin\theta_z)^2 + K_z \cos\theta_y^2 \,. \tag{2.54}$$

2.4.2. Mathematically Modeling the Permeability Tensor

As we have discussed above, when permeability varies in different directions a tensor is required to describe the material's permeability.

Two dimensional permeability tensor models have been used and tested with the cross terms in the matrix having non-zero terms (Leung 1986). Examples are shown with the X-Y local

coordinate axes of the reservoir set up such that they are aligned with the principal permeability axes of the reservoir, but are offset at an angle from the global x-y coordinate. This will be the basis for my three dimensional permeability tensor having rotation around the x, y & z axis.

Chapter 3 Mathematical Modeling

Three different reservoir models, all having the same total volume, were used to test the effects of rotating the permeability tensor to align with the wellpath that is not parallel to either the x-, y- or z-axis. The first is using a single reservoir grid block, Figures 3-1 to 3-10. Second is a 5x5x5 (5 blocks in the x-direction, 5 blocks in the y-direction and 5 blocks in the z-direction) reservoir, Figures 3-11 to 3-29. Finally is the 10x10x10 reservoir, which are represented in Figures 3-30 to 3-48. The grid blocks in all three reservoirs had different sizes that when combined equalled 50 x 50 x 50 ft^3. The different number of blocks in each reservoir model will determine if increasing the grid refinement also increases the error in oil production rates between the full permeability tensor and the diagonal tensor cases. Ideally, we would use even more grid blocks. However, this turned out to be impracticable due to large CPU times, and the grid sizes chosen for this study do indeed reflect the grid size dependency correctly. Every simulation had a specific code wrote for it and was ran using Eclipse E300 on a computer with a Intel® Core™ i5-4570 CPU @ 3.20 GHz processor with 8.00 GB of RAM.

The wellbore was rotated about the y-axis which would account for a downward slope in the well. The z-axis rotation was used when the well was not along the x-axis. The rotations used in the test simulations were counterclockwise rotations in the y-axis being 0°, 343° and 320°, and counterclockwise rotations in the z-axis of 0°, 22° and 45°. These rotations give the full range of

possible wellbore rotation. This can be seen in Figure 2-12 of the directional cosines section, 2.4.1.1.

The permeability of the reservoir simulation grid was 200 milliDarcy (mD) in the x- and y-direction and 64 milliDarcy (mD) in the z-direction. These values were taken as average values in the E-Segment of the Norne Field from publically available data (Statoil 2001). Also taken from (Statoil 2001) was the porosity in the reservoir simulation grid, 25%.

Table 3-1 below is the simulation matrix followed to test the effects of rotating the permeability tensor. A total of 36 reservoir simulations were performed.

The first rotated permeability tensor tests were performed on a single reservoir simulation block, with the x-, y- and z-direction all having a length of 50 feet. This size of block was not the same as used for the 5x5x5 reservoir (10 feet) and the 10x10x10 reservoir (5 feet).

The oil production rate for each run were obtained, for both the full permeability tensor and the diagonal permeability tensor cases, from the use of the Eclipse E300 reservoir simulator. These results will be used for comparison to find differences between the rotated and base case.

Table 3-1: Reservoir Simulation Matrix

Run	Number of Blocks	Rotation (Degrees) about y-axis	Rotation (Degrees) about z-axis	PERMX (mD)	PERMY (mD)	PERMZ (mD)
1	1	0	0	200	200	64
2	1	0	22	200	200	64
3	1	0	45	200	200	64
4	1	343	0	200	200	64
5	1	343	22	200	200	64
6	1	343	45	200	200	64
7	1	320	0	200	200	64
8	1	320	22	200	200	64
9	1	320	45	200	200	64
10	5x5x5 = 125	0	0	200	200	64
11	5x5x5 = 125	0	22	200	200	64
12	5x5x5 = 125	0	45	200	200	64
13	5x5x5 = 125	343	0	200	200	64
14	5x5x5 = 125	343	22	200	200	64
15	5x5x5 = 125	343	45	200	200	64
16	5x5x5 = 125	320	0	200	200	64
17	5x5x5 = 125	320	22	200	200	64
18	5x5x5 = 125	320	45	200	200	64
19	5x5x5 = 125	0	0	200	150	64
20	5x5x5 = 125	0	22	200	150	64
21	5x5x5 = 125	0	45	200	150	64
22	5x5x5 = 125	343	0	200	150	64
23	5x5x5 = 125	343	22	200	150	64
24	5x5x5 = 125	343	45	200	150	64
25	5x5x5 = 125	320	0	200	150	64
26	5x5x5 = 125	320	22	200	150	64
27	5x5x5 = 125	320	45	200	150	64
28	10x10x10= 1000	0	0	200	200	64
29	10x10x10= 1000	0	22	200	200	64
30	10x10x10= 1000	0	45	200	200	64
31	10x10x10= 1000	343	0	200	200	64
32	10x10x10= 1000	343	22	200	200	64
33	10x10x10= 1000	343	45	200	200	64
34	10x10x10= 1000	320	0	200	200	64
35	10x10x10= 1000	320	22	200	200	64
36	10x10x10= 1000	320	45	200	200	64

3.1. Wellpath Modeling in Single Block Reservoir

The wellpath in the simulator can penetrate the block straight through the center in either the x-, y-, or z-direction. The full length of the well is perforated. For the unrotated single block simulation, the well was in the x-direction, shown in Figure 3-1. This meant that when rotating the permeability tensor to align with the wellpath in Runs 1 to 9, the tensor was rotated from the x-axis. The results from Runs 1 to 9 were then compared to the results of the unrotated simulation.

Prior to running the Eclipse simulations, Petrel was used to develop the actual wellpath used for simulation. The Petrel wellpath in the following figures show what the traditional reservoir simulation use for the wellpath. Comparing these to the rotated permeability tensor wellpath, also shown in the figures, indicate that there is a difference depending on which approach used in the reservoir simulation.

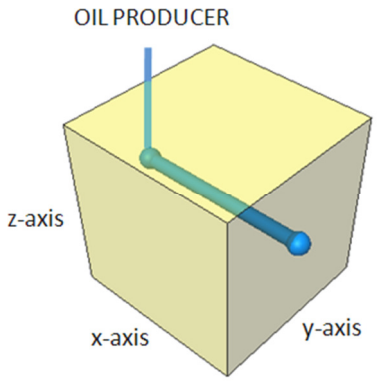

Figure 3-1: Petrel Wellpath for Single Block

Runs 1-9 had the rotated permeability tensor rotated to match the wellpaths displayed in Figures 3-2 to 3-10. Figure 3-1 shows zero rotation about the y- or z-axis. In the simulation code, for this case a full tensor was used while in the unrotated case a diagonal tensor was used. If the oil production results are identical it will prove there is no error in the simulator, as was discussed in Section 2.2.

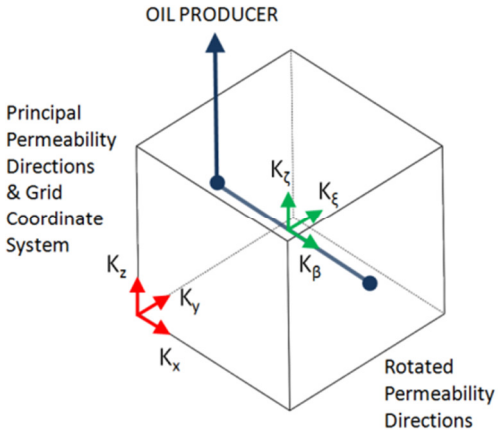

Figure 3-2: Mathematical Wellpath for Run 1 (0° about y-axis and 0° about z-axis; K_x = 200mD, K_y = 200mD and K_z = 64mD)

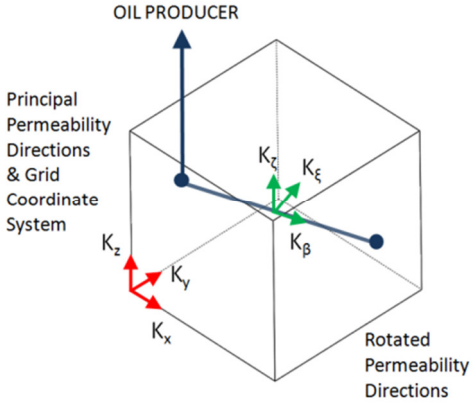

Figure 3-3: Mathematical Wellpath for Run 2 (0° about y-axis and 22° about z-axis; K_x = 200mD, K_y = 200mD and K_z = 64mD)

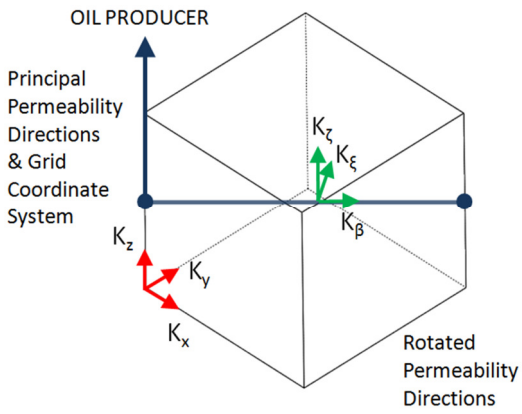

Figure 3-4: Mathematical Wellpath for Run 3 (0° about y-axis and 45° about z-axis;

K_x = 200mD, K_y = 200mD and K_z = 64mD)

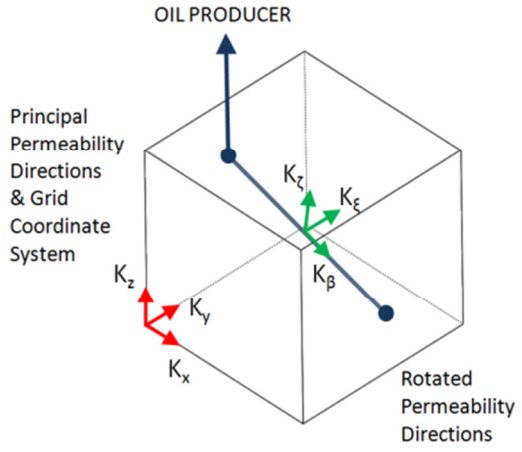

Figure 3-5: Mathematical Wellpath for Run 4 (343° about y-axis and 0° about z-axis;

K_x = 200mD, K_y = 200mD and K_z = 64mD)

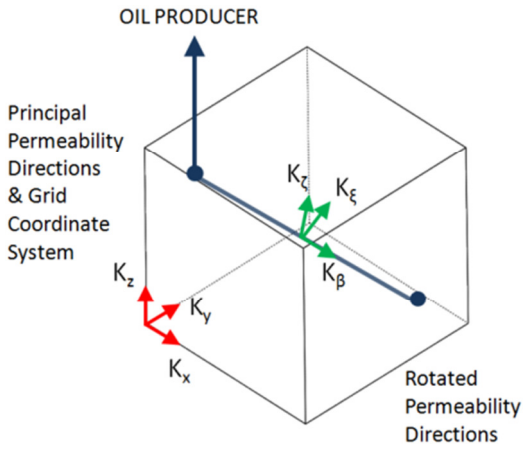

Figure 3-6: Mathematical Wellpath for Run 5 (343° about y-axis and 22° about z-axis;

K_x = 200mD, K_y = 200mD and K_z = 64mD)

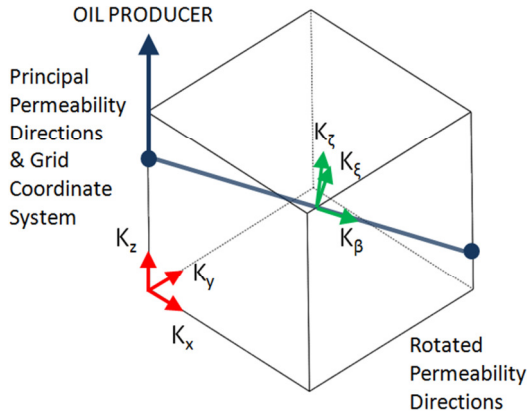

Figure 3-7: Mathematical Wellpath for Run 6 (343° about y-axis and 45° about z-axis;

K_x = 200mD, K_y = 200mD and K_z = 64mD)

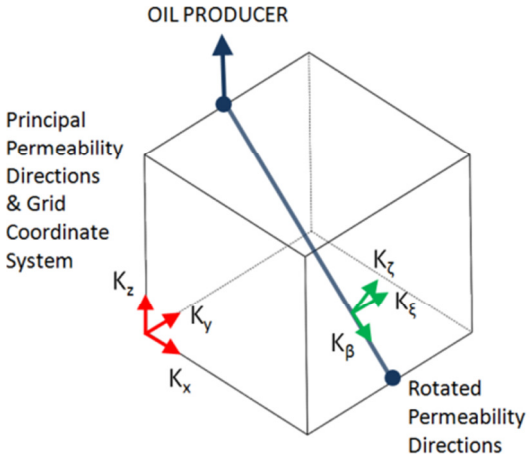

Figure 3-8: Mathematical Wellpath for Run 7 (320° about y-axis and 0° about z-axis;

K_x = 200mD, K_y = 200mD and K_z = 64mD)

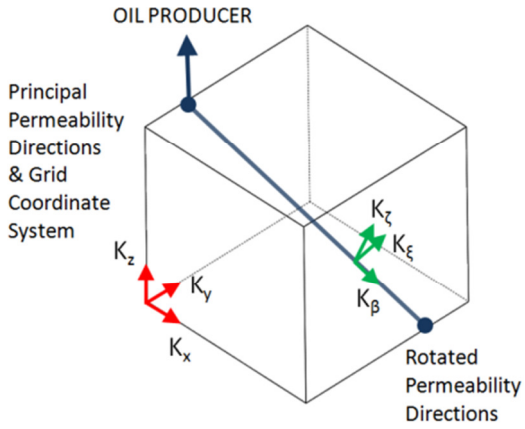

Figure 3-9: Mathematical Wellpath for Run 8 (320° about y-axis and 22° about z-axis;

K_x = 200mD, K_y = 200mD and K_z = 64mD)

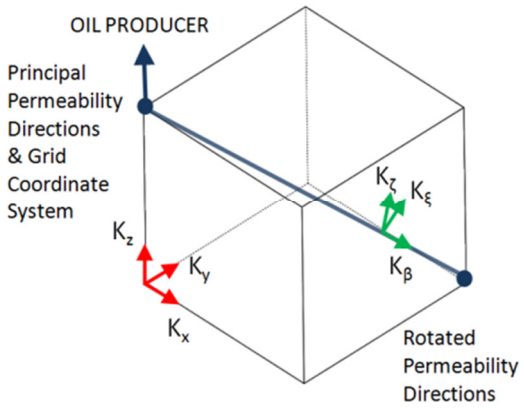

Figure 3-10: Mathematical Wellpath for Run 9 (320° about y-axis and 45° about z-axis;

K_x = 200mD, K_y = 200mD and K_z = 64mD)

3.2. Wellpath Modeling in 5x5x5 Block Reserovir

For the 5x5x5 reservoir grid (Runs 10 to 27 in Table 3-1) there is not just one unrotated case used to compare the other 9 Runs. Instead, each Run (Figures 3-12 to 3-29) have their own unrotated case used for comparison. This happens because the well will follow a different path depending on the set of rotations used in the Run. For instance, the well path for Run 10's unrotated case penetrate blocks (1,3,3), (2,3,3), (3,3,3), (4,3,3) and (5,3,3), while Run 11's unrotated cases has the well going through (1,2,3), (2,3,3), (3,3,3), (4,3,3) and (5,4,3).

Run 10's rotated and unrotated cases follow the exact path because the rotation about the y- and z-axis are both zero. A diagonal tensor was used in the unrotated code and a full tensor in the rotated code. This will indicate the size of the error made in the simulation when ignoring off diagonal elements, as discussed in section 2.2.

Figures 3-12 to 3-29 show the mathematical representation of the wellpath after tensor rotation and the Petrel wellpath for Runs 10 - 18. In Petrel the wellpath only connects the center points of the blocks with wells. It does not show the direction the well is traveling in each block. The direction in each block should be straight through the center of the block and in the x-direction. This can be seen in the simulation code, Appendix C, under COMPDAT.

A Cartesian coordinate system is used to create the well path in the reservoir. For example, the position (2,3,4) would represent 2 blocks in the x-direction, 3 blocks in the y-direction and 4 blocks in the z-direction. Figures 3-11 represents the reference grids for the 5x5x5 block reservoir. Each of these blocks are 10 feet in each direction, totalling the same volume as the single block reservoir.

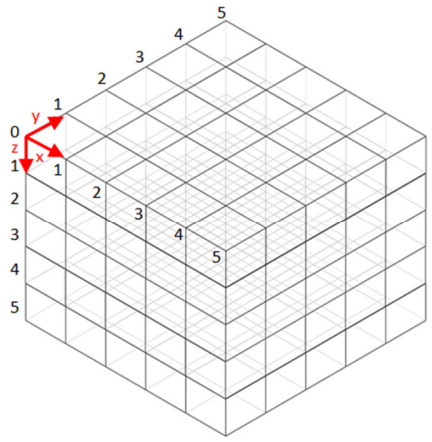

Figure 3-11: 5x5x5 Reservoir Reference Grid

In the 5x5x5 block cases each Run had their own unrotated case to be compared to. In each case the well path would follow through a different set of blocks. For example, Run 10 unrotated case, the well goes through blocks (1,3,3), (2,3,3), (3,3,3), (4,3,3) and (5,3,3), with the well travelling in the x-direction within each block. Run 11 unrotated case travels in blocks (1,2,3), (2,3,3), (3,3,3), (4,3,3) and (5,4,3), which is slightly different from Run 10 because the well is rotated 22 degrees about the z-axis.

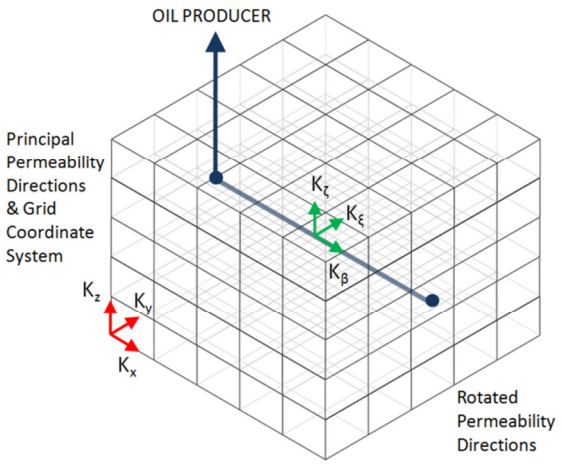

Figure 3-12: Mathematical Wellpath for Run 10 (0° about y-axis and 0° about z-axis; K_x = 200mD, K_y = 200mD and K_z = 64mD)

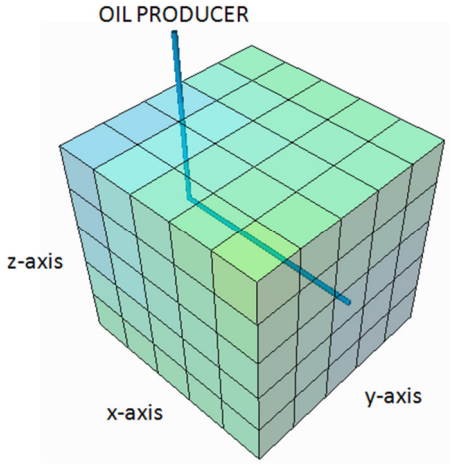

Figure 3-13: Petrel Wellpath for Run 10 (0° about y-axis and 0° about z-axis; K_x = 200mD, K_y = 200mD and K_z = 64mD)

Run 10, Figure 3-12 and 3-13, shows a 0° rotation about both the y- and z-axis. Both the mathematical wellpath and the Petrel wellpath figures are very similar. The wellpath travelled in the reservoir simulation code is (1,3,3), (2,3,3), (3,3,3), (4,3,3) and (5,3,3).

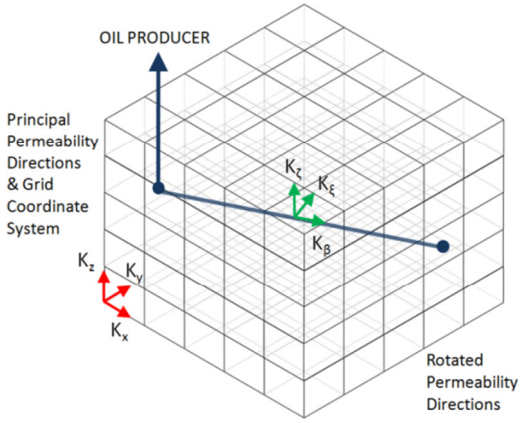

Figure 3-14: Mathematical Wellpath for Run 11 (0° about y-axis and 22° about z-axis; K_x = 200mD, K_y = 200mD and K_z = 64mD)

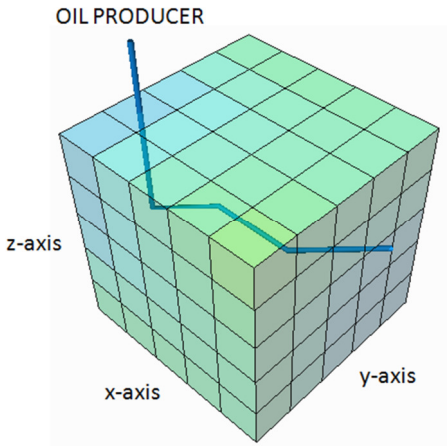

Figure 3-15: Petrel Wellpath for Run 11 (0° about y-axis and 22° about z-axis; K_x = 200mD, K_y = 200mD and K_z = 64mD)

Figures 3-14 and 3-15 depict the mathematical and Petrel wellpaths for Run 11, respectively. The Petrel model shows an irregular wellpath compared to the mathematical model. In Petrel, the wellpath is represented by connecting the center point of each block which the wellpath

passes through. In the reservoir code created for this model the well travels in the x-direction within each cell and passes through cells (1,2,3), (2,3,3), (3,3,3), (4,3,3) and (5,4,3).

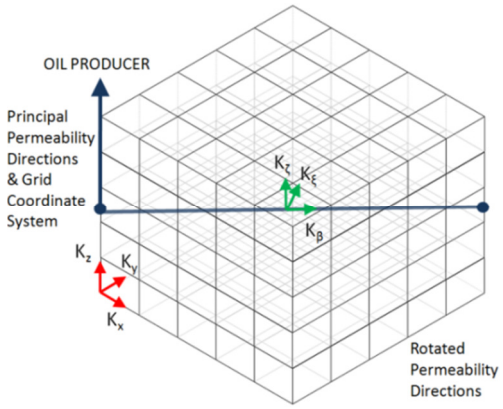

Figure 3-16: Mathematical Wellpath for Run 12 (0° about y-axis and 45° about z-axis; K_x = 200mD, K_y = 200mD and K_z = 64mD)

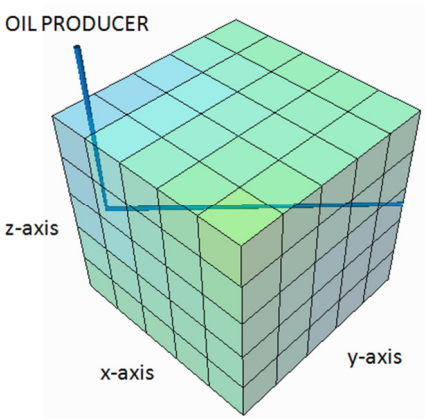

Figure 3-17: Petrel Wellpath for Run 12 (0° about y-axis and 45° about z-axis; K_x = 200mD, K_y = 200mD and K_z = 64mD)

The reservoir simulation code for Run 12 passes through blocks (1,1,3), (2,2,3), (3,3,3), (4,4,3) and (5,5,3), all in the x-direction. In the Petrel model the well starts at the center of block

(1,1,3) rather than at the edge. This is due to Petrel connecting center points to depict their wellpaths.

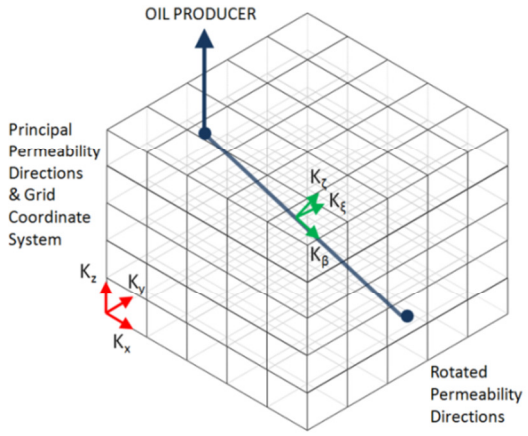

Figure 3-18: Mathematical Wellpath for Run 13 (343° about y-axis and 0° about z-axis; K_x = 200mD, K_y = 200mD and K_z = 64mD)

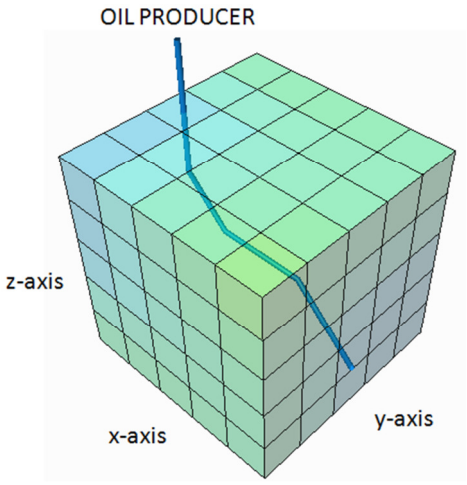

Figure 3-19: Petrel Wellpath for Run 13 (343° about y-axis and 0° about z-axis; K_x = 200mD, K_y = 200mD and K_z = 64mD)

A jagged wellpath is noticed again in the Petrel model for Run 13. The simulation code wellpath for Run 13 is (1,3,2), (2,3,3), (3,3,3), (4,3,3) and (5,3,4).

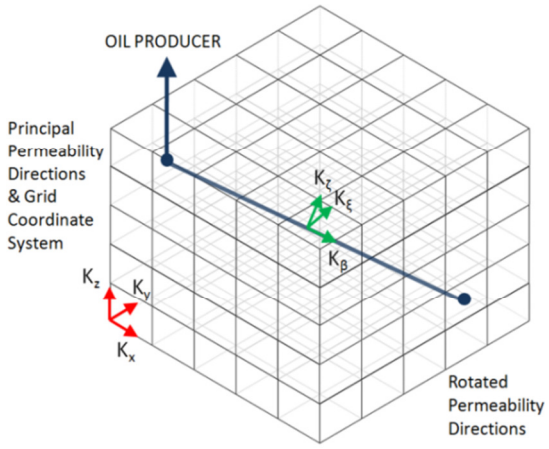

Figure 3-20: Mathematical Wellpath for Run 14 (343° about y-axis and 22° about z-axis; K_x = 200mD, K_y = 200mD and K_z = 64mD)

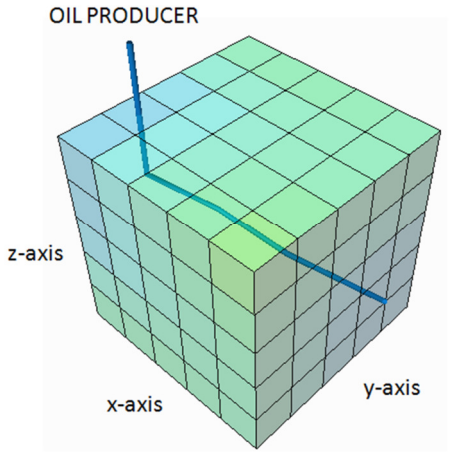

Figure 3-21: Petrel Wellpath for Run 14 (343° about y-axis and 22° about z-axis; K_x = 200mD, K_y = 200mD and K_z = 64mD)

Figure 3-20 and 3-21 show both the mathematical and Petrel wellpaths for Run 14. Blocks (1,2,2), (2,3,3), (3,3,3), (4,3,3) and (5,4,4) were used in the reservoir coded to model the wellpath.

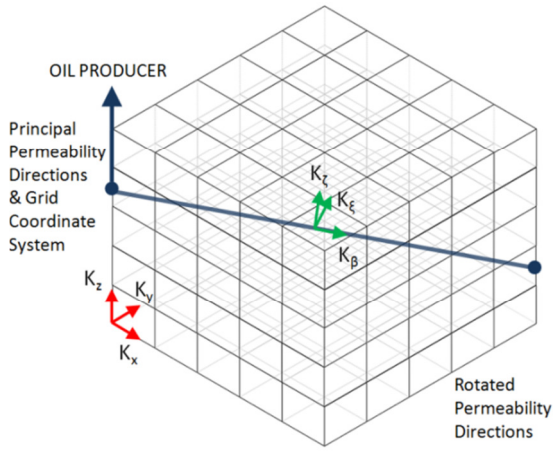

Figure 3-22: Mathematical Wellpath for Run 15 (343° about y-axis and 45° about z-axis; K_x = 200mD, K_y = 200mD and K_z = 64mD)

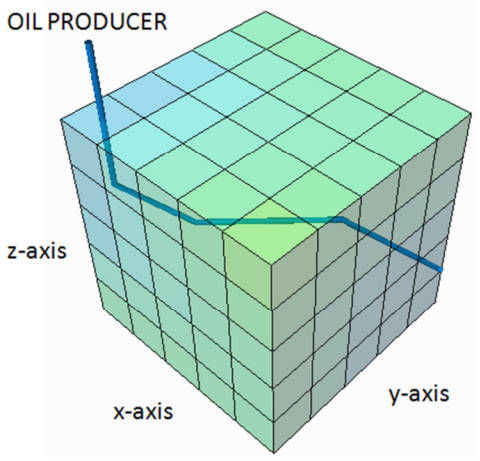

Figure 3-23: Petrel Wellpath for Run 15 (343° about y-axis and 45° about z-axis; K_x = 200mD, K_y = 200mD and K_z = 64mD)

For Run 15 a jagged wellpath is noticed again in the Petrel model. The simulation code wellpath for Run 15 is (1,1,2), (2,2,3), (3,3,3), (4,4,3) and (5,5,4).

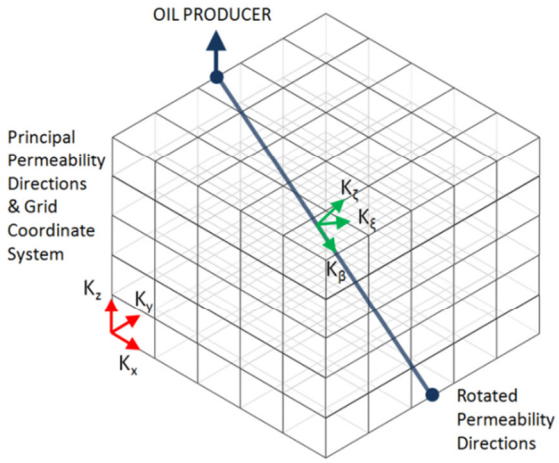

Figure 3-24: Mathematical Wellpath for Run 16 (320° about y-axis and 0° about z-axis; K_x = 200mD, K_y = 200mD and K_z = 64mD)

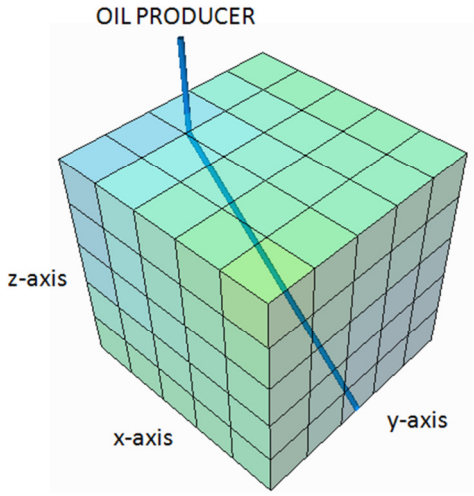

Figure 3-25: Petrel Wellpath for Run 16 (320° about y-axis and 0° about z-axis; K_x = 200mD, K_y = 200mD and K_z = 64mD)

The reservoir simulation code for Run 16 passes through blocks (1,3,1), (2,3,2), (3,3,3), (4,3,4) and (5,3,5), all in the x-direction.

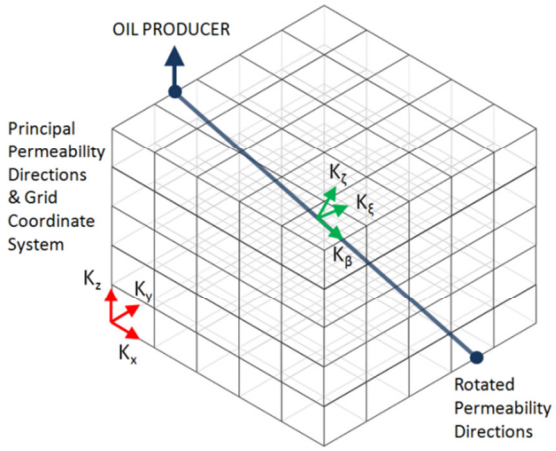

Figure 3-26: Mathematical Wellpath for Run 17 (320° about y-axis and 22° about z-axis; K_x = 200mD, K_y = 200mD and K_z = 64mD)

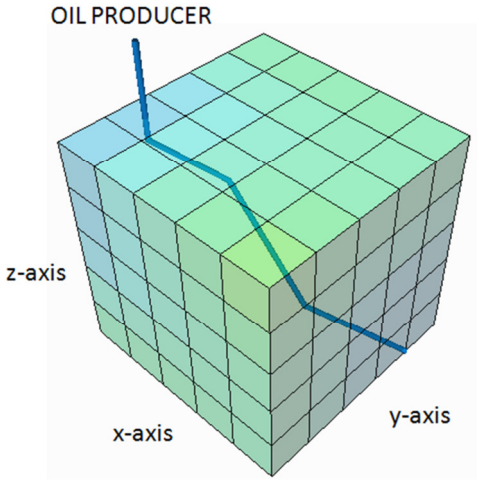

Figure 3-27: Petrel Wellpath for Run 17 (320° about y-axis and 45° about z-axis; K_x = 200mD, K_y = 200mD and K_z = 64mD)

Figures 3-26 and 3-27 are the mathematical wellpath and the Petrel wellpath, respectively, for Run 17. The blocks the wellpath passes through in the code are (1,2,1), (2,3,2), (3,3,3), (4,3,4) and (5,4,5).

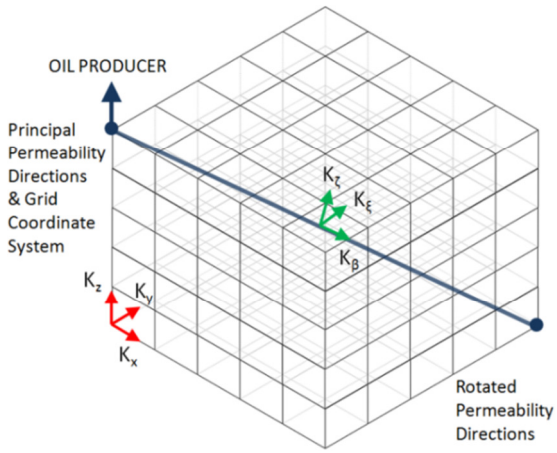

Figure 3-28: Mathematical Wellpath for Run 18 (320° about y-axis and 45° about z-axis; K_x = 200mD, K_y = 200mD and K_z = 64mD)

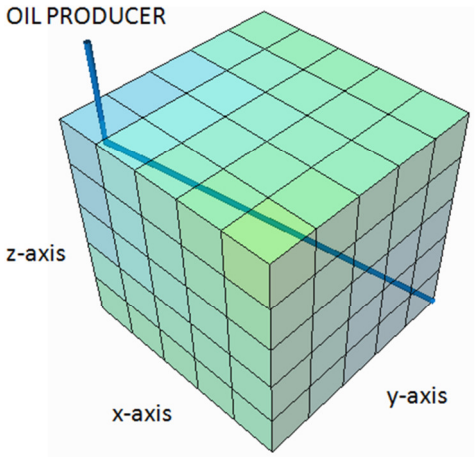

Figure 3-29: Petrel Wellpath for Run 18 (320° about y-axis and 45° about z-axis; K_x = 200mD, K_y = 200mD and K_z = 64mD)

Finally, Figure 3-28 and 3-29 show the wellpaths for Run 18. In the reservoir code the wellpath passes through blocks (1,1,1), (2,2,2), (3,3,3), (4,4,4) and (5,5,5).

Runs 19 - 27 use the 5x5x5 blocks but have the permeability in the x- and y-direction not equal. The principal permeability in the x-direction is still equal to 200 mD, but the principal permeability in the y-direction is changed to 150 mD. This was done in order to see if having a different x and y permeability had an effect on the oil production difference. The wellpath for these Runs are the same as Runs 10-18.

3.3. Wellpath Modeling in 10x10x10 Block Reserovir

Finally, the 10x10x10 reservoir will test the effects of rotating the permeability tensor. This number of reservoir simulation grid blocks has created a more complex well path to follow and is shown in the Figures 3-31 to 3-48.

Once again a Cartesian coordinate system is used to create the well path. Figure 3-30 demonstrates the coordinate system used in the 10x10x10 reservoir. The block sizes now are 5 feet in each direction, totalling the same volume as the single block reservoir and the 5x5x5 block reservoir.

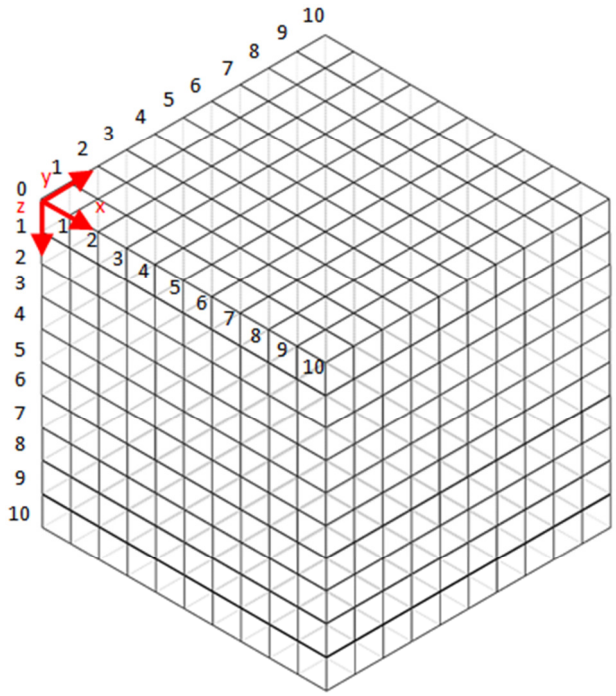

Figure 3-30: 10x10x10 Reservoir Reference Grid

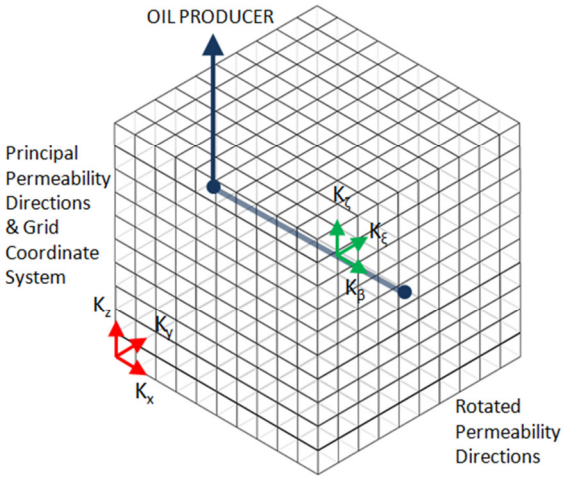

Figure 3-31: Mathematical Wellpath for Run 28 (0° about y-axis and 0° about z-axis; K_x = 200mD, K_y = 200mD and K_z = 64mD)

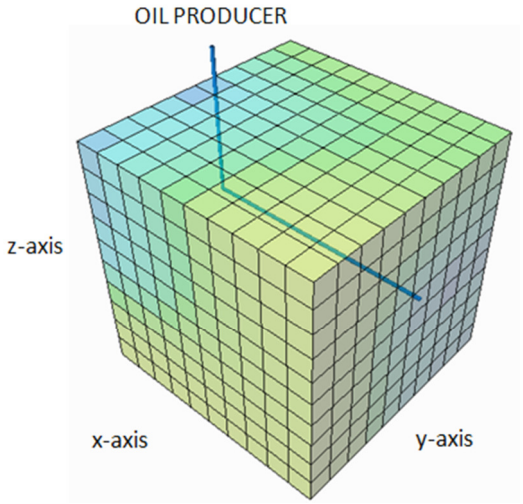

Figure 3-32: Petrel Wellpath for Run 28 (0° about y-axis and 0° about z-axis; K_x = 200mD, K_y = 200mD and K_z = 64mD)

Run 28, Figured 3-31 and 3-32, shows a 0° rotation about both the y- and z-axis. Both the mathematical wellpath and the Petrel wellpath figures are very similar. The wellpath travelled

in the reservoir simulation code is (1,5,5), (2,5,5), (3,5,5), (4,5,5), (5,5,5), (6,5,5), (7,5,5), (8,5,5), (9,5,5) and (10,5,5).

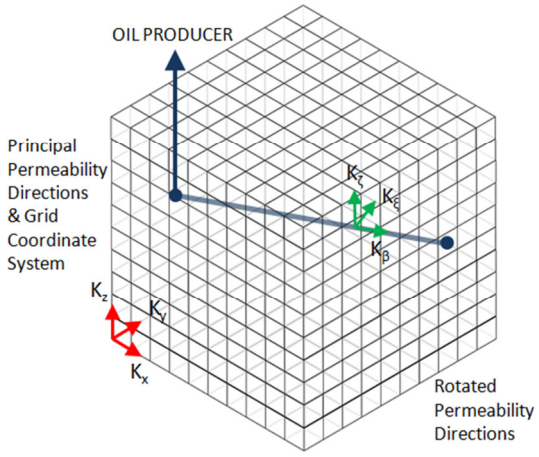

Figure 3-33: Mathematical Wellpath for Run 29 (0° about y-axis and 22° about z-axis; K_x = 200mD, K_y = 200mD and K_z = 64mD)

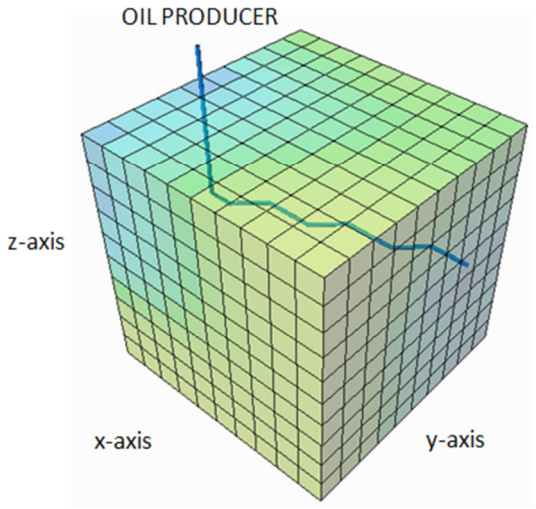

Figure 3-34: Petrel Wellpath for Run 29 (0° about y-axis and 22° about z-axis; K_x = 200mD, K_y = 200mD and K_z = 64mD)

Figures 3-33 and 3-34 depict the mathematical and Petrel wellpaths for Run 29, respectively. The blocks the wells pass through are (1,3,5), (2,3,5), (3,4,5), (4,4,5), (5,4,5), (6,5,5), (7,5,5),

(8,5,5), (9,6,5) and (10,6,5). Similar to the 5x5x5 reservoir model, the Petrel model shows an irregular wellpath compared to the mathematical model.

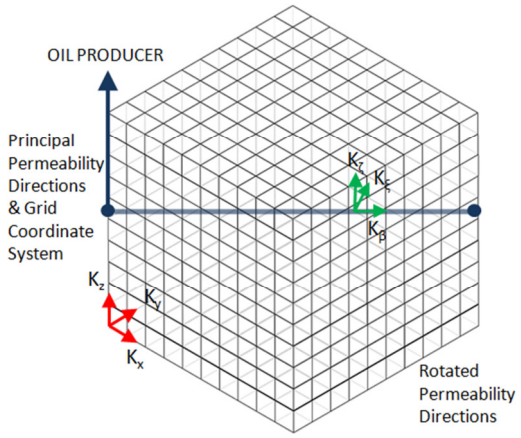

Figure 3-35: Mathematical Wellpath for Run 30 (0° about y-axis and 45° about z-axis; K_x = 200mD, K_y = 200mD and K_z = 64mD)

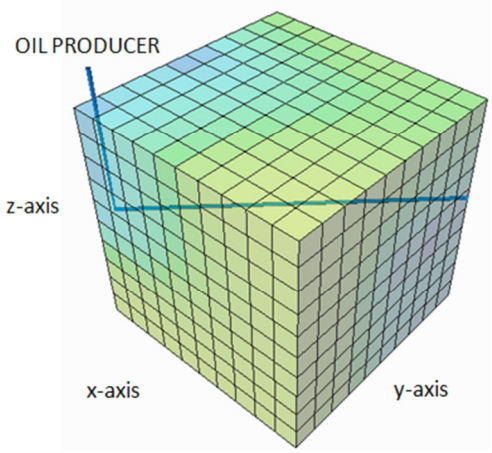

Figure 3-36: Petrel Wellpath for Run 30 (0° about y-axis and 45° about z-axis; K_x = 200mD, K_y = 200mD and K_z = 64mD)

The reservoir simulation code for Run 30 passes through blocks (1,1,5), (2,2,5), (3,3,5), (4,4,5), (5,5,5) (6,6,5), (7,7,5), (8,8,5), (9,9,5) and (10,10,5) all in the x-direction. In the Petrel model,

again the well starts at the center of block (1,1,5) rather than at the edge. This is due to Petrel connecting center points to depict their wellpaths.

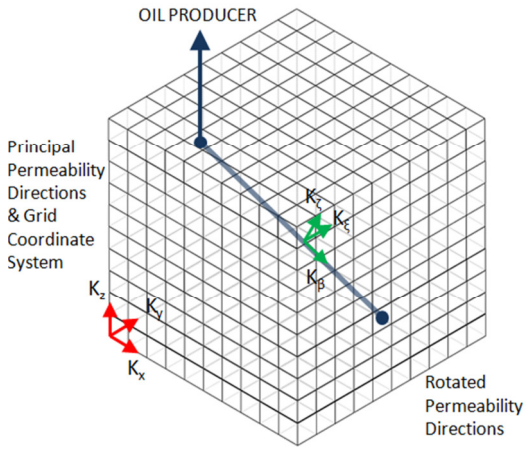

Figure 3-37: Mathematical Wellpath for Run 31 (343° about y-axis and 0° about z-axis; K_x = 200mD, K_y = 200mD and K_z = 64mD)

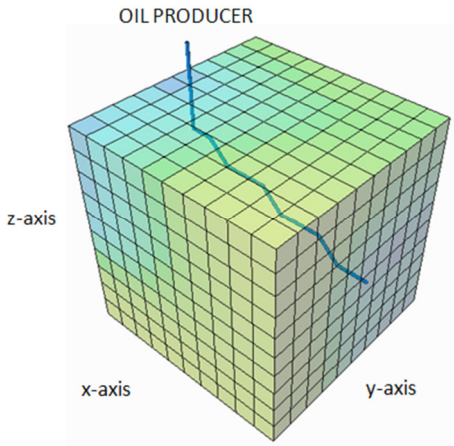

Figure 3-38: Petrel Wellpath for Run 31 (343° about y-axis and 0° about z-axis; K_x = 200mD, K_y = 200mD and K_z = 64mD)

A jagged wellpath is noticed again in the Petrel model for Run 31. The simulation code wellpath for Run 31 is (1,5,3), (2,5,3), (3,5,4), (4,5,4), (5,3,4), (6,5,5), (7,5,5), (8,5,5), (9,5,6) and (10,6,6).

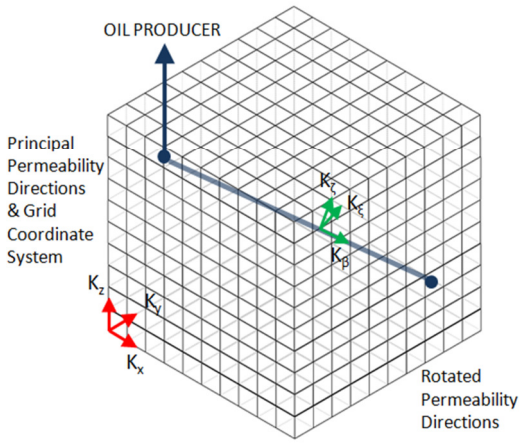

Figure 3-39: Mathematical Wellpath for Run 32 (343° about y-axis and 22° about z-axis; K_x = 200mD, K_y = 200mD and K_z = 64mD)

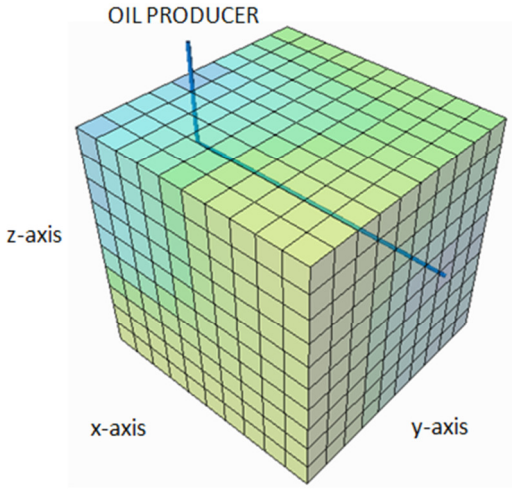

Figure 3-40: Petrel Wellpath for Run 32 (343° about y-axis and 22° about z-axis; K_x = 200mD, K_y = 200mD and K_z = 64mD)

Figure 3-39 and 3-40 show both the mathematical and Petrel wellpaths for Run 32. Blocks (1,3,3), (2,3,3), (3,4,4), (4,4,4), (5,4,4), (6,5,5), (7,5,5), (8,5,5), (9,6,6) and (10,6,6) were used in the reservoir coded to model the wellpath

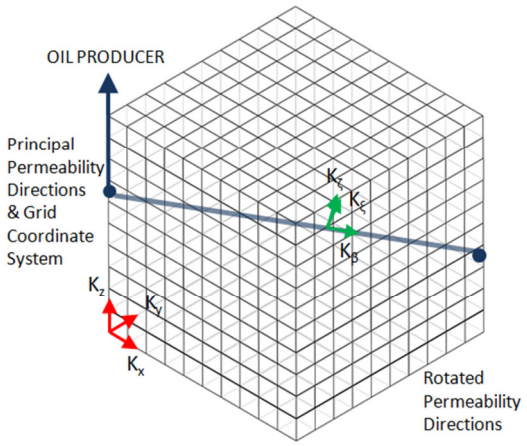

Figure 3-41: Mathematical Wellpath for Run 33 (343° about y-axis and 45° about z-axis; K_x = 200mD, K_y = 200mD and K_z = 64mD)

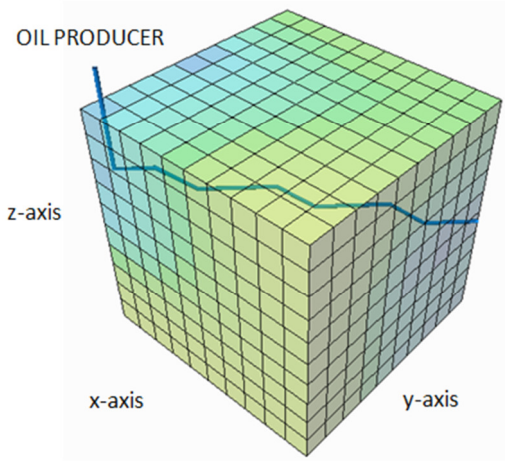

Figure 3-42: Petrel Wellpath for Run 33 (343° about y-axis and 45° about z-axis; K_x = 200mD, K_y = 200mD and K_z = 64mD)

For Run 33 an irregular wellpath is noticed again in the Petrel model. The simulation code wellpath for Run 33 is (1,1,3), (2,2,4), (3,3,4), (4,4,4), (5,5,4), (6,6,5), (7,7,5), (8,8,5), (9,9,6) and (10,10,6).

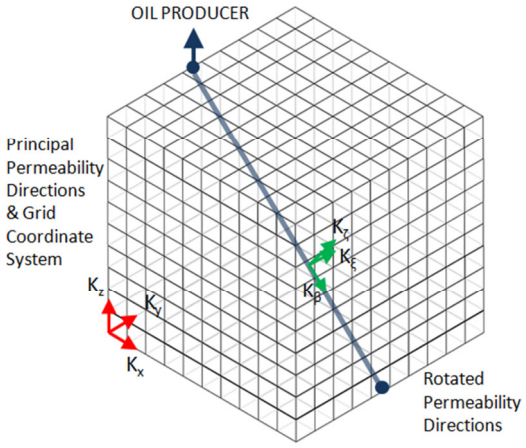

Figure 3-43: Mathematical Wellpath for Run 34 (320° about y-axis and 0° about z-axis; K_x = 200mD, K_y = 200mD and K_z = 64mD)

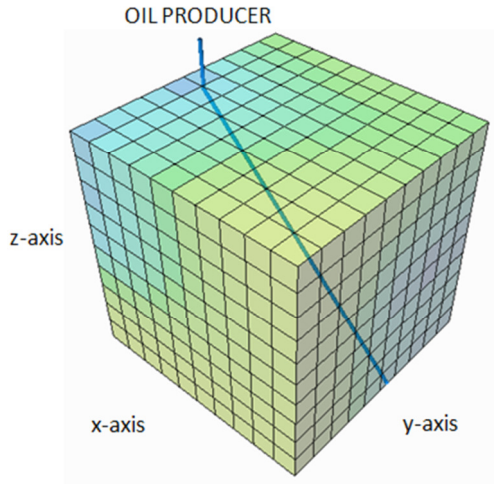

Figure 3-44: Petrel Wellpath for Run 34 (320° about y-axis and 0° about z-axis; K_x = 200mD, K_y = 200mD and K_z = 64mD)

The reservoir simulation code for Run 34 passes through blocks (1,5,1), (2,5,2), (3,5,3), (4,5,4), (5,5,5), (6,5,6), (7,5,7), (8,5,8), (9,5,9) and (10,5,10), all in the x-direction.

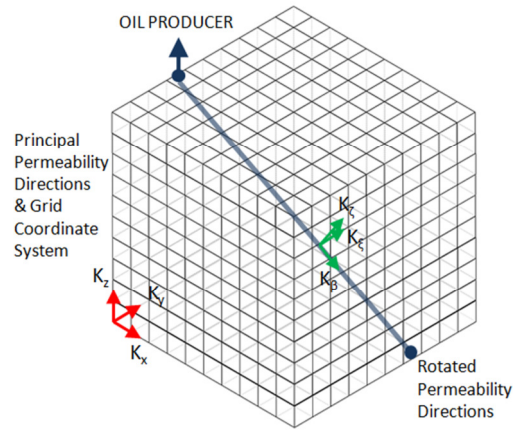

Figure 3-45: Mathematical Wellpath for Run 35 (320° about y-axis and 22° about z-axis; K_x = 200mD, K_y = 200mD and K_z = 64mD)

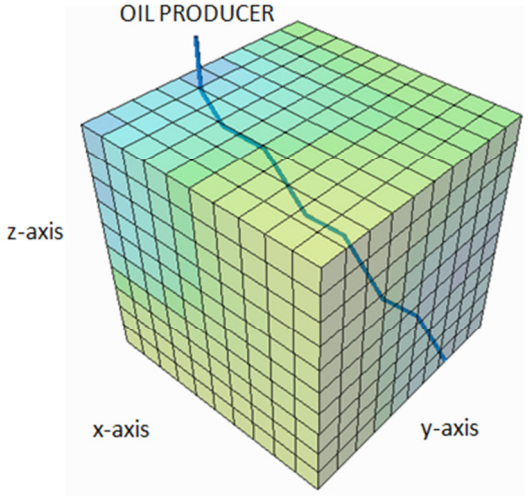

Figure 3-46: Petrel Wellpath for Run 35 (320° about y-axis and 22° about z-axis; K_x = 200mD, K_y = 200mD and K_z = 64mD)

Figures 3-45 and 3-46 are the mathematical wellpath and the Petrel wellpath, respectively, for Run 35. The blocks the wellpath passes through in the code are (1,3,1), (2,3,2), (3,4,3), (4,4,4), (5,4,5), (6,5,6), (7,5,7), (8,5,8), (9,6,9) and (10,6,10).

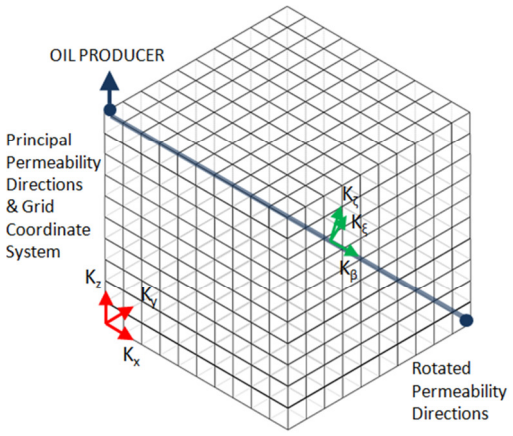

Figure 3-47: Mathematical Wellpath for Run 36 (320° about y-axis and 45° about z-axis; K_x = 200mD, K_y = 200mD and K_z = 64mD)

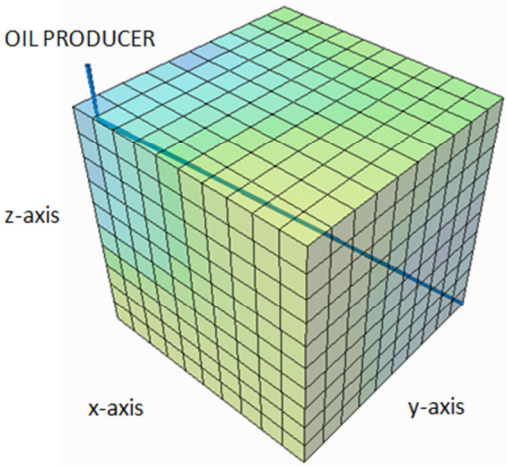

Figure 3-48: Petrel Wellpath for Run 36 (320° about y-axis and 45° about z-axis; K_x = 200mD, K_y = 200mD and K_z = 64mD)

Finally, Figure 3-47 and 3-48 show the wellpaths for Run 36. In the reservoir code the wellpath passes through blocks (1,1,1), (2,2,2), (3,3,3), (4,4,4), (5,5,5), (6,6,6), (7,7,7), (8,8,8), (9,9,9) and (10,10,10).

Once again in the 10x10x10 reservoir Runs (28-36), each Run had their own corresponding unrotated case. The wellpath's for this reservoir followed the same idea as the 5x5x5 reservoir.

The reservoir code was created to Run in a compositional simulator, Eclipse 300. Sample codes for both an unrotated and rotated case are given for the one block, the 5x5x5 reservoir and the 10x10x10 reservoir in the Appendix C.

The only sections of the code that change are DIMENS, DXV, DYV, DZV, and TSTEP, depending on the reservoir size. The keywords PERMX, PERMY, PERMZ, PERMXY, PERMXZ, PERMYZ, WELLSPECS and COMPDAT change depending on the Run. PERMXY, PERMXZ, PERMYZ are not in the unrotated codes. All these keywords and definitions can be found in Appendix C.

Values for the full tensor, PERMX, PERMY, PERMZ, PERMXY, PERMXZ and PERMYZ, were obtained through the tensor rotation calculation in Appendix A and B.

3.4. Procedure for Calculating the Permeability Tensor

The calculation for rotating the permeability tensor was placed in an Excel sheet for ease of calculation. The values in the Excel document, shown in Figure 3-49, that can be varied include the principal permeabilities (K_x, K_y, K_z) and the angles of rotation for the x-, y- and z-axis. The

blue blocks are inputs for the principal permeabilities and the grey blocks are the angles of rotation. Depending on the values in these block, the permeability $\underline{K}$ matrix will change.

K_1 =	Kx =	200
K_2 =	Ky =	200
K_3 =	Kz =	64

	Degrees	Radian	Cos θ	Sin θ
θx =	0	0	1	0
θy =	320	5.59	0.77	-0.64
θz =	45	0.79	0.71	0.71

Figure 3-49: Input Values in Excel Sheet include *Kx*, *Ky* and *Kz* (Blue Cells) and θx, θy and θz (Grey Cells)

Once the input values are included the values for $K_{\beta\beta}, K_{\beta\xi}, K_{\beta\zeta}, K_{\xi\beta}, K_{\xi\xi}, K_{\xi\zeta}, K_{\zeta\beta}, K_{\zeta\xi}, K_{\zeta\zeta}$ are output into a table and a matrix version in the excel sheet, Figure 2-50. These are the values that will make up the new rotated permeability tensor used in the reservoir simulation code. Figure 2-50 also shows the results when inputting the values used in Runs 9, 18 and 36 (320° about y-axis and 45° about z-axis; K_x=200mD, K_y=200mD and K_z=64mD).

Kββ =	144
Kβξ =	0
Kβζ =	-67
Kξβ =	0
Kξξ =	200
Kξζ =	0
Kζβ =	-67
Kζξ =	0
Kζζ =	120

$$K = \begin{vmatrix} K_{\beta\beta} & K_{\beta\xi} & K_{\beta\zeta} \\ K_{\xi\beta} & K_{\xi\xi} & K_{\xi\zeta} \\ K_{\zeta\beta} & K_{\zeta\xi} & K_{\zeta\zeta} \end{vmatrix} = \begin{vmatrix} 144 & 0 & -67 \\ 0 & 200 & 0 \\ -67 & 0 & 120 \end{vmatrix}$$

Figure 3-50: Tensor Rotation Results For Runs 9, 18 and 36 (320° about y-axis and 45° about z-axis; K_x=200mD, K_y=200mD and K_z=64mD)

The results from the tensor rotation show $K\beta\xi = K\xi\beta$, $K\beta\zeta = K\zeta\beta$, and $K\xi\zeta = K\zeta\xi$. This indicates that the tensor rotation is performed correctly. The matrix test also confirms that the calculation is performed without error. The theory behind the matrix test was discussed in Section 2.4.1, Tensor Rotation. Table 3-2 is the matrix test that was included into the excel sheet to verify the calculations (Malvern 1969).

Table 3-2: Invariance Test Using Equations 2.18

$K_{\beta\beta} + K_{\xi\xi} + K_{\zeta\zeta}$ = 464	$K_1 + K_2 + K_2$ = 464
$K_{\beta\beta}K_{\xi\xi} + K_{\xi\xi}K_{\zeta\zeta} + K_{\zeta\zeta}K_{\beta\beta} - K_{\beta\xi}^2 - K_{\xi\zeta}^2 - K_{\beta\zeta}^2$ = 65600	$K_1K_2 + K_2K_3 + K_1K_3$ = 65600
$K_{\beta\beta}K_{\xi\xi}K_{\zeta\zeta} + 2K_{\beta\xi}K_{\xi\zeta}K_{\beta\zeta} - K_{\beta\beta}K_{\xi\zeta}^2 - K_{\xi\xi}K_{\beta\zeta}^2 - K_{\zeta\zeta}K_{\beta\zeta}^2$ = 2.5x10^6	$K_1K_2K_3$ = 2.5x10^6

The permeability values used in Table 3-2 were from both the permeability matrix after rotation and the principal permeability values. The permeability values from the matrix after rotation include $K_{\beta\beta}$ = 144 mD, $K_{\xi\xi}$ = 200 mD, $K_{\zeta\zeta}$ = 120 mD, $K_{\beta\xi}$ =0 mD, $K_{\beta\zeta}$ = -67mD, and $K_{\xi\zeta}$ = 0 mD. The terms K_1, K_2 and K_3 are the principal permeability values for directions x, y and z, respectively. The principal permeability values used in Runs 9, 18 and 36 are $K_1 = K_2 = 200$ mD and $K_3 = 64$ mD. Invariance testing, Table 3-2, confirms that the rotation was performed correctly.

The following tables show the results for all combination of tensor rotations and for both reservoirs permeability types.

Table 3-3: Tensor Rotation Results for Runs 1 to 18 and 28 to 36

Runs	Rotation (Degrees) about y-axis	Rotation (Degrees) about z-axis	PERMX (mD)	PERMY (mD)	PERMZ (mD)	PERMXY (mD)	PERMYZ (mD)	PERMZX (mD)
1, 10, 28	0	0	200	200	64	0	0	0
2, 11, 29	0	22	200	200	64	0	0	0
3, 12, 30	0	45	200	200	64	0	0	0
4, 13, 31	343	0	188	200	76	0	0	-38
5, 14, 32	343	22	188	200	76	0	0	-38
6, 15, 33	343	45	188	200	76	0	0	-38
7, 16, 34	320	0	144	200	120	0	0	-67
8, 17, 35	320	22	144	200	120	0	0	-67
9, 18, 36	320	45	144	200	120	0	0	-67

Table 3-4: Tensor Rotation Results for Runs 19 to 27

Runs	Rotation (Degrees) about y-axis	Rotation (Degrees) about z-axis	PERMX (mD)	PERMY (mD)	PERMZ (mD)	PERMXY (mD)	PERMYZ (mD)	PERMZX (mD)
19	0	0	200	150	64	0	0	0
20	0	22	193	157	64	-17	0	0
21	0	45	175	175	64	-25	0	0
22	343	0	188	150	76	0	0	-38
23	343	22	182	157	75	-16	5	-36
24	343	45	166	175	73	-24	7	-31
25	320	0	144	150	120	0	0	-67
26	320	22	140	157	117	-13	11	-64
27	320	45	129	175	110	-19	16	-55

Chapter 4 Results and Discussion

The oil production simulation results for the single block reservoir, 5x5x5 block reservoir and the 10x10x10 block reservoir at the various well rotations are presented and discussed in his chapter. The different reservoir grid refinements will determine if increasing the number of blocks also increases the difference in oil production rate between cases. The rotations of the wellbore used, as previously discussed, give the full range of possible rotation. The well production schedule was identical for all cases, with a maximum production rate of 250 STB/day. The bottom hole pressure for the wells were given the Eclipse default value of 14.7 psia and the initial reservoir pressure was 10,000 psia.

Included in the 5x5x5 reservoir result section is a test performed to examine cases where permeability in the x- and y-direction are not equal. The x-permeability stays the same at 200 mD, but the y-permeability changes to 150 mD.

4.1. Single Block Reservoir Runs

Runs 1-36, Table 4-1, had a rotated permeability simulation and were compared to their corresponding unrotated permeability simulation. This comparison will show the difference in

oil production rate between using conventional simulator (unrotated, which do not account for the actual well trajectory) and the method of rotating the permeability tensor.

The simulation results for Runs 1-9, single block with 200 mD, 200 mD, and 64 mD in the x-, y- and z-direction, are show in Table 4-1. All production rates shown are in STB/Day. Runs 1-3 (0° about y-axis and varying degrees about z-axis), 4-5 (343° about y-axis and varying degrees about z-axis) and 6-9 (320° about y-axis and varying degrees about z-axis) produced identical oil production rates and therefore can be grouped together for discussion. This means that the rotation about the z-axis, the only variable that is different within the groups, had no effect on the oil production. The reason for this is that the permeability in the x- and y-direction are both 200 mD, meaning the entire x-y plane is 200 mD in all directions, and any rotation about the z-axis has no affect on the x and y permeability.

Since Run 1 (0° about the y-axis and 0° about the z-axis) matches the results from the unrotated case, it proves there is no error in the simulator when it comes to comparing the results from the full tensor and the diagonal tensor when the x-y plane is isotropic.

Table 4-1: Oil Production Rates (STB/DAY) for Runs #1-9 (single block, varying degrees about the y-axis and z-axis, K_x=200mD, K_y=200mD and K_z=64mD)

Time (Days)	Unrotated	Run #1	Run #2	Run #3	Run #4	Run #5	Run #6	Run #7	Run #8	Run #9
1	250	250	250	250	250	250	250	250	250	250
2	250	250	250	250	250	250	250	250	250	250
3	208	208	208	208	220	220	220	231	231	231
4	27.9	27.9	27.9	27.9	29.0	29.0	29.0	30.2	30.2	30.2
5	18.3	18.3	18.3	18.3	18.7	18.7	18.7	19.1	19.1	19.1
6	13.0	13.0	13.0	13.0	13.0	13.0	13.0	13.0	13.0	13.0
7	9.7	9.7	9.7	9.7	9.7	9.7	9.7	9.7	9.7	9.7

Each Run in the single block cases were compared to the same unrotated case. The unrotated case is where the single block has the horizontal well running horizontally through the center of the block in the x-direction.

Table 4-2, Figure 4-1 and Figure 4-2 shows the grouped simulation results. Figure 4-1 show the grouped production rates for Runs 1 to 9. The oil production percent difference from the unrotated case and group rotated tensor cases are shown in Table 4-2 and graphically in Figure 4-2. Runs 1-3 (single block, 0° about the y-axis and varying degrees about the z-axis) have no rotation about the y-axis and yield identical production data as the unrotated case, therefore Runs 1-3 were grouped with the unrotated case and are identified as the blue blocks in the table. Runs 4-6 (single block, 343° about the y-axis and varying degrees about the z-axis) show a slight difference in production data from the unrotated case. Finally Runs 7-9 (single block, 320° about the y-axis and varying degrees about the z-axis) show a considerable difference in production data from the unrotated case, due to the irregular well path.

The unrotated case, which used the diagonal tensor in the simulation, had identical oil production results as the full tensor Runs 1-3 (single block, 0° about the y-axis and varying degrees about the z-axis). Table 4-1 shows that after the tensor rotation, the tensor for Runs 1-3 were the same. This group had the smallest production rate at the first time step after production started to decline from the maximum permitted. Runs 4-6 had the second highest production rate at the first time step of the decline and Runs 7-9 had the lowest production

rate. This reveals that as the permeability tensor is rotated at greater degrees from the principal permeability directions the higher the production rate becomes.

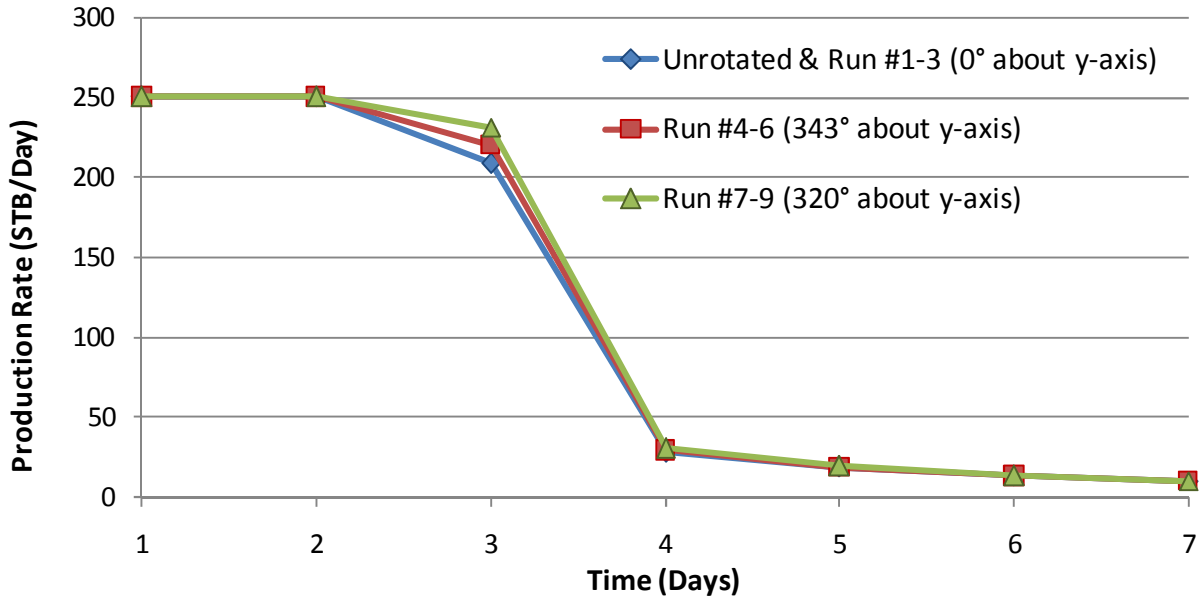

Figure 4-1: Oil Production Rates Combining Runs with Identical Results (Unrotated with Runs 1-3, Runs 4-6 & Runs 7-9)

The unrotated tensor simulation is considered the way conventional simulators would represent Runs 1-9 in a single block case. Therefore a percent difference between the unrotated simulation and Runs 1-9 is useful in describing the results. A percentage difference of the oil production rate between the unrotated case and the three groups are shown in Figure 4-2 and Table 4-2.

Table 4-2: Oil Production Percentage Difference from Unrotated Case and Grouped Rotated Tensor Cases (Runs 1-3, Runs 4-6 & Runs 7-9)

	0° about y-axis	**343° about y-axis**	**320°** about y-axis
Time (Days)	**Run 1-3 (%)**	**Run 4-6 (%)**	**Run 7-9 (%)**
1	0	0	0
2	0	0	0
3	0	5	10
4	0	4	8
5	0	2	4
6	0	0	0
7	0	0	0

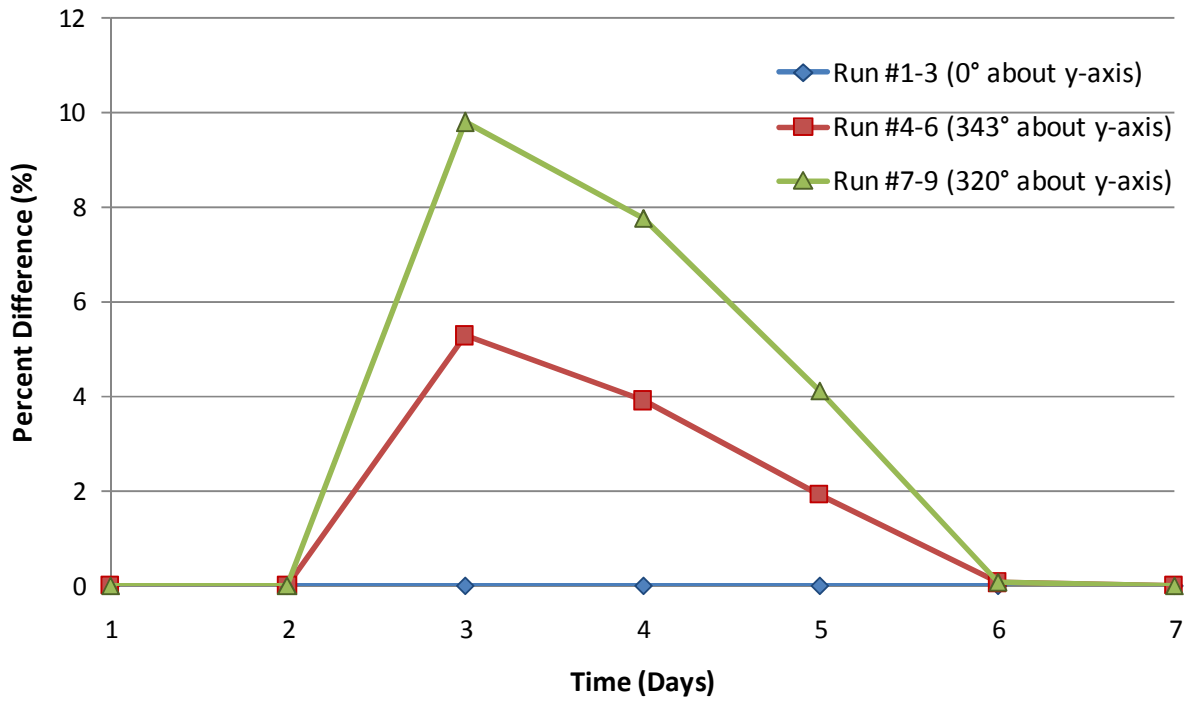

Figure 4-2: Graph of Oil Production Percentage Difference for Unrotated Case and Grouped Rotated Tensor Cases (Runs 1-3, Runs 4-6 & Runs 7-9)

The results show zero percent difference between Runs 1-3 and the unrotated case. The unrotated case has identical production rate results as Runs 1-3, therefore zero production difference in the figure.

Runs 4-6 (red in the figure) had a production rate 5% higher than the unrotated case at the first time step of production decline (3 days). As the production continued, Runs 4-6 gradually declined until it started producing at the same rate as the unrotated case. Similar results can be seen when comparing Runs 7-9 (green in the figures) to the unrotated case, but with a more drastic effect.

Table 4-2 shows that the overall oil production rate for each simulation drops fast within the first few time steps. The unrotated production rate starts at 250 STB/day and drops to 9.7 STB/day in 7 days. Production rate comparison in the higher time steps are comparing lower oil production rate. These low rates can be accounted for from the size of the reservoir simulation grid used. For all the cases the reservoir is only 50 feet x 50 feet x 50 feet, 125,000 ft^3.

The single block simulations show that rotations about the z-axis had no effect on oil production. As the rotation about the y-axis increased so did the difference in production rates between the rotated and unrotated cases.

4.2. 5x5x5 Block Reservoir Runs

The next set of simulations were performed on a 5x5x5 reservoir grid. Each block in this reservoir is smaller than the single block reservoir, but when combined equal the same total volume as the single block reservoir. This increased number of reservoir grid blocks will indicate the effect of increasing the number of blocks on the oil production difference.

Once again it was noticed that the rotation about the z-axis had little to no effect on production. Runs 10-12 (zero rotation about the y-axis and changing z-axis rotation) showed that the z-axis rotation had zero effect on oil production difference between the unrotated and rotated cases for each Run. The table below shows the results for Runs 10-12 (0° rotation about the y-axis and changing rotation about the z-axis).

Table 4-3: Oil Production and Percent Difference Results for Runs 10-12 (5x5x5 Reservoir, 0° rotation about the y-axis and changing rotation about the z-axis, K_x=200mD, K_y=200mD and K_z=64mD)

	0° about y-axis, 0° about z-axis			0° about y-axis, 22° about z-axis			0° about y-axis, 45° about z-axis		
Time (Days)	Run #10 Unrotated (STB/Day)	Run #10 Rotated (STB/Day)	Run #10 Percent Difference	Run #11 Unrotated (STB/Day)	Run #11 Rotated (STB/Day)	Run #11 Percent Difference	Run #12 Unrotated (STB/Day)	Run #12 Rotated (STB/Day)	Run #12 Percent Difference
1	250	250	0	250	250	0	250	250	0
2	250	250	0	250	250	0	250	250	0
3	249	249	0	249	249	0	249	249	0
4	22.2	22.2	0	23.1	23.1	0	22.6	22.6	0
5	17.4	17.4	0	17.8	17.8	0	17.4	17.4	0
6	13.8	13.8	0	13.9	13.9	0	13.7	13.7	0
7	10.9	10.9	0	11.0	11.0	0	10.8	10.8	0

Runs 13-15 (343° rotation about y-axis and changing z-axis rotation) shows nearly identical results when compared to the difference between each Runs unrotated case. In the percentage difference column, below in the table, we see that the Runs 13 (0° rotation about the y-axis and 0° about the z-axis), 14 (0° about the y-axis and 22° about the z-axis) and 15 (0° about the y-axis and 45° about the z-axis) have a very similar percentage difference when production starts to drop off. With the slight difference in production coming from the wells following different paths and having different lengths in each simulation, see Figures 3-12 to 3-29.

Table 4-4: Oil Production and Percent Difference Results for Runs 13-15 (5x5x5 Reservoir, 343° rotation about the y-axis and changing rotation about the z-axis, K_x=200mD, K_y=200mD and K_z=64mD)

	343° about y-axis, 0° about z-axis			343° about y-axis, 22° about z-axis			343° about y-axis, 45° about z-axis		
Time (Days)	Run #13 Unrotated (STB/Day)	Run #13 Rotated (STB/Day)	Run #13 Percent Difference	Run #14 Unrotated (STB/Day)	Run #14 Rotated (STB/Day)	Run #14 Percent Difference	Run #15 Unrotated (STB/Day)	Run #15 Rotated (STB/Day)	Run #15 Percent Difference
1	250	250	0	250	250	0	250	250	0
2	250	250	0	250	250	0	250	250	0
3	249	249	0	249	249	0	249	249	0
4	24.9	26.3	5.3	24.9	26.5	6.0	24.3	26.5	8.2
5	19.1	19.9	3.9	19.1	19.9	4.3	18.6	19.7	5.7
6	14.5	14.8	2.2	14.4	14.8	2.7	14.3	14.8	3.3
7	11.1	11.3	1.2	11.1	11.3	1.4	11.0	11.2	1.7

Finally, Runs 16-18 (320 degree rotation about the y-axis and changing z-axis rotation) shows a larger difference in unrotated and rotated production values then was observe in Runs 13-15. It shows a similar pattern, with a greater difference as production drops towards zero. In Runs 13-15, table above, the difference reached 8.2% difference as production dropped, while the results for Runs 16-18 shows the production difference reach 15.2% as production drops.

The higher difference in production in Runs 16-18 reveals that the rotation about the y-axis has a larger effect on the production difference between the rotated and unrotated cases. The final time step in Run 18 has a percent difference of 15.2%.

Table 4-5: Oil Production and Percent Difference Results for Runs 16-18 (5x5x5 Reservoir, 320° rotation about the y-axis and changing rotation about the z-axis, K_x=200mD, K_y=200mD and K_z=64mD)

	320° about y-axis, 0° about z-axis			320° about y-axis, 22° about z-axis			320° about y-axis, 45° about z-axis		
Time (Days)	Run #16 Unrotated (STB/Day)	Run #16 Rotated (STB/Day)	Run #16 Percent Difference	Run #17 Unrotated (STB/Day)	Run #17 Rotated (STB/Day)	Run #17 Percent Difference	Run #18 Unrotated (STB/Day)	Run #18 Rotated (STB/Day)	Run #18 Percent Difference
1	250	250	0	250	250	0	250	250	0
2	250	250	0	250	250	0	250	250	0
3	249	249	0	249	249	0	249	249	0
4	26.6	30.6	13.2	26.2	30.5	14.1	25.1	29.6	15.2
5	20.0	21.8	8.0	20.1	21.9	8.3	19.1	21.2	9.8
6	14.8	15.4	3.7	14.9	15.5	4.1	14.5	15.3	5.1
7	11.2	11.3	1.3	11.2	11.4	1.6	11.1	11.4	2.1

Figure 4-3 illustrates the production rate differences for Runs 10-18 (5x5x5 block reservoir, changing rotation about the y- and z-axis, K_x=200mD, K_y=200mD and K_z=64mD). It shows the change in z-axis rotation has little effect on the oil production rate and the y-axis rotation having a large effect on oil production rate. The main reason for the little effect caused by the z-axis rotation is the permeability in the x- and y-direction equal. When the tensor is only rotated on the x-y plane, rotation about the z-axis, the x-y plane is isotropic and therefore the rotation has no effect.

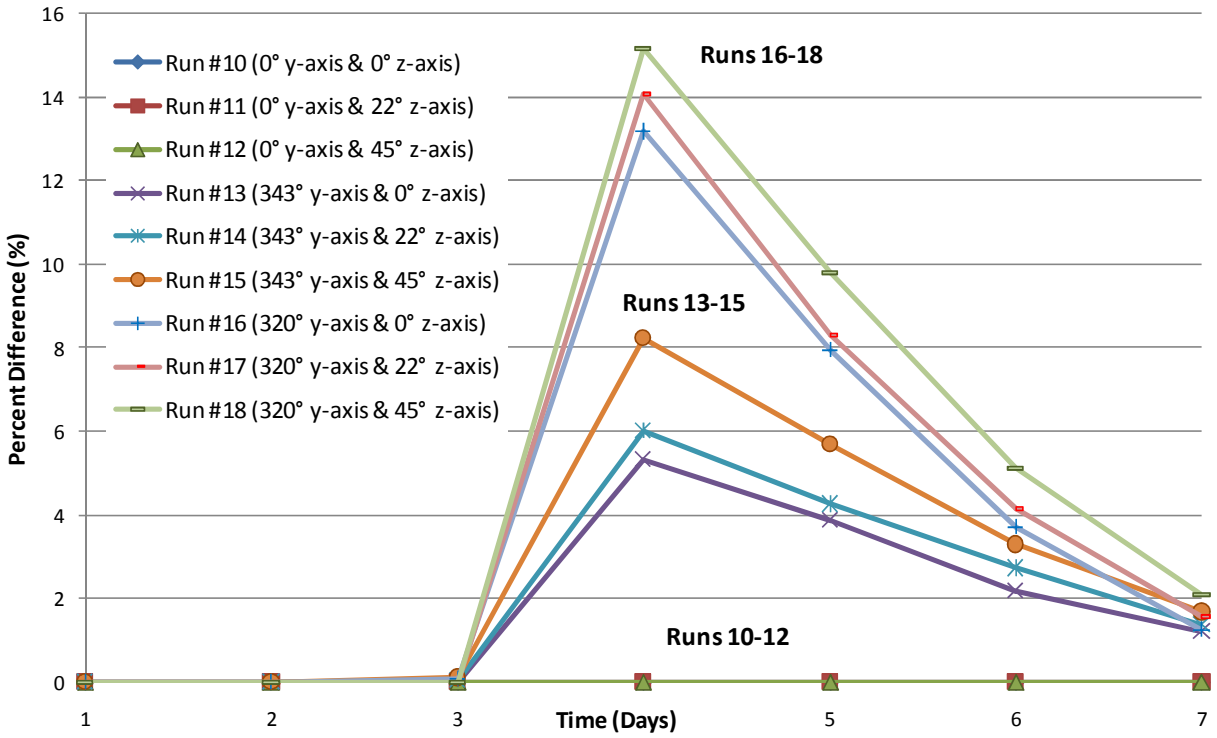

Figure 4-3 Oil Production Rate Percent Difference for Runs 10-18 (5x5x5 block reservoir, changing rotation about the y- & z-axis, K_x=200mD, K_y=200mD and K_z=64mD)

The next set of simulation tests were performed on the same 5x5x5 reservoir as Runs 10-18, except the permeability in the y-direction was changed to 150 mD. This was done to see the effect of the z-axis rotation when permeability in the x- and y-direction were not equal.

Table 4-6 shows the simulation results for Runs 19-20 (0° rotation about the y-axis and a changing rotation about the z-axis). In this set of simulations the rotation about the z-axis does have an effect on the oil production rate. In the previous set of simulations, Runs 10-18, there was no effect. Runs 20 and 21 (0° rotation about the y-axis and a changing rotation about the z-axis) in Table 4-6 show that rotation about the z-axis now effects the production rate.

Previously when the x- and y-permeability were both 200 mD there was no production difference when there was a rotation about the z-axis.

Once again the first Run, zero rotation about both the y-axis and z-axis, has identical oil production results. This shows there is no significant difference in comparing results from the diagonal tensor and full tensor.

Table 4-6: Oil Production and Percent Difference Results for Runs 19-21 (5x5x5 Reservoir, 0° rotation about the y-axis and changing rotation about the z-axis, K_x=200mD, K_y=150mD and K_z=64mD)

	0° about y-axis, 0° about z-axis			0° about y-axis, 22° about z-axis			0° about y-axis, 45° about z-axis		
Time (Days)	Run #19 Unrotated (STB/Day)	Run #19 Rotated (STB/Day)	Run #19 Percent Difference	Run #20 Unrotated (STB/Day)	Run #20 Rotated (STB/Day)	Run #20 Percent Difference	Run #21 Unrotated (STB/Day)	Run #21 Rotated (STB/Day)	Run #21 Percent Difference
1	250	250	0	250	250	0	250	250	0
2	250	250	0	250	250	0	250	250	0
3	249	249	0	249	249	0	249	249	0
4	20.1	20.1	0	20.8	21.2	1.7	20.6	21.2	2.6
5	16.1	16.1	0	16.6	16.8	1.3	16.5	16.8	1.8
6	13.1	13.1	0	13.3	13.4	0.5	13.3	13.5	0.8
7	10.7	10.7	0	10.8	10.8	0.2	10.7	10.7	0.4

The next set of production results, Runs 22-24 (343° rotation about the y-axis and changing rotation about the z-axis), are shown in Table 4-7. The results are similar to Runs 13-15, Table 4-4, with Runs 22-24 having larger differences in oil production rates compared to the unroated tensor case. These results show that the rotation about the z-axis is now affecting the oil production rate.

Table 4-7: Oil Production and Percent Difference Results for Runs 22-24 (5x5x5 Reservoir, 343° rotation about the y-axis and changing rotation about the z-axis, K_x=200mD, K_y=150mD and K_z=64mD)

	343° about y-axis, 0° about z-axis			343° about y-axis, 22° about z-axis			343° about y-axis, 45° about z-axis		
Time (Days)	Run #22 Unrotated (STB/Day)	Run #22 Rotated (STB/Day)	Run #22 Percent Difference	Run #23 Unrotated (STB/Day)	Run #23 Rotated (STB/Day)	Run #23 Percent Difference	Run #24 Unrotated (STB/Day)	Run #24 Rotated (STB/Day)	Run #24 Percent Difference
1	250	250	0	250	250	0	250	250	0
2	250	250	0	250	250	0	250	250	0
3	249	249	0	249	249	0	249	249	0
4	22.4	23.5	4.8	22.1	23.7	6.4	22.1	24.1	8.3
5	17.5	18.2	3.4	17.9	18.9	5.3	17.6	18.7	6.0
6	13.9	14.3	2.6	13.9	14.4	3.3	13.8	14.3	3.7
7	11.0	11.1	1.4	11.0	11.1	1.5	10.9	11.1	2.0

The final set of simulations performed on the 5x5x5 reservoir are Runs 25-27 (320° rotation about the y-axis and changing rotation about the z-axis), with Table 4-8 below show the results.

Table 4-8: Oil Production and Percent Difference Results for Runs 25-27 (5x5x5 Reservoir, 320° rotation about the y-axis and changing rotation about the z-axis, K_x=200mD, K_y=150mD and K_z=64mD)

	320° about y-axis, 0° about z-axis			320° about y-axis, 22° about z-axis			320° about y-axis, 45° about z-axis		
Time (Days)	Run #25 Unrotated (STB/Day)	Run #25 Rotated (STB/Day)	Run #25 Percent Difference	Run #26 Unrotated (STB/Day)	Run #26 Rotated (STB/Day)	Run #26 Percent Difference	Run #27 Unrotated (STB/Day)	Run #27 Rotated (STB/Day)	Run #27 Percent Difference
1	250	250	0	250	250	0	250	250	0
2	250	250	0	250	250	0	250	250	0
3	249	249	0	249	249	0	249	249	0
4	23.6	27.4	13.7	23.9	28.2	15.2	22.2	27.0	17.8
5	18.7	20.4	8.2	18.7	20.8	9.8	17.8	20.0	10.7
6	14.3	15.0	4.8	14.3	15.1	5.1	13.9	14.9	6.5
7	11.1	11.3	2.1	11.1	11.3	2.0	10.9	11.3	3.3

Similar results as Runs 10-18 are observed for Runs 19-27, with the z-axis rotation now having more of an effect on production because the x and y principal permeabilities are not equal. Runs 10-12, in Figure 4-3, and Runs 19-21, in Figure 4-4, both have 0° rotation about the y-axis

and varying rotation about the z-axis, with the only difference being the principal permeability in the x and y direction are equal in Runs 10-12 and not equal in Runs 19-21. From the figures it is observed that when the x and y permeabilities are not equal and there is a rotation about the z-axis, it causes there to be a difference in the percent difference in the oil production between the unrotated and rotated tensor cases.

Figure 4-4 illustrates the percent difference results for Runs 19-27. The figure shows that all rotated tensor cases produced at a higher rate than their unrotated case when production rate started to decline. At steps 1 to 3 days all cases were producing at their maximum oil production rate, 250 STB/day. Once the production rate started to decline (time step 4) the differences in oil production rates were noticed.

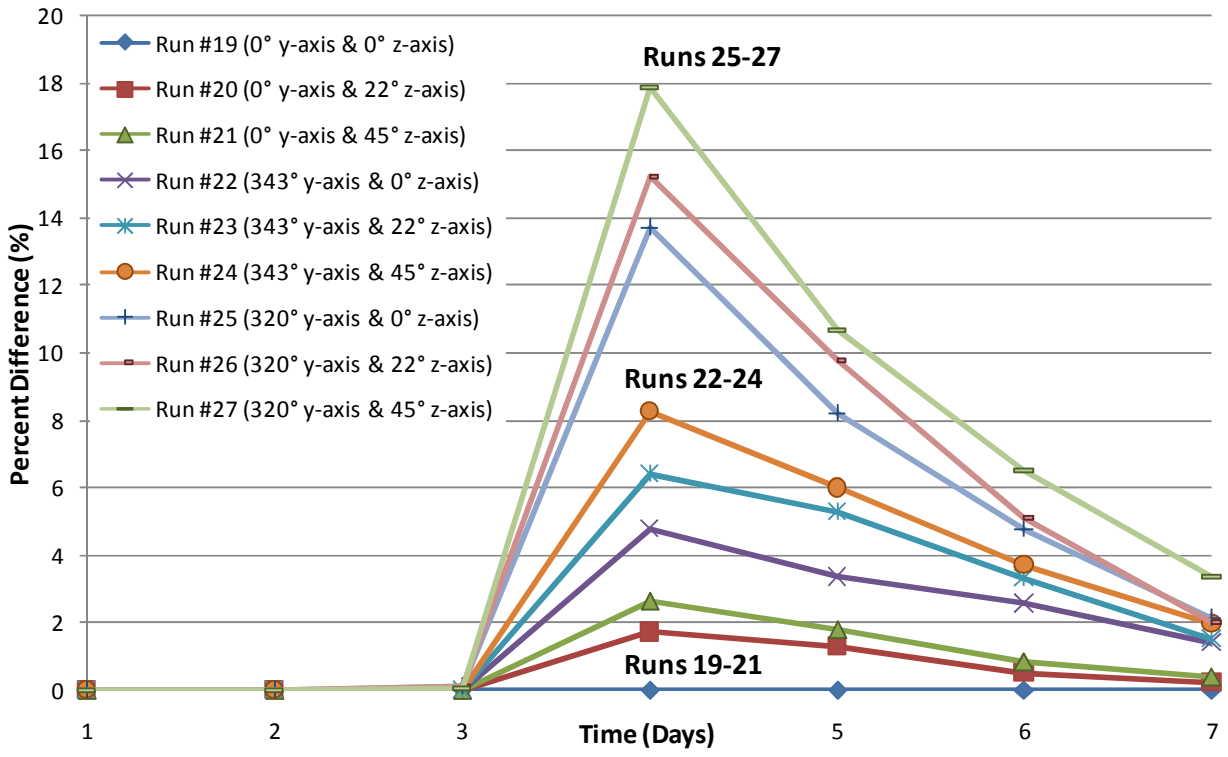

Figure 4-4: Oil Production Rate Percent Difference for Runs 19-27 (5x5x5 block reservoir, changing rotation about the y- & z-axis, K_x=200mD, K_y=150mD and K_z=64mD)

Results in Figures 4-3 and 4-4 prove that having the permeability in the x- and y-direction not equal effects the production rate difference. At the point in the 5x5x5 reservoir simulation where the production rate starts to decline (4 days) we notice a percent difference at the first step in the production rate decline.

4.3. 10x10x10 Block Reservoir Runs

Simulations for Runs 28-36 (changing rotation about the y- & z-axis, K_x=200mD, K_y=200mD and K_z=64mD) were performed on a 10x10x10 block reservoir grid. The larger simulation grid will show if grid scaling has an effect on percent difference between the rotated and unrotated permeability tensor. Runs 10-18 and Runs 28-36 have identical principal permeability values and followed the same set of tensor rotations. Comparing the results for Runs 28-36 to the results found in Runs 10-18 will show if more reservoir blocks increases the production rate difference between the rotated and unrotated tensor cases.

The first set of simulation for the 10x10x10 reservoir, Runs 28-30, yields the same result as Runs 10-12 of the 5x5x5 reservoir, which was zero percent difference between the unrotated and rotated cases.

Table 4-9: Oil Production and Percent Difference Results for Runs 28-30 (10x10x10 Reservoir, 0° rotation about the y-axis and changing rotation about the z-axis, K_x=200mD, K_y=200mD and K_z=64mD)

	0° about y-axis, 0° about z-axis			0° about y-axis, 22° about z-axis			0° about y-axis, 45° about z-axis		
Time (Days)	Run #28 Unrotated (STB/Day)	Run #28 Rotated (STB/Day)	Run #28 Percent Difference	Run #29 Unrotated (STB/Day)	Run #29 Rotated (STB/Day)	Run #29 Percent Difference	Run #30 Unrotated (STB/Day)	Run #30 Rotated (STB/Day)	Run #30 Percent Difference
1	250	250	0	250	250	0	250	250	0
2	250	250	0	250	250	0	250	250	0
3	249	249	0	249	249	0	249	249	0
4	23.8	23.8	0	23.7	23.7	0	25.3	25.3	0
5	19.1	19.1	0	18.9	18.9	0	19.3	19.3	0
6	15.0	15.0	0	15.0	15.0	0	15.0	15.0	0
7	11.9	11.9	0	12.0	12.0	0	12.0	12.0	0

The simulation results for Runs 31-33 are shown in Table 4-10. The rotations for these Runs are the same as Runs 13-15 in the 5x5x5 block simulations. The difference in oil production rates for Runs 31-33 are similar to results in Runs 13-15 (5x5x5 block reservoir), with the percent difference being greater in Runs 31-33 (10x10x10 block reservoir).

Table 4-10: Oil Production and Percent Difference Results for Runs 31-33 (10x10x10 Reservoir, 343° rotation about the y-axis and changing rotation about the z-axis, K_x=200mD, K_y=200mD and K_z=64mD)

	343° about y-axis, 0° about z-axis			343° about y-axis, 22° about z-axis			343° about y-axis, 45° about z-axis		
Time (Days)	Run #31 Unrotated (STB/Day)	Run #31 Rotated (STB/Day)	Run #31 Percent Difference	Run #32 Unrotated (STB/Day)	Run #32 Rotated (STB/Day)	Run #32 Percent Difference	Run #33 Unrotated (STB/Day)	Run #33 Rotated (STB/Day)	Run #33 Percent Difference
1	250	250	0	250	250	0	250	250	0
2	250	250	0	250	250	0	250	250	0
3	249	249	0	249	249	0	249	249	0
4	25.8	27.8	7.3	25.2	27.7	9.0	25.9	29.0	10.7
5	19.6	20.5	4.6	19.6	20.9	5.9	19.8	21.3	7.0
6	15.2	15.6	2.8	15.2	15.7	3.2	15.3	15.9	3.3
7	12.0	12.2	1.3	11.9	12.2	2.1	11.9	12.2	2.3

Once again we see a similar result in Run 34-36 (320° rotation about the y-axis and changing rotation about the z-axis), Table 4-11, as was seen in the corresponding rotations in the 5x5x5 reservoir, Runs 16-18. Both sets of simulation results showed the largest percent difference between the unrotated and rotated cases when the y-axis rotation was 320°. With the highest difference in oil production rate coming when the permeability tensor is rotated 320° about the y-axis and 45° about the z-axis.

Table 4-11: Oil Production and Percent Difference Results for Runs 34-36 (10x10x10 Reservoir, 320° rotation about the y-axis and changing rotation about the z-axis, K_x=200mD, K_y=200mD and K_z=64mD)

	320° about y-axis, 0° about z-axis			320° about y-axis, 22° about z-axis			320° about y-axis, 45° about z-axis		
Time (Days)	Run #34 Unrotated (STB/Day)	Run #34 Rotated (STB/Day)	Run #34 Percent Difference	Run #35 Unrotated (STB/Day)	Run #35 Rotated (STB/Day)	Run #35 Percent Difference	Run #36 Unrotated (STB/Day)	Run #36 Rotated (STB/Day)	Run #36 Percent Difference
1	250	250	0	250	250	0	250	250	0
2	250	250	0	250	250	0	250	250	0
3	249	249	0	249	249	0	249	249	0
4	29.6	34.9	15.3	29.7	35.9	17.3	28.2	35.6	20.7
5	22.1	24.1	8.2	21.8	24.4	10.8	21.2	24.1	12.2
6	16.0	16.8	4.5	15.9	16.7	4.8	15.9	16.8	5.0
7	12.1	12.4	2.5	12.0	12.4	2.9	12.1	12.5	3.6

The percent difference results for Runs 28-36 (10x10x10 block reservoir, changing rotation about the y- & z-axis, K_x=200mD, K_y=150mD and K_z=64mD) are shown in Figure 4-5. The results show a similar graph as Runs 10-18, Figure 4-4. That is, Runs 28-30 (0° about the y-axis and varying degrees about the z-axis) have a zero percent difference in oil production rate between the unrotated and rotated tensor. Runs 31-33 (343° about the y-axis and varying degrees about the z-axis) show an increase in oil production difference as the days increase. Finally Runs 34-36 (320° about the y-axis and varying degrees about the z-axis) show the largest difference in oil production rate, reaching 20.7% in Run 36.

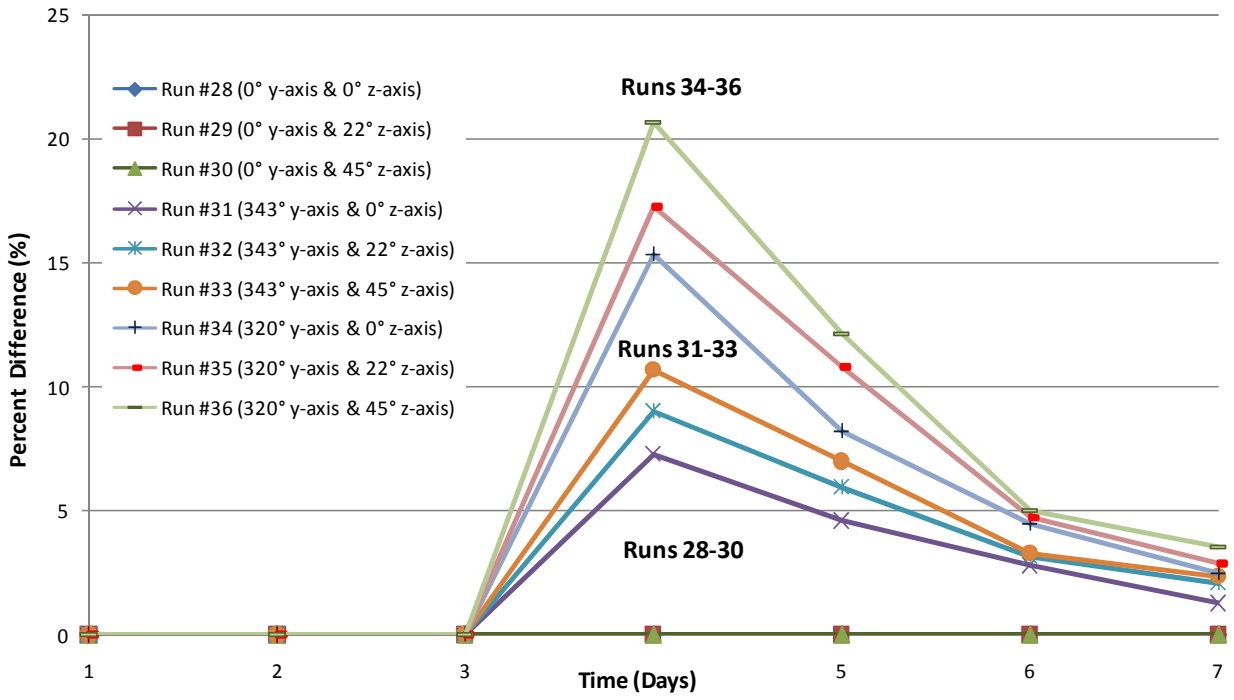

Figure 4-5: Oil Production Rate Percent Difference for Runs 28-36 (10x10x10 block reservoir, changing rotation about the y- & z-axis, K_x=200mD, K_y=200mD and K_z=64mD)

Runs 28-36 also have negative percent differences in oil production when the oil production rates start to drop from their maximum allowed rate, the rotated tensor first produces more than the unrotated. As production rates continue to decrease the percent difference between the rotated and unrotated cases increases, in Runs with a rotation about the y-axis.

It was noticed once again that as the number of reservoir grid blocks increased, the difference oil production has also increased. In the final step of Run 36 the percent difference is 20.7%.

When comparing the results from the single block case, the 5x5x5 block reservoir and the 10x10x10 block reservoir we see that increasing the grid refinement of the reservoir simulation grid slightly increases the percent difference between the rotated and unrotated cases.

Chapter 5 Conclusion and Recommendations

A total of 64 reservoir simulations (10 for the single block, 36 for the 5x5x5 block reservoir and 18 for the 10x10x10 block reservoir) were performed to obtain the results needed for this research. These results show that the way conventional reservoir simulator create the wellpath and the rotated permeability tensor to align with the actual wellpath method gives different oil production rate results.

5.1. Conclusion

Simulation results from comparing the oil production rates of the unrotated tensor (traditional reservoir simulator) to the rotated tensor (aligning the permeability tensor with the actual well path) demonstrate a difference in oil production rates depending if the rotation is done about the y- or z-axis. It was found that the rotation about the z-axis had no effect on the oil production difference when both the x and y principal permeability are equal and there is no rotation about the y-axis. As the y-axis rotation increased from 0° to 343° to 320° (counterclockwise), the percent difference between the rotated and unrotated simulations also increased.

The single block reservoir simulations, Runs 1-9 (single block, changing rotation about the y- & z-axis, K_x=200mD, K_y=200mD and K_z=64mD), had the unrotated tensor case producing at a higher production rate than the rotated cases when rates dropped from the maximum oil production rate.

In the 5x5x5 block reservoir, oil production rate differences increased as the rotation about the y-axis increased. There was a zero percent difference when the rotation about the y-axis was zero. When the rotation about the y-axis increased so did the oil production difference.

Tests were performed on the 5x5x5 block reservoir to determine the effect on oil production rates when the principal permeability in the x- and y-direction were not equal, Runs 19-27 (5x5x5 block reservoir, changing rotation about the y- & z-axis, K_x=200mD, K_y=150mD and K_z=64mD). It was found that rotation about the y-axis and the z-axis both had an effect on oil production rates. With the largest oil production difference occurring in Run 26 (320° about the y-axis and 22° about the z-axis).

As the number of reservoir grid blocks increased, so did the maximum oil production percent difference. In the 5x5x5 block reservoir (Runs 10-18), five blocks within the reservoir had production wells penetrating them. While in the 10x10x10 block reservoir (Runs 28-36) there was 10 blocks having wells. The more blocks used in the simulation the greater the difference in oil production rate becomes. In both the 5x5x5 block reservoir and the 10x10x10 block

reservoir, the oil production difference was zero when the rotation about the y-axis was zero. When the rotation about the y-axis was 343° the 5x5x5 block reservoir had an oil production difference of 8.2%, while the 10x10x10 block reservoir reached a 10.7% oil production difference. In the 320° rotation about the y-axis cases the 5x5x5 block reservoir had a 15.7% oil production difference and the 10x10x10 block reservoir had the highest oil production difference of all simulations, 20.7%. This indicates that increasing the grid refinement also increased the difference in production rate.

These results show there are large differences in production rates depending on which tensor approach used. The permeability tensor rotation to align with the well trajectory may prove to be more accurate in predict reservoir production rates. This would be extremely valuable to oil and gas reservoir operators in predicting future production rates.

5.2. Recommendations

The results show that the wellpath in traditional reservoir simulators are producing at a rate that may not be emulating true reservoir production. More accurate production rates may come from rotating the permeability tensor to align the tensor parallel to the well trajectories.

Further variations using the full tensorial permeability aligning with the well trajectory should be performed, such as using a greater number of grid blocks and different well trajectories. The

cause for these oil production rate differences may be better understood with further reservoir simulations using full tensorial permeability and interpreting the well lengths used in the simulation.

Also, a cost based analysis on computational time between the traditional reservoir simulation approach and the full tensorial permeability aligning with the well trajectory should be performed.

Finally, research using this technique in a full field applications need to be performed. The more accurate tensor approach would be found by comparing the reservoir simulation results of the full permeability tensor and the diagonal permeability tensor to the actual field production data. If the full tensorial simulation is demonstrated to be the more accurate way for reservoir simulation it will be beneficial in the oil and gas industry when making large capital decision, to estimate reserves, and to diagnose and improve the performance of producing reservoirs.

References

Bagheri, M. S. (2003). Metods for Modelling Full Tensor Permeability in Reservoir Simulators. *Society of Petroleum Engineering Journal*.

Bear, J. (1988). *Dynamics of Fluids in Porous Media.* Dover.

Case, C., & Cochran, G. (1972). Transformation of the Tensor Form of Darcy's Law in Inhomogeneous and Anisotropic Soils. *Water Resources Research*, 728-733.

Coats, K. H. (1980). An Equation of State Compositional Model. *Society of Petroleum Engineering Journal*, 363-376.

Dalen, V., Hegre, T., & Henriquez, A. (1986). Generalized Transmissibilites for Distorted Grids in Reservoir Simulation. *SPE Annual Technical Conference and Exhibition.* New Orleans, Louisiana: Society of Petroleum Engineers.

Dullemond, K., & Peeters, K. (2010). *Introduction to Tensor Calculus.* University of Heidelberg.

Durlofsky, L. (1991). Numerical Calculation of Equivalent Grid Block Permeability Tensors for Heterogeneous Porous Media. *Water Resources Research*, 699-708.

Fanchi, J. (2006). *Principals of Applied Reservoir Simulation, 3rd Edition.* Gulf Professional Publishing.

Johansen, T. (2008). *Principals of Reservoir Engineering.* Memorial University.

Johansen, T. (2013). *Inflow Modeling for Wells with Arbitrary Trajectories in Anisotropic Media.* Memorial University Research Note.

Johnson, W., & Breston, J. (1951). Directional Permeability Measurements on Oil Sandstones from Various States. *Producers Monthly*, 10-19.

Johnson, W., & Hughes, R. (1948). Directional Permeability Measurements and their Significance. *Producers Monthly*, 17-25.

Lake, L. W. (1988). The Origins of Anisotropy. *SPE Technology Today Series*.

Leung, W. (1986). A Tensor Model for Anisotropic and Heterogeneous Reservoirs with Variable Directional Permeabilities. *Society of Petroleum Engineers*.

Liakopoulos. (1965). Darcy's Coefficient of Permeability as Symmetric Tensor of Second Rank. *International Association of Scientific Hydrology*, 41-48.

Liakopoulos, C. (1960). Variation of the Permeability Tensor Ellipsoid in Homogeneous Anisotropic Soils. *Civil Engineering Department, College of Engineering, Riyadh, Saudi Arabia*.

Malvern, L. E. (1969). *Introduction to the Mechanics of a Continuous Medium.* Englewood Cliffs, New Jersey: Prentice-Hall, Inc.

Peaceman, D. (1983). Interpretation of Well-Block Pressures in Numerical Reservoir Simulation With Nonsquare Grid Blocks and Anisotropic Permeability. *Society of Petroleum Engineering Journal* , 531-543.

Rose, W. (1982). A New Method to Measure Directional Permeability . *Pet. Tech*.

Scheidegger, E. (1958). *The Physics of Flow Through Porous Media.* The MacMillian Company, New York.

Schlumberger. (2014). *Schlumberger Eclipse Software*. Retrieved from Schlumberger Limited: https://www.software.slb.com/products/foundation/Pages/eclipse.aspx

Sheldon, J. W., & Cardwell, W. T. (1959). One-Dimensional, Incompressible, Noncapillary, Two-Phase Fluid Flow in a Porous Medium. *Society of Petroleum Engineering*.

Statoil. (2001). *PL128-Norne Field Reservoir Management Plan.*

Szabo, B. (1968). Permeability of Orthotropic Porous Mediums. *Water Resources Research*, 801-808.

Tyldesley, J. (1975). *An Introduction to Tensor Analysis for Engineering and Applied Scientists.* Longman.

Whitaker, S. (1969). Advances in Theory of Fluid Motion in Porous Media. *Industrial and Engineering Chemistry*, 14-28.

Appendix A. Tensor Rotation Using Directional Cosines Method

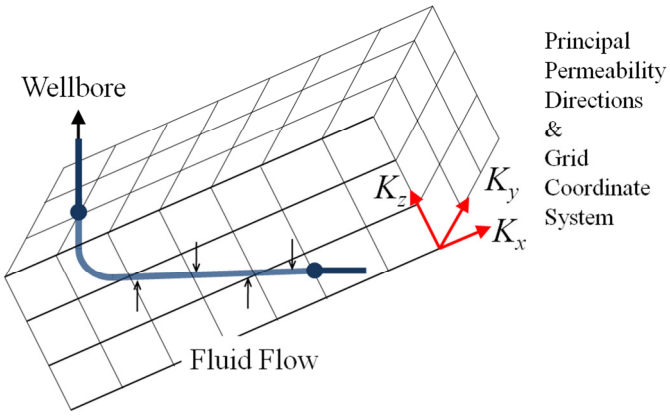

Figure 1

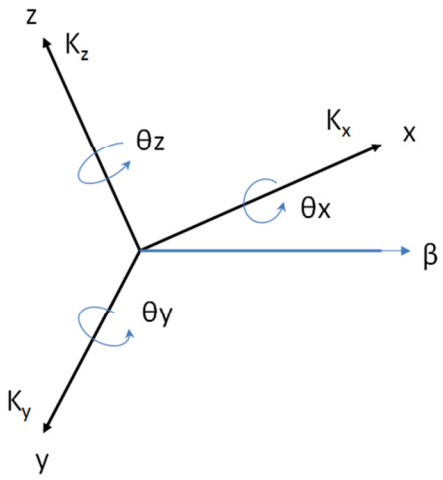

Figure 2

Figure 1 above depicts a three dimensional Cartesian coordinate system (*x, y, z*), which corresponds to principal permeability directions of the reservoir, and a well path that does not align with the coordinate system. The well path will be represented in a coordinate system that is different from the principal directions. The β axis, shown in figure 2, will align with the well and has the β axis rotated at an angle of ϑ_x from the x-axis, ϑ_y from the y-axis and then ϑ_z from the z-axis.

According to Darcy's Law, the velocity vector is

$$\vec{u} = -\frac{1}{\mu}\underline{K} \cdot \nabla p \,, \tag{A.1}$$

or

$$\begin{bmatrix} u_x \\ u_y \\ u_z \end{bmatrix} = -\frac{1}{\mu}\begin{pmatrix} K_{xx} & K_{xy} & K_{xz} \\ K_{yx} & K_{yy} & K_{yz} \\ K_{zx} & K_{zy} & K_{zz} \end{pmatrix} \cdot \begin{pmatrix} {}^{\partial p}/_{\partial x} \\ {}^{\partial p}/_{\partial y} \\ {}^{\partial p}/_{\partial z} \end{pmatrix}, \tag{A.2}$$

where we for simplicity have ignored gravity.

From (A.2), the components of $\vec{u}$ are

$$u_x = -\frac{1}{\mu}\left[K_{xx}\frac{\partial p}{\partial x} + K_{xy}\frac{\partial p}{\partial y} + K_{xz}\frac{\partial p}{\partial z}\right], \tag{A.3}$$

$$u_y = -\frac{1}{\mu}\left[K_{yx}\frac{\partial p}{\partial x} + K_{yy}\frac{\partial p}{\partial y} + K_{yz}\frac{\partial p}{\partial z}\right], \tag{A.4}$$

$$u_z = -\frac{1}{\mu}\left[K_{zx}\frac{\partial p}{\partial x} + K_{zy}\frac{\partial p}{\partial y} + K_{zz}\frac{\partial p}{\partial z}\right]. \tag{A.5}$$

A three dimensional rotated coordinate system is given by a matrix *R*.

$$\begin{pmatrix} \beta \\ \xi \\ \zeta \end{pmatrix} = R \cdot \begin{pmatrix} x \\ y \\ z \end{pmatrix} \tag{A.6}$$

where R equals;

$$R = R_x(\theta_x) \cdot R_y(\theta_y) \cdot R_z(\theta_z), \tag{A.7}$$

with coordinate system rotations of the x, y and z-axis in a counter clockwise direction when looking towards the origin give the matrices;

$$R_x(\theta_x) = \begin{bmatrix} 1 & 0 & 0 \\ 0 & \cos\theta_x & \sin\theta_x \\ 0 & -\sin\theta_x & \cos\theta_x \end{bmatrix}, \tag{A.8}$$

$$R_y(\theta_y) = \begin{bmatrix} \cos\theta_y & 0 & -\sin\theta_y \\ 0 & 1 & 0 \\ \sin\theta_y & 0 & \cos\theta_y \end{bmatrix}, \tag{A.9}$$

$$R_z(\theta_z) = \begin{bmatrix} \cos\theta_z & \sin\theta_z & 0 \\ -\sin\theta_z & \cos\theta_z & 0 \\ 0 & 0 & 1 \end{bmatrix}. \tag{A.10}$$

We find

$$R = R_x(\theta_x) R_y(\theta_y) \cdot R_z(\theta_z)$$

$$= \begin{bmatrix} 1 & 0 & 0 \\ 0 & \cos\theta_x & \sin\theta_x \\ 0 & -\sin\theta_x & \cos\theta_x \end{bmatrix} \cdot \begin{bmatrix} \cos\theta_y & 0 & -\sin\theta_y \\ 0 & 1 & 0 \\ \sin\theta_y & 0 & \cos\theta_y \end{bmatrix} \cdot \begin{bmatrix} \cos\theta_z & \sin\theta_z & 0 \\ -\sin\theta_z & \cos\theta_z & 0 \\ 0 & 0 & 1 \end{bmatrix}$$

$$= \begin{bmatrix} \cos\theta_y \cos\theta_z + 0 + 0 & \cos\theta_y \sin\theta_z + 0 + 0 & 0 + 0 - \sin\theta_y \\ \cos\theta_z \sin\theta_x \sin\theta_y - \cos\theta_x \sin\theta_z + 0 & \sin\theta_x \sin\theta_y \sin\theta_z + \cos\theta_x \cos\theta_z + 0 & 0 + 0 + \cos\theta_y \sin\theta_x \\ \cos\theta_x \cos\theta_z \sin\theta_y + \sin\theta_x \sin\theta_z + 0 & \cos\theta_x \sin\theta_y \sin\theta_z - \cos\theta_z \sin\theta_x + 0 & 0 + 0 + \cos\theta_x \cos\theta_y \end{bmatrix}$$

$$= \begin{bmatrix} \cos\theta_y \cos\theta_z & \cos\theta_y \sin\theta_z & -\sin\theta_y \\ \cos\theta_z \sin\theta_x \sin\theta_y - \cos\theta_x \sin\theta_z & \sin\theta_x \sin\theta_y \sin\theta_z + \cos\theta_x \cos\theta_z & \cos\theta_y \sin\theta_x \\ \cos\theta_x \cos\theta_z \sin\theta_y + \sin\theta_x \sin\theta_z & \cos\theta_x \sin\theta_y \sin\theta_z - \cos\theta_z \sin\theta_x & \cos\theta_x \cos\theta_y \end{bmatrix}. \qquad \text{(A.11)}$$

From (A.6),

$$\begin{pmatrix} \beta \\ \xi \\ \zeta \end{pmatrix} = \begin{bmatrix} \cos\theta_y \cos\theta_z & \cos\theta_y \sin\theta_z & -\sin\theta_y \\ \cos\theta_z \sin\theta_x \sin\theta_y - \cos\theta_x \sin\theta_z & \sin\theta_x \sin\theta_y \sin\theta_z + \cos\theta_x \cos\theta_z & \cos\theta_y \sin\theta_x \\ \cos\theta_x \cos\theta_z \sin\theta_y + \sin\theta_x \sin\theta_z & \cos\theta_x \sin\theta_y \sin\theta_z - \cos\theta_z \sin\theta_x & \cos\theta_x \cos\theta_y \end{bmatrix} \cdot \begin{pmatrix} x \\ y \\ z \end{pmatrix},$$

which gives

$$\beta = x \cos\theta_y \cos\theta_z + y \cos\theta_y \sin\theta_z - z \sin\theta_y, \qquad \text{(A.12)}$$

$$\xi = x(\cos\theta_z \sin\theta_x \sin\theta_y - \cos\theta_x \sin\theta_z) + y(\cos\theta_x \cos\theta_z + \sin\theta_x \sin\theta_y \sin\theta_z)$$
$$+z\cos\theta_y \sin\theta_x, \tag{A.13}$$

$$\zeta = x(\sin\theta_x \sin\theta_z + \cos\theta_x \cos\theta_z \sin\theta_y) + y(\cos\theta_x \sin\theta_y \sin\theta_z - \cos\theta_z \sin\theta_x)$$
$$+z\cos\theta_x \cos\theta_y. \tag{A.14}$$

Using the chain rule for differentiation,

$$\frac{\partial p}{\partial x} = \frac{\partial p}{\partial \beta}\frac{\partial \beta}{\partial x} + \frac{\partial p}{\partial \xi}\frac{\partial \xi}{\partial x} + \frac{\partial p}{\partial \zeta}\frac{\partial \zeta}{\partial x}$$
$$= \cos\theta_y \cos\theta_z \frac{\partial p}{\partial \beta} + (\cos\theta_z \sin\theta_x \sin\theta_y - \cos\theta_x \sin\theta_z)\frac{\partial p}{\partial \xi} + (\sin\theta_x \sin\theta_z$$
$$+ \cos\theta_x \cos\theta_z \sin\theta_y)\frac{\partial p}{\partial \zeta}, \tag{A.15}$$

and

$$\frac{\partial p}{\partial y} = \frac{\partial p}{\partial \beta}\frac{\partial \beta}{\partial y} + \frac{\partial p}{\partial \xi}\frac{\partial \xi}{\partial y} + \frac{\partial p}{\partial \zeta}\frac{\partial \zeta}{\partial y}$$
$$= \cos\theta_y \sin\theta_z \frac{\partial p}{\partial \beta} + (\cos\theta_x \cos\theta_z + \sin\theta_x \sin\theta_y \sin\theta_z)\frac{\partial p}{\partial \xi} + (\cos\theta_x \sin\theta_y \sin\theta_z$$
$$- \cos\theta_z \sin\theta_x)\frac{\partial p}{\partial \zeta}, \tag{A.16}$$

and

$$\frac{\partial p}{\partial z} = \frac{\partial p}{\partial \beta}\frac{\partial \beta}{\partial z} + \frac{\partial p}{\partial \xi}\frac{\partial \xi}{\partial z} + \frac{\partial p}{\partial \zeta}\frac{\partial \zeta}{\partial z}$$

$$= -\sin\theta_y \frac{\partial p}{\partial \beta} + \cos\theta_y \sin\theta_x \frac{\partial p}{\partial \xi} + \cos\theta_x \cos\theta_y \frac{\partial p}{\partial \zeta}. \quad \text{(A.17)}$$

Using Darcy's law in the principal directions x, y, z,

$$u_x = K_x \frac{\partial p}{\partial x}, \quad \text{(A.18)}$$

$$u_y = K_y \frac{\partial p}{\partial y}, \quad \text{(A.19)}$$

$$u_z = K_z \frac{\partial p}{\partial z}. \quad \text{(A.20)}$$

Then applying the rotation (A.11) to the Darcy velocities (A.18), (A.19) and (A.20) as follows:

$$R \cdot \begin{pmatrix} u_x \\ u_y \\ u_z \end{pmatrix}$$

$$= \begin{bmatrix} \cos\theta_y \cos\theta_z & \cos\theta_y \sin\theta_z & -\sin\theta_y \\ \cos\theta_z \sin\theta_x \sin\theta_y - \cos\theta_x \sin\theta_z & \sin\theta_x \sin\theta_y \sin\theta_z + \cos\theta_x \cos\theta_z & \cos\theta_y \sin\theta_x \\ \cos\theta_x \cos\theta_z \sin\theta_y + \sin\theta_x \sin\theta_z & \cos\theta_x \sin\theta_y \sin\theta_z - \cos\theta_z \sin\theta_x & \cos\theta_x \cos\theta_y \end{bmatrix}$$

$$\cdot \begin{pmatrix} K_x \cos\theta_y \cos\theta_z \dfrac{\partial p}{\partial \beta} + K_x(\cos\theta_z \sin\theta_x \sin\theta_y - \cos\theta_x \sin\theta_z) \dfrac{\partial p}{\partial \xi} + K_x(\sin\theta_x \sin\theta_z + \cos\theta_x \cos\theta_z \sin\theta_y) \dfrac{\partial p}{\partial \zeta} \\ K_y \cos\theta_y \sin\theta_z \dfrac{\partial p}{\partial \beta} + K_y(\cos\theta_x \cos\theta_z + \sin\theta_x \sin\theta_y \sin\theta_z) \dfrac{\partial p}{\partial \xi} + K_y(\cos\theta_x \sin\theta_y \sin\theta_z - \cos\theta_z \sin\theta_x) \dfrac{\partial p}{\partial \zeta} \\ -K_z \sin\theta_y \dfrac{\partial p}{\partial \beta} + K_z \cos\theta_y \sin\theta_x \dfrac{\partial p}{\partial \xi} + K_z \cos\theta_x \cos\theta_y \dfrac{\partial p}{\partial \zeta} \end{pmatrix}$$

$$= \begin{pmatrix} Term\ 1 \\ Term\ 2 \\ Term\ 3 \end{pmatrix} \tag{A.21}$$

where

$$Term\ 1 = K_x \cos^2\theta_y \cos^2\theta_z \frac{\partial p}{\partial \beta} + K_x(\cos\theta_z \sin\theta_x \sin\theta_y - \cos\theta_x \sin\theta_z) \cos\theta_y \cos\theta_z \frac{\partial p}{\partial \xi} +$$

$$K_x(\sin\theta_x \sin\theta_z + \cos\theta_x \cos\theta_z \sin\theta_y) \cos\theta_y \cos\theta_z \frac{\partial p}{\partial \zeta} + K_y \cos^2\theta_y \sin^2\theta_z \frac{\partial p}{\partial \beta} -$$

$$K_y(\cos\theta_x \cos\theta_z + \sin\theta_x \sin\theta_y \sin\theta_z) \cos\theta_y \sin\theta_z \frac{\partial p}{\partial \xi} + K_y(\cos\theta_x \sin\theta_y \sin\theta_z -$$

$$\cos\theta_z \sin\theta_x) \cos\theta_y \sin\theta_z \frac{\partial p}{\partial \zeta} + K_z \sin^2\theta_y \frac{\partial p}{\partial \beta} - K_z \cos\theta_y \sin\theta_x \sin\theta_y \frac{\partial p}{\partial \xi} -$$

$$K_z \cos\theta_x \cos\theta_y \sin\theta_y \frac{\partial p}{\partial \zeta}, \tag{A.22}$$

$$Term\ 2 = K_x \cos\theta_y \cos\theta_z(\cos\theta_z \sin\theta_x \sin\theta_y - \cos\theta_x \sin\theta_z)\frac{\partial p}{\partial \beta} + K_x(\cos\theta_z \sin\theta_x \sin\theta_y -$$

$$\cos\theta_x \sin\theta_z)^2 \frac{\partial p}{\partial \xi} + K_x(\sin\theta_x \sin\theta_z + \cos\theta_x \cos\theta_z \sin\theta_y)(\cos\theta_z \sin\theta_x \sin\theta_y -$$

$$\cos\theta_x \sin\theta_z)\frac{\partial p}{\partial \zeta} + K_y \cos\theta_y \sin\theta_z(\cos\theta_x \cos\theta_z + \sin\theta_x \sin\theta_y \sin\theta_z)\frac{\partial p}{\partial \beta} +$$

$$K_y(\cos\theta_x \cos\theta_z + \sin\theta_x \sin\theta_y \sin\theta_z)^2 \frac{\partial p}{\partial \xi} + K_y(\cos\theta_x \sin\theta_y \sin\theta_z - \cos\theta_z \sin\theta_x) *$$

$$(\cos\theta_x \cos\theta_z + \sin\theta_x \sin\theta_y \sin\theta_z)\frac{\partial p}{\partial \zeta} - K_z \cos\theta_y \sin\theta_x \sin\theta_y \frac{\partial p}{\partial \beta} +$$

$$K_z \cos^2\theta_y \sin^2\theta_x \frac{\partial p}{\partial \xi} + K_z \cos\theta_x \cos^2\theta_y \sin\theta_x \frac{\partial p}{\partial \zeta}, \qquad \text{(A.23)}$$

and

$$Term\ 3 = K_x \cos\theta_y \cos\theta_z(\cos\theta_x \cos\theta_z \sin\theta_y + \sin\theta_x \sin\theta_z)\frac{\partial p}{\partial \beta} + K_x(\cos\theta_z \sin\theta_x \sin\theta_y -$$

$$\cos\theta_x \sin\theta_z)(\cos\theta_x \cos\theta_z \sin\theta_y + \sin\theta_x \sin\theta_z)\frac{\partial p}{\partial \xi} + K_x(\sin\theta_x \sin\theta_y +$$

$$\cos\theta_x \cos\theta_z \sin\theta_y)^2 \frac{\partial p}{\partial \zeta} + K_y \cos\theta_y \sin\theta_z(\cos\theta_x \sin\theta_y \sin\theta_z - \cos\theta_z \sin\theta_x)\frac{\partial p}{\partial \beta} +$$

$$K_y(\cos\theta_x \cos\theta_z + \sin\theta_x \sin\theta_y \sin\theta_z)(\cos\theta_x \sin\theta_y \sin\theta_z - \cos\theta_z \sin\theta_x)\frac{\partial p}{\partial \xi} +$$

$$K_y(\cos\theta_x \sin\theta_y \sin\theta_z - \cos\theta_z \sin\theta_x)^2 \frac{\partial p}{\partial \zeta} - K_z \sin\theta_y \cos\theta_x \cos\theta_y \frac{\partial p}{\partial \beta} +$$

$$K_z \cos\theta_x \cos^2\theta_y \sin\theta_x \frac{\partial p}{\partial \xi} + K_z \cos^2\theta_x \cos^2\theta_y \frac{\partial p}{\partial \zeta}. \qquad \text{(A.24)}$$

This is the volumetric flux in β, ξ, ζ coordinates. Hence it must be equal to

$$\begin{pmatrix} Term\ 1 \\ Term\ 2 \\ Term\ 3 \end{pmatrix} = \begin{pmatrix} K_{\beta\beta} & K_{\beta\xi} & K_{\beta\zeta} \\ K_{\xi\beta} & K_{\xi\xi} & K_{\xi\zeta} \\ K_{\zeta\beta} & K_{\zeta\xi} & K_{\zeta\zeta} \end{pmatrix} \cdot \begin{pmatrix} {}^{\partial p}/_{\partial \beta} \\ {}^{\partial p}/_{\partial \xi} \\ {}^{\partial p}/_{\partial \zeta} \end{pmatrix} \tag{A.25}$$

by carrying out the above matrix multiplication we find that the permeabilities $K_{\beta\beta}$, $K_{\beta\xi}$, $K_{\beta\zeta}$, $K_{\xi\beta}$, $K_{\xi\xi}$, $K_{\xi\zeta}$, $K_{\zeta\beta}$, $K_{\zeta\xi}$, and $K_{\zeta\zeta}$ are given by

$$K_{\beta\beta} = K_x \cos^2\theta_y \cos^2\theta_z + K_y \cos^2\theta_y \sin^2\theta_z + K_z \sin^2\theta_y, \tag{A.26}$$

$$K_{\beta\xi} = K_x(\cos\theta_z \sin\theta_x \sin\theta_y - \cos\theta_x \sin\theta_z)\cos\theta_y \cos\theta_z + K_y(\cos\theta_x \cos\theta_z + \sin\theta_x \sin\theta_y \sin\theta_z)\cos\theta_y \sin\theta_z - K_z \cos\theta_y \sin\theta_x \sin\theta_y, \tag{A.27}$$

$$K_{\beta\zeta} = K_x(\sin\theta_x \sin\theta_z + \cos\theta_x \cos\theta_z \sin\theta_y)\cos\theta_y \cos\theta_z + K_y(\cos\theta_x \sin\theta_y \sin\theta_z - \cos\theta_z \sin\theta_x) * \cos\theta_y \sin\theta_z - K_z \cos\theta_x \cos\theta_y \sin\theta_y, \tag{A.28}$$

$$K_{\xi\beta} = K_x(\cos\theta_z \sin\theta_x \sin\theta_y - \cos\theta_x \sin\theta_z)\cos\theta_y \cos\theta_z + K_y(\cos\theta_x \cos\theta_z + \sin\theta_x \sin\theta_y \sin\theta_z) * \cos\theta_y \sin\theta_z - K_z \sin\theta_y \cos\theta_y \sin\theta_x, \tag{A.29}$$

$$K_{\xi\xi} = K_x(\cos\theta_x \sin\theta_x \sin\theta_z - \cos\theta_x \sin\theta_z)^2 + K_y(\cos\theta_x \cos\theta_z + \sin\theta_x \sin\theta_y \sin\theta_z)^2$$
$$+K_z \cos^2\theta_y \sin^2\theta_x, \quad \text{(A.30)}$$

$$K_{\xi\zeta} = K_x(\sin\theta_x \sin\theta_y + \cos\theta_x \cos\theta_z \sin\theta_y)(\cos\theta_z \sin\theta_x \sin\theta_y - \cos\theta_x \sin\theta_z)$$
$$+K_y(-\cos\theta_z \sin\theta_x + \cos\theta_x \sin\theta_y \sin\theta_z)(\cos\theta_x \cos\theta_z + \sin\theta_x \sin\theta_y \sin\theta_z)$$
$$+K_z \cos\theta_x \cos^2\theta_y \sin\theta_x \quad \text{(A.31)}$$

$$K_{\zeta\beta} = K_x(\sin\theta_x \sin\theta_z + \cos\theta_x \cos\theta_z \sin\theta_y)\cos\theta_y \cos\theta_z + K_y(\cos\theta_x \sin\theta_y \sin\theta_z$$
$$-\cos\theta_z \sin\theta_x) * \cos\theta_y \sin\theta_z - K_z \cos\theta_x \cos\theta_y \sin\theta_y, \quad \text{(A.32)}$$

$$K_{\zeta\xi} = K_x(\sin\theta_x \sin\theta_z + \cos\theta_x \cos\theta_z \sin\theta_y)(\cos\theta_z \sin\theta_x \sin\theta_y - \cos\theta_x \sin\theta_z)$$
$$+K_y(-\cos\theta_z \sin\theta_x + \cos\theta_x \sin\theta_y \sin\theta_z)(\cos\theta_x \cos\theta_z + \sin\theta_x \sin\theta_y \sin\theta_z)$$
$$+K_z \cos\theta_x \cos^2\theta_y \sin\theta_x, \quad \text{(A.33)}$$

$$K_{\zeta\zeta} = K_x(\sin\theta_x \sin\theta_z + \cos\theta_x \cos\theta_z \sin\theta_y)^2 + K_y(\cos\theta_x \sin\theta_y \sin\theta_z - \cos\theta_z \sin\theta_x)^2$$
$$+K_z \cos^2\theta_x \cos^2\theta_y. \quad \text{(A.34)}$$

Appendix B. Tensor Rotation Using Two Axis Rotation Method

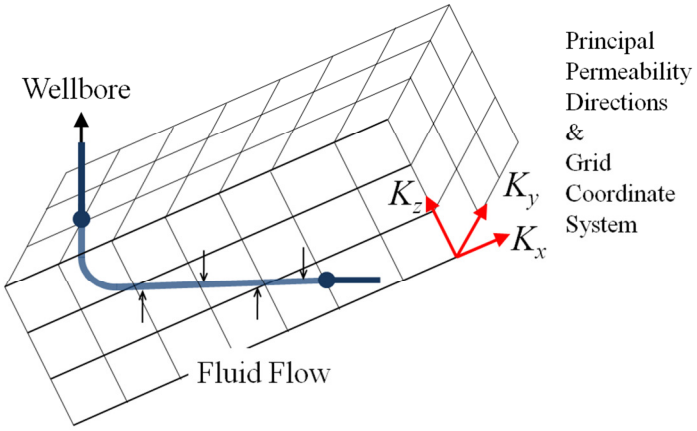

Figure 1

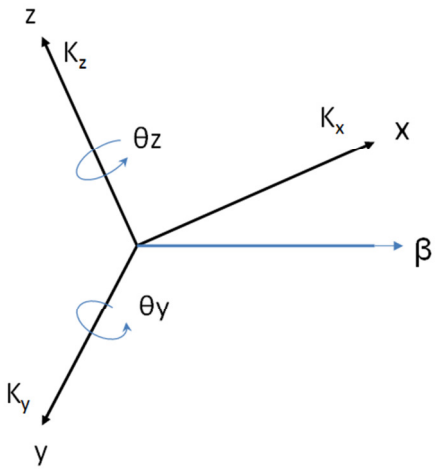

Figure 2

Figure 1 above depicts a three dimensional Cartesian coordinate system (*x, y, z*), which corresponds to principal permeability directions of the reservoir, and a well path that does not align with the coordinate system. The well path will be represented in a coordinate system that is different from the principal directions. In order to align the x-axis with the *β* axis in figure 2, a rotation around the y-axis, ϑ_y, followed by a rotation about the z-axis, ϑ_z, is required.

According to Darcy's Law, the velocity vector is

$$\vec{u} = -\frac{1}{\mu}\underline{K} \cdot \nabla p \,, \tag{B.1}$$

or

$$\begin{bmatrix} u_x \\ u_y \\ u_z \end{bmatrix} = -\frac{1}{\mu}\begin{pmatrix} K_{xx} & K_{xy} & K_{xz} \\ K_{yx} & K_{yy} & K_{yz} \\ K_{zx} & K_{zy} & K_{zz} \end{pmatrix} \cdot \begin{pmatrix} {}^{\partial p}/_{\partial x} \\ {}^{\partial p}/_{\partial y} \\ {}^{\partial p}/_{\partial z} \end{pmatrix}, \tag{B.2}$$

where we for simplicity have ignored gravity.

From (B.2), the components of $\vec{u}$ are

$$u_x = -\frac{1}{\mu}\left[K_{xx}\frac{\partial p}{\partial x} + K_{xy}\frac{\partial p}{\partial y} + K_{xz}\frac{\partial p}{\partial z}\right], \tag{B.3}$$

$$u_y = -\frac{1}{\mu}\left[K_{yx}\frac{\partial p}{\partial x} + K_{yy}\frac{\partial p}{\partial y} + K_{yz}\frac{\partial p}{\partial z}\right], \tag{B.4}$$

$$u_z = -\frac{1}{\mu}\left[K_{zx}\frac{\partial p}{\partial x} + K_{zy}\frac{\partial p}{\partial y} + K_{zz}\frac{\partial p}{\partial z}\right]. \tag{B.5}$$

A three dimensional rotated coordinate system is given by a matrix *R*.

$$\begin{pmatrix} \beta \\ \xi \\ \zeta \end{pmatrix} = R \cdot \begin{pmatrix} x \\ y \\ z \end{pmatrix} \tag{B.6}$$

where R equals;

$$R = R_y(\theta_y) \cdot R_z(\theta_z), \tag{B.7}$$

with coordinate system rotations of the y and z-axis in a counter clockwise direction when looking towards the origin give the matrices;

$$R_y(\theta_y) = \begin{bmatrix} \cos\theta_y & 0 & -\sin\theta_y \\ 0 & 1 & 0 \\ \sin\theta_y & 0 & \cos\theta_y \end{bmatrix}, \tag{B.8}$$

$$R_z(\theta_z) = \begin{bmatrix} \cos\theta_z & \sin\theta_z & 0 \\ -\sin\theta_z & \cos\theta_z & 0 \\ 0 & 0 & 1 \end{bmatrix}. \tag{B.9}$$

We find

$R = R_y(\theta_y) \cdot R_z(\theta_z)$

$$= \begin{bmatrix} \cos\theta_y & 0 & -\sin\theta_y \\ 0 & 1 & 0 \\ \sin\theta_y & 0 & \cos\theta_y \end{bmatrix} \cdot \begin{bmatrix} \cos\theta_z & \sin\theta_z & 0 \\ -\sin\theta_z & \cos\theta_z & 0 \\ 0 & 0 & 1 \end{bmatrix}$$

$$= \begin{bmatrix} \cos\theta_y\cos\theta_z + 0 + 0 & \cos\theta_y\sin\theta_z + 0 + 0 & 0 + 0 - \sin\theta_y \\ 0 - \sin\theta_z + 0 & 0 + \cos\theta_z + 0 & 0 + 0 + 0 \\ \sin\theta_y\cos\theta_z + 0 + 0 & \sin\theta_z\sin\theta_y + 0 + 0 & 0 + 0 + \cos\theta_y \end{bmatrix}$$

$$= \begin{bmatrix} \cos\theta_y\cos\theta_z & \cos\theta_y\sin\theta_z & -\sin\theta_y \\ -\sin\theta_z & \cos\theta_z & 0 \\ \cos\theta_z\sin\theta_y & \sin\theta_z\sin\theta_y & \cos\theta_y \end{bmatrix}. \tag{B.10}$$

From (B.6),

$$\begin{pmatrix}\beta\\ \xi\\ \zeta\end{pmatrix}=\begin{bmatrix}\cos\theta_y\cos\theta_z & \cos\theta_y\sin\theta_z & -\sin\theta_y\\ -\sin\theta_z & \cos\theta_z & 0\\ \cos\theta_z\sin\theta_y & \sin\theta_z\sin\theta_y & \cos\theta_y\end{bmatrix}\cdot\begin{pmatrix}x\\ y\\ z\end{pmatrix}$$

which gives

$$\beta = x\cos\theta_y\cos\theta_z + y\cos\theta_y\sin\theta_z - z\sin\theta_y, \tag{B.11}$$

$$\xi = -x\sin\theta_z + y\cos\theta_z, \tag{B.12}$$

$$\zeta = x\cos\theta_z\sin\theta_y + y\sin\theta_z\sin\theta_y + z\cos\theta_y. \tag{B.13}$$

Using the chain rule for differentiation,

$$\frac{\partial p}{\partial x}=\frac{\partial p}{\partial\beta}\frac{\partial\beta}{\partial x}+\frac{\partial p}{\partial\xi}\frac{\partial\xi}{\partial x}+\frac{\partial p}{\partial\zeta}\frac{\partial\zeta}{\partial x}$$

$$= \cos\theta_y\cos\theta_z\frac{\partial p}{\partial\beta} - \sin\theta_z\frac{\partial p}{\partial\xi} + \cos\theta_z\sin\theta_y\frac{\partial p}{\partial\zeta}, \tag{B.14}$$

and

$$\frac{\partial p}{\partial y} = \frac{\partial p}{\partial \beta}\frac{\partial \beta}{\partial y} + \frac{\partial p}{\partial \xi}\frac{\partial \xi}{\partial y} + \frac{\partial p}{\partial \zeta}\frac{\partial \zeta}{\partial y}$$

$$= \cos\theta_y \sin\theta_z \frac{\partial p}{\partial \beta} + \cos\theta_z \frac{\partial p}{\partial \xi} + \sin\theta_z \sin\theta_y \frac{\partial p}{\partial \zeta}, \tag{B.15}$$

and

$$\frac{\partial p}{\partial z} = \frac{\partial p}{\partial \beta}\frac{\partial \beta}{\partial z} + \frac{\partial p}{\partial \xi}\frac{\partial \xi}{\partial z} + \frac{\partial p}{\partial \zeta}\frac{\partial \zeta}{\partial z}$$

$$= -\sin\theta_y \frac{\partial p}{\partial \beta} + \cos\theta_y \frac{\partial p}{\partial \zeta}. \tag{B.16}$$

Using Darcy's law in the principal directions x, y, z,

$$u_x = K_x \frac{\partial p}{\partial x}, \tag{B.17}$$

$$u_y = K_y \frac{\partial p}{\partial y}, \tag{B.18}$$

$$u_z = K_z \frac{\partial p}{\partial z}. \tag{B.19}$$

Then applying the rotation (B.10) to the Darcy velocities (B.17), (B.18) and (B.19) as follows:

$$R \cdot \begin{pmatrix} u_x \\ u_y \\ u_z \end{pmatrix} = \begin{bmatrix} \cos\theta_y \cos\theta_z & \cos\theta_y \sin\theta_z & -\sin\theta_y \\ -\sin\theta_z & \cos\theta_z & 0 \\ \cos\theta_z \sin\theta_y & \sin\theta_z \sin\theta_y & \cos\theta_y \end{bmatrix}$$

$$\cdot \begin{bmatrix} \mathrm{K_x}\cos\theta_y \cos\theta_z \dfrac{\partial p}{\partial \beta} - \mathrm{K_x}\sin\theta_z \dfrac{\partial p}{\partial \xi} + \mathrm{K_x}\cos\theta_z \sin\theta_y \dfrac{\partial p}{\partial \zeta} \\ K_y \cos\theta_y \sin\theta_z \dfrac{\partial p}{\partial \beta} + K_y \cos\theta_z \dfrac{\partial p}{\partial \xi} + K_y \sin\theta_z \sin\theta_y \dfrac{\partial p}{\partial \zeta} \\ -\mathrm{K_z}\sin\theta_y \dfrac{\partial p}{\partial \beta} + \mathrm{K_z}\cos\theta_y \dfrac{\partial p}{\partial \zeta} \end{bmatrix}$$

$$= \begin{pmatrix} Term\ 1 \\ Term\ 2 \\ Term\ 3 \end{pmatrix}, \tag{B.20}$$

where

$$Term\ 1 = K_x(\cos\theta_y \cos\theta_z)^2 \frac{\partial p}{\partial \beta} - K_x \cos\theta_y \cos\theta_z \sin\theta_z \frac{\partial p}{\partial \xi} + K_x \cos\theta_y \cos\theta_z^2 \sin\theta_y \frac{\partial p}{\partial \zeta} +$$

$$K_y(\cos\theta_y \sin\theta_z)^2 \frac{\partial p}{\partial \beta} + K_y \cos\theta_y \cos\theta_z \sin\theta_z \frac{\partial p}{\partial \xi} + K_y \cos\theta_y \sin\theta_y \sin\theta_z^2 \frac{\partial p}{\partial \zeta} +$$

$$K_z \sin\theta_y^2 \frac{\partial p}{\partial \beta} - K_z \cos\theta_y \sin\theta_y \frac{\partial p}{\partial \zeta}, \tag{B.21}$$

$$Term\ 2 = -K_x \cos\theta_y \cos\theta_z \sin\theta_z \frac{\partial p}{\partial \beta} + K_x \sin\theta_z^2 \frac{\partial p}{\partial \xi} - K_x \cos\theta_z \sin\theta_y \sin\theta_z \frac{\partial p}{\partial \zeta} +$$

$$K_y \cos\theta_y \cos\theta_z \sin\theta_z \frac{\partial p}{\partial \beta} + K_y \cos\theta_z^2 \frac{\partial p}{\partial \xi} + K_y \cos\theta_z \sin\theta_y \sin\theta_z \frac{\partial p}{\partial \zeta}, \tag{B.22}$$

$$Term\ 3 = K_x \cos\theta_y \cos\theta_z^2 \sin\theta_y \frac{\partial p}{\partial \beta} - K_x \cos\theta_z \sin\theta_y \sin\theta_z \frac{\partial p}{\partial \xi} + K_x (\cos\theta_z \sin\theta_y)^2 \frac{\partial p}{\partial \zeta} +$$

$$K_y \cos\theta_y \sin\theta_y \sin\theta_z^2 \frac{\partial p}{\partial \beta} + K_y \cos\theta_z \sin\theta_y \sin\theta_z \frac{\partial p}{\partial \xi} + K_y (\sin\theta_y \sin\theta_z)^2 \frac{\partial p}{\partial \zeta} -$$

$$K_z \cos\theta_y \sin\theta_y \frac{\partial p}{\partial \beta} + K_z \cos\theta_y^2 \frac{\partial p}{\partial \zeta}\,. \tag{B.23}$$

This is the volumetric flux in β, ξ, ζ coordinates. Hence it must be equal to

$$\begin{pmatrix} Term\ 1 \\ Term\ 2 \\ Term\ 3 \end{pmatrix} = \begin{pmatrix} K_{\beta\beta} & K_{\beta\xi} & K_{\beta\zeta} \\ K_{\xi\beta} & K_{\xi\xi} & K_{\xi\zeta} \\ K_{\zeta\beta} & K_{\zeta\xi} & K_{\zeta\zeta} \end{pmatrix} \cdot \begin{pmatrix} {\partial p}/{\partial \beta} \\ {\partial p}/{\partial \xi} \\ {\partial p}/{\partial \zeta} \end{pmatrix} \tag{B.24}$$

by carrying out the above matrix multiplication we find that the permeabilities $K_{\beta\beta}$, $K_{\beta\xi}$, $K_{\beta\zeta}$, $K_{\xi\beta}$, $K_{\xi\xi}$, $K_{\xi\zeta}$, $K_{\zeta\beta}$, $K_{\zeta\xi}$, and $K_{\zeta\zeta}$ are given by

$$K_{\beta\beta} = K_x (\cos\theta_y \cos\theta_z)^2 + K_y (\cos\theta_y \sin\theta_z)^2 + K_z \sin\theta_y^2\,, \tag{B.25}$$

$$K_{\beta\xi} = -K_x \cos\theta_y \cos\theta_z \sin\theta_z + K_y \cos\theta_y \cos\theta_z \sin\theta_z\,, \tag{B.26}$$

$$K_{\beta\zeta} = K_x \cos\theta_y \cos\theta_z^2 \sin\theta_y + K_y \cos\theta_y \sin\theta_y \sin\theta_z^2 - K_z \cos\theta_y \sin\theta_y\,, \tag{B.27}$$

$$K_{\xi\beta} = -K_x \cos\theta_y \cos\theta_z \sin\theta_z + K_y \cos\theta_y \cos\theta_z \sin\theta_z \,, \tag{B.28}$$

$$K_{\xi\xi} = K_x \sin\theta_z^2 + K_y \cos\theta_z^2 \,, \tag{B.29}$$

$$K_{\xi\zeta} = -K_x \cos\theta_z \sin\theta_y \sin\theta_z + K_y \cos\theta_z \sin\theta_y \sin\theta_z \,, \tag{B.30}$$

$$K_{\zeta\beta} = K_x \cos\theta_y \cos\theta_z^2 \sin\theta_y + K_y \cos\theta_y \sin\theta_y \sin\theta_z^2 - K_z \cos\theta_y \sin\theta_y \,, \tag{B.31}$$

$$K_{\zeta\xi} = -K_x \cos\theta_z \sin\theta_y \sin\theta_z + K_y \cos\theta_z \sin\theta_y \sin\theta_z \,, \tag{B.32}$$

$$K_{\zeta\zeta} = K_x(\cos\theta_z \sin\theta_y)^2 + K_y(\sin\theta_y \sin\theta_z)^2 + K_z \cos\theta_y^2 \,. \tag{B.33}$$

Appendix C. Sample Reservoir Simulation Code

Code for Run#1-9 unrotated (Single Block)

RUNSPEC --- Beginning Section of the Code.

TITLE --- Gives the code its title.
RUN#1-9 UNROTATED

FIELD --- Request the Field unit set.

HWELLS --- Horizontal wells present, needed in 300 code.

--- Indicates that the Run may contain oil, water and gas.
OIL
WATER
GAS

CO2SOL --- Allows CO_2 to exist in all three phases.

AIM --- Selects the AIM (Adaptive IMplicit) solution option for 300 code.

COMPS --- Activates the compositional mode.
9 /

EOS --- Equation of state being used is Peng-Robinson.
PR /

DIMENS --- Number of blocks in x-, y-, and z-directions. This is a part of the code that will be changed, depending on the number of blocks in the reservoir.
1 1 1 /

TABDIMS --- Table dimensions.
1 1 200 200 /

START --- Specifies the start date of the simulation.
1 JAN 2014 /

GRID --- Grid section of the code.

DXV --- x-direction grid block sizes, 50 feet per block. Change depending on the reservoir.
1*50 /
DYV --- y-direction grid block sizes, 50 feet per block. Change depending on the reservoir.
1*50 /
DZV --- z-direction grid block sizes, 50 feet per block. Change depending on the reservoir.
1*50 /

TOPS --- Depth to the top of the reservoir, 1000 feet.
1*10000 /

EQUALS --- Assigns or replaces the value of a property for a box of cells within the grid.

PORO --- Porosity, 25%.
0.25 /

--- The location in the code where the permeability is changed, depending on the Run.
PERMX 200 / --- Principal permeability in the x-direction, 200 mD.
PERMY 200 / --- Principal permeability in the y-direction, 200 mD.
PERMZ 64 / --- Principal permeability in the z-direction, 64mD.

PROPS --- Properties section of the code.

NCOMPS --- Confirm number of components
9 /

STCOND --- Standard temperature and pressure in degree F and PSIA.
60.0 14.7 /

CNAMES --- Component names.
CO2 N2 C1 C2 C3 C4-6 C7+ C7+2 C7+3 /

HYDRO --- Define hydrocarbon type.
N N H H H H A A A /

TCRIT --- Critical temperature, degree R.
548.46000 227.16000 343.08000 549.77400 665.64000
806.54054 838.11282 1058.03863 1291.89071 /

PCRIT --- Critical pressure, PSA
1071.33111 492.31265 667.78170 708.34238 618.69739

514.92549 410.74956 247.56341 160.41589 /

ZCRIT --- Critical z-factor.
.27408 .29115 .28473 .28463 .27748
.27640 .26120 .22706 .20137 /

ACF --- Acentric factor.
.22500 .04000 .01300 .09860 .15240
.21575 .31230 .55670 .91692 /

MW --- Molecular weights.
44.01000 28.01300 16.04300 30.07000 44.09700
66.86942 107.77943 198.56203 335.19790 /

OMEGAA --- Omega_A values.
.4572355 .4572355 .5340210 .4572355 .4572355
.4572355 .6373344 .6373344 .6373344 /

OMEGAB --- Omega_B values.
.0777961 .0777961 .0777961 .0777961 .0777961
.0777961 .0872878 .0872878 .0872878 /

ZMFVD --- Default fluid sample composition.
1 0.0852 0.13774 0.468529 0.061628 0.041961 0.068657 0.03195 0.0994 0.001633
10000 0.0852 0.13774 0.468529 0.061628 0.041961 0.068657 0.03195 0.0994 0.001633 /

TBOIL --- Boiling point temperature, degree R.
350.46000 139.32000 201.06000 332.10000 415.98000
523.33222 689.67140 958.31604 1270.40061 /

TREF --- Reference temperature, degree R.
527.40000 140.58000 201.06000 329.40000 415.80000
526.05233 519.67000 519.67000 519.67000 /

DREF --- Reference densities, lb/ft3.
48.50653 50.19209 26.53189 34.21053 36.33308
37.87047 45.60035 50.88507 55.89861 /

PARACHOR --- Parachors, dynes/cm.
78.00000 41.00000 77.00000 108.00000 150.30000

213.52089 331.78241 516.45301 853.48860 /

BIC --- Binary interaction coefficients.
-.0200
.1000 .0360
.1300 .0500 .000000
.1350 .0800 .000000 .000
.1277 .1002 .092810 .000 .000
.1000 .1000 .130663 .006 .006 .0
.1000 .1000 .130663 .006 .006 .0 .0
.1000 .1000 .130663 .006 .006 .0 .0 .0 /

RTEMP --- Reservoir temperature, degree F.
230.0 /

SWFN --- Water saturation functions.
0.16 0 3
0.18 0 2
0.20 0.002 1
0.44 0.090 0.5
0.68 0.330 0.1
0.8 0.540 0.05
1.00 1.000 0.0 /

SGFN --- Gas saturation functions.
0.00 0.000 0.0
0.04 0.005 0.0
0.12 0.026 0.0
0.24 0.078 0.0
0.36 0.156 0.0
0.48 0.260 0.0
0.60 0.400 0.0
0.72 0.562 0.0
0.84 0.800 0.0
/

SOF3 --- Oil saturation functions (three-phase)
0.00 0.000 0.000
0.24 0.000 0.000

```
0.28 0.005 0.005
0.32 0.012 0.012
0.44 0.060 0.060
0.56 0.150 0.150
0.72 0.400 0.400
0.84 0.800 0.800 /

ROCK --- Rock compressibility.
4351.1 0.00001577 /

PVTW  --- Water pressure tables.
4351.1 1.0 0.000004 0.2476 0.0 /

DENSITY  --- Surface density.
1* 63.02 1* /

SOLUTION --- Solution section of the code.
EQUIL --- Equilibration data specification.
10000 10000 10250 3 10000  0.001/

OUTSOL --- Outputs at every report step.
PRESSURE SOIL SWAT SGAS /

SUMMARY --- Summary section of the code.
RUNSUM --- Requests table output of summary data.
FOPR
FWPR
FOPT
FGOR
FPR

RPTONLY --- Requests that summary data be written to the summary file only at report times.

SCHEDULE  --- Schedule section of the code.
RPTSCHED --- Controls the output from the schedule section of the code.
PRESSURE SWAT SOIL SGAS /

WELSPECS  --- General specification data for wells. Will change depending on the Run.
P FIELD 1 1 10000 OIL  /
/
```

COMPDAT --- Well completion specification data. Will change depending on the Run. In the single block reservoir the well is in the only block and traveling in the x-direction.
well name, x, y, z, second z, open wellbore, default 6, well direction in the block.

```
P  1  1  1  1  open  6*  'X' /
/
```

WCONPROD ---- Controls data for the production wells.

```
P OPEN LRAT 1* 1* 1* 250 1* 1/
/
```

TSTEP --- After each time step a report of the current state of the reservoir is produced. The time step will also change depending on the reservoir used.

```
7*1 /
```

END --- End of the code.

Code for Run#4 rotated (Single block reservoir, 343° about the y-axis and 0° about the z-axis)

```
RUNSPEC

TITLE
RUN#4 ROTATED

FIELD

HWELLS

OIL
WATER
GAS

CO2SOL

AIM

COMPS
9 /

EOS
PR /

DIMENS
1 1 1 /

TABDIMS
1 1 200 200 /

START
1 JAN 2014 /

GRID

DXV
1*50 /
DYV
1*50 /
```

```
DZV
1*50 /

TOPS
1*10000 /

EQUALS

PORO
0.25 /
```

--- PERMXY, PERMYZ, PERMZX used in the rotated tensor cases. They represent he off diagonal terms in the permeability matrix that appear after the rotation. This is the only section of the code that changes in Runs 1-9.

```
PERMX  188.37    /
PERMY  200       /
PERMZ  75.625    /
PERMXY 0         /
PERMYZ 0         /
PERMZX -38.025   /
/

PROPS

NCOMPS
9 /

STCOND
60.0 14.7 /

CNAMES
CO2 N2 C1 C2 C3 C4-6 C7+ C7+2 C7+3 /
HYDRO
N N H H H H A A A /

TCRIT
548.46000 227.16000 343.08000 549.77400 665.64000
806.54054 838.11282 1058.03863 1291.89071 /
```

PCRIT
1071.33111 492.31265 667.78170 708.34238 618.69739
514.92549 410.74956 247.56341 160.41589 /

ZCRIT
.27408 .29115 .28473 .28463 .27748
.27640 .26120 .22706 .20137 /

ACF
.22500 .04000 .01300 .09860 .15240
.21575 .31230 .55670 .91692 /

MW
44.01000 28.01300 16.04300 30.07000 44.09700
66.86942 107.77943 198.56203 335.19790 /

OMEGAA
.4572355 .4572355 .5340210 .4572355 .4572355
.4572355 .6373344 .6373344 .6373344 /

OMEGAB
.0777961 .0777961 .0777961 .0777961 .0777961
.0777961 .0872878 .0872878 .0872878 /

ZMFVD
1 0.0852 0.13774 0.468529 0.061628 0.041961 0.068657 0.03195 0.0994 0.001633
10000 0.0852 0.13774 0.468529 0.061628 0.041961 0.068657 0.03195 0.0994 0.001633 /

TBOIL
350.46000 139.32000 201.06000 332.10000 415.98000
523.33222 689.67140 958.31604 1270.40061 /

TREF
527.40000 140.58000 201.06000 329.40000 415.80000
526.05233 519.67000 519.67000 519.67000 /

DREF
48.50653 50.19209 26.53189 34.21053 36.33308
37.87047 45.60035 50.88507 55.89861 /

PARACHOR
78.00000 41.00000 77.00000 108.00000 150.30000
213.52089 331.78241 516.45301 853.48860 /

BIC
-.0200
.1000 .0360
.1300 .0500 .000000
.1350 .0800 .000000 .000
.1277 .1002 .092810 .000 .000
.1000 .1000 .130663 .006 .006 .0
.1000 .1000 .130663 .006 .006 .0 .0 /

RTEMP
230.0 /

SWFN
0.16 0 3
0.18 0 2
0.20 0.002 1
0.44 0.090 0.5
0.68 0.330 0.1
0.8 0.540 0.05
1.00 1.000 0.0 /

SGFN
0.00 0.000 0.0
0.04 0.005 0.0
0.12 0.026 0.0
0.24 0.078 0.0
0.36 0.156 0.0
0.48 0.260 0.0
0.60 0.400 0.0
0.72 0.562 0.0
0.84 0.800 0.0
/

SOF3
0.00 0.000 0.000
0.24 0.000 0.000
0.28 0.005 0.005

```
0.32 0.012 0.012
0.44 0.060 0.060
0.56 0.150 0.150
0.72 0.400 0.400
0.84 0.800 0.800 /

ROCK
4351.1 0.00001577 /

PVTW
4351.1 1.0 0.000004 0.2476 0.0 /

DENSITY
1* 63.02 1* /


SOLUTION
EQUIL
10000 10000 10250 3 10000  0.001/

OUTSOL
PRESSURE SOIL SWAT SGAS /

SUMMARY
RUNSUM
FOPR
FWPR
FOPT
FGOR
FPR

RPTONLY

SCHEDULE
RPTSCHED
PRESSURE SWAT SOIL SGAS /

WELSPECS
P FIELD 1 1 10000 OIL  /
/
```

```
COMPDAT
P  1  1  1  1  open  6*  'X' /
/

WCONPROD
P OPEN LRAT 1* 1* 1* 250 1* 1/
/

TSTEP
7*1 /

END
```

Code for Run#15 unrotated (5x5x5 Reservoir)

```
RUNSPEC

TITLE
RUN#15 UNROTATED

FIELD

HWELLS

OIL
WATER
GAS

CO2SOL

AIM

COMPS
9 /

EOS
PR /

DIMENS  --- Since this is now a 5x5x5 reservoir, the dimensions are changed.
5 5 5 /

TABDIMS
1 1 200 200 /

START
1 JAN 2014 /

GRID

--- The number of blocks in this section is also changed.
DXV
5*10 /
DYV
```

```
5*10 /
DZV
5*10 /

TOPS
125*10000 /

EQUALS

PORO
0.25 /

--- The unrotated permeability is still the same in the 5x5x5 reservoir.
PERMX 200 /
PERMY 200 /
PERMZ 64  /
/

PROPS

NCOMPS
9 /

STCOND
60.0 14.7 /

CNAMES
CO2 N2 C1 C2 C3 C4-6 C7+ C7+2 C7+3 /
HYDRO
N N H H H H A A A /

TCRIT
548.46000 227.16000 343.08000 549.77400 665.64000
806.54054 838.11282 1058.03863 1291.89071 /

PCRIT
1071.33111 492.31265 667.78170 708.34238 618.69739
514.92549 410.74956 247.56341 160.41589 /

ZCRIT
.27408 .29115 .28473 .28463 .27748
```

.27640 .26120 .22706 .20137 /
ACF
.22500 .04000 .01300 .09860 .15240
.21575 .31230 .55670 .91692 /

MW
44.01000 28.01300 16.04300 30.07000 44.09700
66.86942 107.77943 198.56203 335.19790 /

OMEGAA
.4572355 .4572355 .5340210 .4572355 .4572355
.4572355 .6373344 .6373344 .6373344 /

OMEGAB
.0777961 .0777961 .0777961 .0777961 .0777961
.0777961 .0872878 .0872878 .0872878 /

ZMFVD
1 0.0852 0.13774 0.468529 0.061628 0.041961 0.068657 0.03195 0.0994 0.001633
10000 0.0852 0.13774 0.468529 0.061628 0.041961 0.068657 0.03195 0.0994 0.001633 /

TBOIL
350.46000 139.32000 201.06000 332.10000 415.98000
523.33222 689.67140 958.31604 1270.40061 /

TREF
527.40000 140.58000 201.06000 329.40000 415.80000
526.05233 519.67000 519.67000 519.67000 /

DREF
48.50653 50.19209 26.53189 34.21053 36.33308
37.87047 45.60035 50.88507 55.89861 /

PARACHOR
78.00000 41.00000 77.00000 108.00000 150.30000
213.52089 331.78241 516.45301 853.48860 /

BIC
-.0200
.1000 .0360
.1300 .0500 .000000

.1350 .0800 .000000 .000
.1277 .1002 .092810 .000 .000
.1000 .1000 .130663 .006 .006 .0
.1000 .1000 .130663 .006 .006 .0 .0 /

RTEMP
230.0 /

SWFN
0.16 0 3
0.18 0 2
0.20 0.002 1
0.44 0.090 0.5
0.68 0.330 0.1
0.8 0.540 0.05
1.00 1.000 0.0 /

SGFN
0.00 0.000 0.0
0.04 0.005 0.0
0.12 0.026 0.0
0.24 0.078 0.0
0.36 0.156 0.0
0.48 0.260 0.0
0.60 0.400 0.0
0.72 0.562 0.0
0.84 0.800 0.0
/

SOF3
0.00 0.000 0.000
0.24 0.000 0.000
0.28 0.005 0.005
0.32 0.012 0.012
0.44 0.060 0.060
0.56 0.150 0.150
0.72 0.400 0.400
0.84 0.800 0.800 /

ROCK
4351.1 0.00001577 /

```
PVTW
4351.1 1.0 0.000004 0.2476 0.0 /

DENSITY
1* 63.02 1* /

SOLUTION
EQUIL
10000 10000 10250 3 10000  0.001/

OUTSOL
PRESSURE SOIL SWAT SGAS /

SUMMARY
RUNSUM
FOPR
FWPR
FOPT
FGOR
FPR

RPTONLY

SCHEDULE
RPTSCHED
PRESSURE SWAT SOIL SGAS /

WELSPECS
P FIELD 1 1 10000 OIL  /
/

--- The wellpath in Run 15 starts at block (1,1,2) and finishes at block (5,5,4). In every block the
well penetrates the center and travels in the x-direction.
COMPDAT
P  1  1  2  2  open  6*  'X' /
P  2  2  3  3  open  6*  'X' /
P  3  3  3  3  open  6*  'X' /
P  4  4  3  3  open  6*  'X' /
P  5  5  4  4  open  6*  'X' /
/
```

```
WCONPROD
P OPEN LRAT 1* 1* 1* 250 1* 1/
/

TSTEP
7*1 /

END
```

Code for Run#15 rotated (5x5x5 block reservoir, 343° about the y-axis and 45° about the z-axis)

```
RUNSPEC

TITLE
RUN#15 ROTATED

FIELD

HWELLS

OIL
WATER
GAS

CO2SOL

AIM

COMPS
9 /

EOS
PR /

DIMENS
5 5 5 /

TABDIMS
1 1 200 200 /

START
1 JAN 2014 /

GRID

DXV
5*10 /
DYV
5*10 /
```

```
DZV
5*10 /

TOPS
125*10000 /

EQUALS

PORO
0.25 /

--- The only section in the code that changes from Run 15 unrotated to Run 15 rotated.
PERMX  188.38   /
PERMY  200      /
PERMZ  75.625   /
PERMXY 0        /
PERMYZ 3.6E-15  /
PERMZX -38.025  /
/
PROPS

NCOMPS
9 /

STCOND
60.0 14.7 /

CNAMES
CO2 N2 C1 C2 C3 C4-6 C7+ C7+2 C7+3 /
HYDRO
N N H H H H A A A /

TCRIT
548.46000 227.16000 343.08000 549.77400 665.64000
806.54054 838.11282 1058.03863 1291.89071 /

PCRIT
1071.33111 492.31265 667.78170 708.34238 618.69739
514.92549 410.74956 247.56341 160.41589 /
```

ZCRIT
.27408 .29115 .28473 .28463 .27748
.27640 .26120 .22706 .20137 /

ACF
.22500 .04000 .01300 .09860 .15240
.21575 .31230 .55670 .91692 /

MW
44.01000 28.01300 16.04300 30.07000 44.09700
66.86942 107.77943 198.56203 335.19790 /

OMEGAA
.4572355 .4572355 .5340210 .4572355 .4572355
.4572355 .6373344 .6373344 .6373344 /

OMEGAB
.0777961 .0777961 .0777961 .0777961 .0777961
.0777961 .0872878 .0872878 .0872878 /

ZMFVD
1 0.0852 0.13774 0.468529 0.061628 0.041961 0.068657 0.03195 0.0994 0.001633
10000 0.0852 0.13774 0.468529 0.061628 0.041961 0.068657 0.03195 0.0994 0.001633 /

TBOIL
350.46000 139.32000 201.06000 332.10000 415.98000
523.33222 689.67140 958.31604 1270.40061 /

TREF
527.40000 140.58000 201.06000 329.40000 415.80000
526.05233 519.67000 519.67000 519.67000 /

DREF
48.50653 50.19209 26.53189 34.21053 36.33308
37.87047 45.60035 50.88507 55.89861 /

PARACHOR
78.00000 41.00000 77.00000 108.00000 150.30000
213.52089 331.78241 516.45301 853.48860 /

```
BIC
-.0200
.1000 .0360
.1300 .0500 .000000
.1350 .0800 .000000 .000
.1277 .1002 .092810 .000 .000
.1000 .1000 .130663 .006 .006 .0
.1000 .1000 .130663 .006 .006 .0 .0 /

RTEMP
230.0 /

SWFN
0.16 0 3
0.18 0 2
0.20 0.002 1
0.44 0.090 0.5
0.68 0.330 0.1
0.8 0.540 0.05
1.00 1.000 0.0 /

SGFN
0.00 0.000 0.0
0.04 0.005 0.0
0.12 0.026 0.0
0.24 0.078 0.0
0.36 0.156 0.0
0.48 0.260 0.0
0.60 0.400 0.0
0.72 0.562 0.0
0.84 0.800 0.0
/

SOF3
0.00 0.000 0.000
0.24 0.000 0.000
0.28 0.005 0.005
0.32 0.012 0.012
0.44 0.060 0.060
0.56 0.150 0.150
```

```
0.72 0.400 0.400/

ROCK
4351.1 0.00001577 /

PVTW
4351.1 1.0 0.000004 0.2476 0.0 /

DENSITY
1* 63.02 1* /


SOLUTION
EQUIL
10000 10000 10250 3 10000  0.001/

OUTSOL
PRESSURE SOIL SWAT SGAS /

SUMMARY
RUNSUM
FOPR
FWPR
FOPT
FGOR
FPR

RPTONLY

SCHEDULE
RPTSCHED
PRESSURE SWAT SOIL SGAS /

WELSPECS
P FIELD 1 1 10000 OIL  /
/
```

--- The wellpath in Run 15 rotated and unrotated are identical.

```
COMPDAT
P  1  1  2  2  open  6*  'X' /
P  2  2  3  3  open  6*  'X' /
P  3  3  3  3  open  6*  'X' /
P  4  4  3  3  open  6*  'X' /
P  5  5  4  4  open  6*  'X' /
/

WCONPROD
P OPEN LRAT 1* 1* 1* 250 1* 1/
/

TSTEP
7*1 /

END
```

Code for Run#26 unrotated (5x5x5 block reservoir)

```
RUNSPEC

TITLE
RUN#26 UNROTATED

FIELD

HWELLS

OIL
WATER
GAS

CO2SOL

AIM

COMPS
9 /

EOS
PR /

DIMENS
5 5 5 /

TABDIMS
1 1 200 200 /

START
1 JAN 2014 /

GRID

DXV
5*10 /
DYV
5*10 /
```

```
DZV
5*10 /

TOPS
125*10000 /

EQUALS

PORO
0.25 /
```

--- The only section in the code that changes from Runs 10-18 to 19-27. Runs 19-27 use the permeability in the y-direction to equal 150.

```
PERMX 200 /
PERMY 150 /
PERMZ 64  /
/
PROPS

NCOMPS
9 /

STCOND
60.0 14.7 /

CNAMES
CO2 N2 C1 C2 C3 C4-6 C7+ C7+2 C7+3 /

HYDRO
N N H H H H A A A /

TCRIT
548.46000 227.16000 343.08000 549.77400 665.64000
806.54054 838.11282 1058.03863 1291.89071 /

PCRIT
1071.33111 492.31265 667.78170 708.34238 618.69739
514.92549 410.74956 247.56341 160.41589 /
```

ZCRIT
.27408 .29115 .28473 .28463 .27748
.27640 .26120 .22706 .20137 /

ACF
.22500 .04000 .01300 .09860 .15240
.21575 .31230 .55670 .91692 /

MW
44.01000 28.01300 16.04300 30.07000 44.09700
66.86942 107.77943 198.56203 335.19790 /

OMEGAA
.4572355 .4572355 .5340210 .4572355 .4572355
.4572355 .6373344 .6373344 .6373344 /

OMEGAB
.0777961 .0777961 .0777961 .0777961 .0777961
.0777961 .0872878 .0872878 .0872878 /

ZMFVD
1 0.0852 0.13774 0.468529 0.061628 0.041961 0.068657 0.03195 0.0994 0.001633
10000 0.0852 0.13774 0.468529 0.061628 0.041961 0.068657 0.03195 0.0994 0.001633 /

TBOIL
350.46000 139.32000 201.06000 332.10000 415.98000
523.33222 689.67140 958.31604 1270.40061 /

TREF
527.40000 140.58000 201.06000 329.40000 415.80000
526.05233 519.67000 519.67000 519.67000 /

DREF
48.50653 50.19209 26.53189 34.21053 36.33308
37.87047 45.60035 50.88507 55.89861 /

PARACHOR
78.00000 41.00000 77.00000 108.00000 150.30000
213.52089 331.78241 516.45301 853.48860 /

```
BIC
-.0200
.1000 .0360
.1300 .0500 .000000
.1350 .0800 .000000 .000
.1277 .1002 .092810 .000 .000
.1000 .1000 .130663 .006 .006 .0
.1000 .1000 .130663 .006 .006 .0 .0 /

RTEMP
230.0 /

SWFN
0.16 0 3
0.18 0 2
0.20 0.002 1
0.44 0.090 0.5
0.68 0.330 0.1
0.8 0.540 0.05
1.00 1.000 0.0 /

SGFN
0.00 0.000 0.0
0.04 0.005 0.0
0.12 0.026 0.0
0.24 0.078 0.0
0.36 0.156 0.0
0.48 0.260 0.0
0.60 0.400 0.0
0.72 0.562 0.0
0.84 0.800 0.0
/

SOF3
0.00 0.000 0.000
0.24 0.000 0.000
0.28 0.005 0.005
0.32 0.012 0.012
0.44 0.060 0.060
0.56 0.150 0.150
0.72 0.400 0.400 /
```

```
ROCK
4351.1 0.00001577 /

PVTW
4351.1 1.0 0.000004 0.2476 0.0 /

DENSITY
1* 63.02 1* /

SOLUTION

EQUIL
10000 10000 10250 3 10000  0.001/
OUTSOL
PRESSURE SOIL SWAT SGAS /

SUMMARY
RUNSUM
FOPR
FWPR
FOPT
FGOR
FPR

RPTONLY

SCHEDULE
RPTSCHED
PRESSURE SWAT SOIL SGAS /

WELSPECS
P FIELD 1 1 10000 OIL  /
/
```

--- The wellpath in Run 10-18 are identical to the well paths in Runs 19-27. Both these sets of Runs use the 5x5x5 reservoir.

```
COMPDAT
P  1  1  2  2  open  6*  'X' /
P  2  2  3  3  open  6*  'X' /
P  3  3  3  3  open  6*  'X' /
P  4  4  3  3  open  6*  'X' /
P  5  5  4  4  open  6*  'X' /
/

WCONPROD
P OPEN LRAT 1* 1* 1* 250 1* 1/
/

TSTEP
7*1 /

END
```

Code for Run#32 unrotated (10x10x10 block reservoir)

```
RUNSPEC

TITLE
RUN#32 UNROTATED

FIELD

HWELLS

OIL
WATER
GAS

CO2SOL

AIM

COMPS
9 /

EOS
PR /

DIMENS --- Changes from the 5x5x5 reservoir to the 10x10x10 reservoir dimensions.
10  10  10 /

TABDIMS
1 1 200 200 /

START
1 JAN 2014 /

GRID

--- The 5 blocks in the code are changed to 10.
DXV
10*5 /
```

```
DYV
10*5 /

DZV
10*5 /

TOPS
1000*10000 /

EQUALS

PORO
0.25 /

--- The only section in the code is the same as Runs 1-9 and Runs 10-18.
PERMX 200 /
PERMY 200 /
PERMZ 64  /
/
PROPS

NCOMPS
9 /

STCOND
60.0 14.7 /

CNAMES
CO2 N2 C1 C2 C3 C4-6 C7+ C7+2 C7+3 /

HYDRO
N N H H H H A A A /

TCRIT
548.46000 227.16000 343.08000 549.77400 665.64000
806.54054 838.11282 1058.03863 1291.89071 /

PCRIT
1071.33111 492.31265 667.78170 708.34238 618.69739
514.92549 410.74956 247.56341 160.41589 /
```

ZCRIT
.27408 .29115 .28473 .28463 .27748
.27640 .26120 .22706 .20137 /

ACF
.22500 .04000 .01300 .09860 .15240
.21575 .31230 .55670 .91692 /

MW
44.01000 28.01300 16.04300 30.07000 44.09700
66.86942 107.77943 198.56203 335.19790 /

OMEGAA
.4572355 .4572355 .5340210 .4572355 .4572355
.4572355 .6373344 .6373344 .6373344 /

OMEGAB
.0777961 .0777961 .0777961 .0777961 .0777961
.0777961 .0872878 .0872878 .0872878 /

ZMFVD
1 0.0852 0.13774 0.468529 0.061628 0.041961 0.068657 0.03195 0.0994 0.001633
10000 0.0852 0.13774 0.468529 0.061628 0.041961 0.068657 0.03195 0.0994 0.001633 /

TBOIL
350.46000 139.32000 201.06000 332.10000 415.98000
523.33222 689.67140 958.31604 1270.40061 /

TREF
527.40000 140.58000 201.06000 329.40000 415.80000
526.05233 519.67000 519.67000 519.67000 /

DREF
48.50653 50.19209 26.53189 34.21053 36.33308
37.87047 45.60035 50.88507 55.89861 /

PARACHOR
78.00000 41.00000 77.00000 108.00000 150.30000
213.52089 331.78241 516.45301 853.48860 /

```
BIC
-.0200
.1000 .0360
.1300 .0500 .000000
.1350 .0800 .000000 .000
.1277 .1002 .092810 .000 .000
.1000 .1000 .130663 .006 .006 .0
.1000 .1000 .130663 .006 .006 .0 .0 /

RTEMP
230.0 /

SWFN
0.16 0 3
0.18 0 2
0.20 0.002 1
0.44 0.090 0.5
0.68 0.330 0.1
0.8 0.540 0.05
1.00 1.000 0.0 /

SGFN
0.00 0.000 0.0
0.04 0.005 0.0
0.12 0.026 0.0
0.24 0.078 0.0
0.36 0.156 0.0
0.48 0.260 0.0
0.60 0.400 0.0
0.72 0.562 0.0
0.84 0.800 0.0
/

SOF3
0.00 0.000 0.000
0.24 0.000 0.000
0.28 0.005 0.005
0.32 0.012 0.012
0.44 0.060 0.060
0.56 0.150 0.150
0.72 0.400 0.400
```

```
0.84 0.800 0.800 /

ROCK
4351.1 0.00001577 /

PVTW
4351.1 1.0 0.000004 0.2476 0.0 /

DENSITY
1* 63.02 1* /

SOLUTION

EQUIL
10000 10000 10250 3 10000  0.001/

OUTSOL
PRESSURE SOIL SWAT SGAS /

SUMMARY
RUNSUM
FOPR
FWPR
FOPT
FGOR
FPR

RPTONLY

SCHEDULE
RPTSCHED
PRESSURE SWAT SOIL SGAS /

WELSPECS
P FIELD 1 3 10000 OIL  /
/

--- The wellpath is longer because the reservoir is now 10x10x10.
COMPDAT
P  1   3  3  3  open  6*  'X' /
P  2   3  3  3  open  6*  'X' /
```

```
P  3   4  4  4  open  6*  'X' /
P  4   4  4  4  open  6*  'X' /
P  5   4  4  4  open  6*  'X' /
P  6   5  5  5  open  6*  'X' /
P  7   5  5  5  open  6*  'X' /
P  8   5  5  5  open  6*  'X' /
P  9   6  6  6  open  6*  'X' /
P  10 6  6  6  open  6*  'X' /
/

WCONPROD
P OPEN LRAT 1* 1* 1* 250 1* 1/
/

TSTEP --- Larger time step to allow for more Running time in the larger reservoir.
7*1 /

END
```

Code for Run#32 rotated (10x10x10 block reservoir, 343° about the y-axis and 22° about the z-axis)

```
RUNSPEC

TITLE
RUN#32 ROTATED

FIELD

HWELLS

OIL
WATER
GAS

CO2SOL

AIM

COMPS
9 /

EOS
PR /

DIMENS
10  10  10 /

TABDIMS
1 1 200 200 /

START
1 JAN 2014 /

GRID

DXV
10*5 /
```

```
DYV
10*5 /
DZV
10*5 /


TOPS
1000*10000 /

EQUALS

PORO
0.25 /

--- This is the only section in the code that is different than the Run 32 unrotated case.
PERMX  188.38    /
PERMY  200       /
PERMZ  75.63     /
PERMXY 0         /
PERMYZ 3.6E-15   /
PERMZX -38.03    /
/
PROPS

NCOMPS
9 /

STCOND
60.0 14.7 /

CNAMES
CO2 N2 C1 C2 C3 C4-6 C7+ C7+2 C7+3 /
HYDRO
N N H H H H A A A /

TCRIT
548.46000 227.16000 343.08000 549.77400 665.64000
806.54054 838.11282 1058.03863 1291.89071 /

PCRIT
1071.33111 492.31265 667.78170 708.34238 618.69739
```

514.92549 410.74956 247.56341 160.41589 /

ZCRIT
.27408 .29115 .28473 .28463 .27748
.27640 .26120 .22706 .20137 /

ACF
.22500 .04000 .01300 .09860 .15240
.21575 .31230 .55670 .91692 /

MW
44.01000 28.01300 16.04300 30.07000 44.09700
66.86942 107.77943 198.56203 335.19790 /

OMEGAA
.4572355 .4572355 .5340210 .4572355 .4572355
.4572355 .6373344 .6373344 .6373344 /

OMEGAB
.0777961 .0777961 .0777961 .0777961 .0777961
.0777961 .0872878 .0872878 .0872878 /

ZMFVD
1 0.0852 0.13774 0.468529 0.061628 0.041961 0.068657 0.03195 0.0994 0.001633
10000 0.0852 0.13774 0.468529 0.061628 0.041961 0.068657 0.03195 0.0994 0.001633 /

TBOIL
350.46000 139.32000 201.06000 332.10000 415.98000
523.33222 689.67140 958.31604 1270.40061 /

TREF
527.40000 140.58000 201.06000 329.40000 415.80000
526.05233 519.67000 519.67000 519.67000 /

DREF
48.50653 50.19209 26.53189 34.21053 36.33308
37.87047 45.60035 50.88507 55.89861 /

PARACHOR
78.00000 41.00000 77.00000 108.00000 150.30000
213.52089 331.78241 516.45301 853.48860 /

```
BIC
-.0200
.1000 .0360
.1300 .0500 .000000
.1350 .0800 .000000 .000
.1277 .1002 .092810 .000 .000
.1000 .1000 .130663 .006 .006 .0
.1000 .1000 .130663 .006 .006 .0 .0 /

RTEMP
230.0 /

SWFN
0.16 0 3
0.18 0 2
0.20 0.002 1
0.44 0.090 0.5
0.68 0.330 0.1
0.8 0.540 0.05
1.00 1.000 0.0 /

SGFN
0.00 0.000 0.0
0.04 0.005 0.0
0.12 0.026 0.0
0.24 0.078 0.0
0.36 0.156 0.0
0.48 0.260 0.0
0.60 0.400 0.0
0.72 0.562 0.0
0.84 0.800 0.0
/

SOF3
0.00 0.000 0.000
0.24 0.000 0.000
0.28 0.005 0.005
0.32 0.012 0.012
0.44 0.060 0.060
0.56 0.150 0.150
0.72 0.400 0.400 /
```

```
ROCK
4351.1 0.00001577 /

PVTW
4351.1 1.0 0.000004 0.2476 0.0 /

DENSITY
1* 63.02 1* /

SOLUTION

EQUIL
10000 10000 10250 3 10000  0.001/

OUTSOL
PRESSURE SOIL SWAT SGAS /

SUMMARY
RUNSUM
FOPR
FWPR
FOPT
FGOR
FPR

RPTONLY

SCHEDULE

RPTSCHED
PRESSURE SWAT SOIL SGAS /

WELSPECS
P FIELD 1 3 10000 OIL  /
/

--- The wellpath is the same as the unrotated case.
COMPDAT
P  1   3  3  3  open  6*  'X' /
P  2   3  3  3  open  6*  'X' /
P  3   4  4  4  open  6*  'X' /
```

```
P  4   4  4  4  open  6*  'X' /
P  5   4  4  4  open  6*  'X' /
P  6   5  5  5  open  6*  'X' /
P  7   5  5  5  open  6*  'X' /
P  8   5  5  5  open  6*  'X' /
P  9   6  6  6  open  6*  'X' /
P  10 6  6  6  open  6*  'X' /
/

WCONPROD
P OPEN LRAT 1* 1* 1* 250 1* 1/
/

TSTEP
7*1 /

END
```